Elektrospinnen en functionalisatie van siliciumoxidenanovezels met behulp van sol-geltechnologie

Electrospinning and Functionalization of Silicon Oxide Nanofibers via Sol-Gel Technology

Jozefien Geltmeyer

Promotoren: prof. dr. ir. K. De Clerck, prof. dr. K. De Buysser
Proefschrift ingediend tot het behalen van de graad van
Doctor in de ingenieurswetenschappen: materiaalkunde

UNIVERSITEIT
GENT

Vakgroep Textielkunde
Voorzitter: prof. dr. P. Kiekens
Faculteit Ingenieurswetenschappen en Architectuur
Academiejaar 2016 - 2017

ISBN 978-90-8578-967-3
NUR 971
Wettelijk depot: D/2017/10.500/2

Examencommissie:

Prof. dr. ir. Karen De Clerck, promotor	Universiteit Gent
Prof. dr. Klaartje De Buysser, promotor	Universiteit Gent
Prof. dr. ir. Gert De Cooman, voorzitter	Universiteit Gent
Prof. dr. Paul Kiekens, secretaris	Universiteit Gent
Prof. dr. ir. Dagmar D'hooge	Universiteit Gent
Prof. dr. Richard Hoogenboom	Universiteit Gent
Prof. dr. ir. Joris Thybaut	Universiteit Gent
Prof. dr. ir. André ten Elshof	Universiteit Twente
Prof. dr. Tamer Uyar	Bilkent University

This work was supported by the Agency for Innovation by Science and Technology (IWT). Results in this PhD were obtained within the framework of the IWT Strategic Basic Research grant 121241.

Woord vooraf

Er bestaan twee soorten families: de maternalistische, waar een vrouw aan het hoofd staat, en de paternalistische, waar een man aan het hoofd staat. Bij de Geltmeyers hadden we een mater familias, ons mamie. Een van de levenswijsheden die ze ons bijbracht was deze over arbeidsvreugde. Hoe belangrijk het is om een job te doen die je graag doet en waar je energie kunt uithalen. Om eerlijk te zijn, er zijn dagen geweest dat ik mijn doctoraat beu was en dat de deadline nog ver weg leek, maar gelukkig namen de leuke, boeiende en leerrijke momenten de bovenhand. Nu, op het einde van de rit ben ik eigenlijk zeer trots op wat ik bereikt heb en ook zeer dankbaar voor wat ik bijgeleerd heb.

Een doctoraat schrijven doe je uiteraard niet alleen. Er zijn nog een paar mensen die ik graag wil bedanken. In de eerste plaats wil ik Karen en Klaartje bedanken, mijn twee promotoren. Jullie deur stond steeds open en elke vraag mocht gesteld worden. Zonder jullie was dit niet mogelijk geweest en daar ben ik jullie zeer erkentelijk voor.

In de vakgroep Textielkunde waren er ook nog veel collega's waar ik steeds kon op rekenen. Vooral mijn bureaugenootjes wil ik bedanken: Iline, Sofie, Ella, Nuray en Ana. Bedankt voor de leuke en grappige babbels, de interessante discussies, het gezelschap en de vriendschap. Daarnaast wil ik ook Lien bedanken, mijn thesisbegeleidster, waar ik ongelooflijk veel van heb bijgeleerd. Waaronder ook de passie voor onderzoek. Ook Sabine, Katrien, Martine, Els, Johanna, Carla en Thierry wil ik bedanken. Niet alleen voor de hulp, maar vooral voor de gezellige lunchpauzes.

De volgende in het rijtje om te bedanken zijn mijn thesisstudenten Bet, Helena, Paulien, Lakshmi en Eva. Alle samenwerkingen waren stuk voor stuk zeer leerrijk en boeiend.

Daarnaast heb ik tijdens mijn doctoraat ook de kans gekregen om samen te werken met andere professoren en vakgroepen. Hierbij wil ik prof. Richard Hoogenboom bedanken voor de uiterst interessante samenwerking rond kleurstof immobilisatie in siliciumoxidenanovezels. Het is onder meer dankzij hem dat het ons gelukt is om de paper in Advanced Functional Materials te publiceren. Ik wil ook Gertjan en

Kathleen bedanken voor hun werk in het labo en het mee begeleiden van de thesisstudenten. Ook prof. Stijn Van Hulle wil ik bedanken voor de zeer interessante samenwerking rond nanovezels voor filtratie. Daarnaast hebben ook de praktische tips en kennis van Nele ervoor gezorgd dat we haar onderzoek op een vruchtbare manier konden verderzetten. Prof. José Martins, Freya en Jonathan ben ik erg dankbaar voor alle NMR metingen en hun hulp bij de interpretatie van de data.

Tot slot bedank ik mijn dichtste vrienden en zeker mijn huisgenootjes van de voorbije vier jaar voor hun vriendschap, de ontspanning, steun en hun interesse in mijn doctoraat. Uiteraard kon ik de voorbije vier jaar ook steeds terugvallen op de steun van mijn familie. In de eerste plaats wil ik mijn ouders bedanken. Het is dankzij jullie steun, liefde en duwtjes in de rug dat ik hier ben geraakt. Ook mijn broer en zus, Adriaan en Klara, wil ik bedanken. Oma en opa, mamie en papie, ook jullie goede zorgen en wijze raad waren mij zeer dierbaar. Als laatste wil ik nog Ruben bedanken. De laatste maanden en weken stond je altijd voor mij klaar, tijdens de leuke en lastige momenten en het verdriet om mamie de voorbije dagen. Bedankt om mijn steun en toeverlaat te zijn en mij zo veel liefde te geven.

Na vier jaar doctoreren ben ik op vele vlakken wijzer geworden, maar heb ik ook beseft dat er nog heel veel dingen zijn die we nog niet weten of begrijpen. Nu, op het einde van de rit, ben ik zeer fier op wat ik de voorbije vier jaar heb bereikt, maar de drang om te leren is nog niet gestild.

Jozefien Geltmeyer
Gent, 28 december 2016

Table of contents

Summary – Dutch Samenvatting

Traditionele keramische materialen, gebaseerd op klei, worden al meer dan 25 000 jaar gebruikt. Typische eigenschappen geassocieerd met keramische materialen zijn brosheid, een goed druksterkte en een uitstekende stabiliteit in extreme chemische en thermische omstandigheden. Keramische materialen kunnen geproduceerd worden via sol-geltechnologie. Het sol-gelproces is een lage temperatuursmethode die toelaat om keramische materialen te maken met een uitstekende controle van de zuiverheid en samenstelling van het product. De ontwikkeling van geavanceerde keramische materialen nam significant toe gedurende de laatste decennia. Recenter breidde ook de interesse in nanotechnologie sterk uit. Nanovezels, die typisch een diameter hebben kleiner dan 500 nm, zijn gekend omwille van hun uitzonderlijke eigenschappen zoals een hoge specifieke oppervlakte, een hoge porositeit en kleine poriëngrootte. Keramische nanovezels kunnen geproduceerd worden door het elektrospinproces te combineren met sol-geltechnologie. De combinatie van de unieke eigenschappen van nanovezels met de veelzijdigheid van het sol-gelproces laat toe om keramische nanovezels te produceren die bruikbaar zijn in uiteenlopende geavanceerde toepassingen.

Binnen dit doctoraat wordt de productie van nieuwe silicananovezels verkend. Deze silicananovezels worden geproduceerd via een techniek die sterk afwijkt van wat typisch gebruikt wordt in de literatuur. In tegenstelling tot de gebruikelijke productietechniek van keramische nanovezels wordt er in dit werk geen organisch polymeer toegevoegd aan de elektrospinoplossing. Hierdoor kan de hittebehandeling, die normaal gebruikt wordt om het polymeer te verwijderen na het elektrospinnen, vermeden worden. Deze hittebehandeling geeft doorgaans aanleiding tot fragiele membranen, die de neiging hebben om in kleine deeltjes uit elkaar te vallen. Door deze hittebehandeling te vermijden wordt de schade aan zowel de nanovezelmembranen zelf als de schade aan toegevoegde functionaliteiten beperkt. Het sol-gelproces en het elektrospinproces laten beiden toe om op een eenvoudige manier extra functionaliteiten in te bouwen in de silicananovezels, waardoor deze membranen voor

uiteenlopende toepassingen gebruikt kunnen worden. In dit doctoraat wordt de focus gelegd op twee toepassingsdomeinen, namelijk waterbehandeling en colorimetrische sensoren. Hoofdstuk 1 bevat een inleiding tot sol-geltechnologie, het elektrospinproces en de beoogde toepassingen. Hierna worden de algemene materialen en methodes beschreven in hoofdstuk 2.

Wanneer het elektrospinnen van silicananovezels wordt uitgevoerd zonder het toevoegen van een organisch polymeer aan de elektrospinoplossing, is het essentieel om de reologie van de oplossing te controleren om een stabiel en opschaalbaar elektrospinproces te bekomen. Een van de eigenschappen van een elektrospinoplossing die de verspinbaarheid sterk beïnvloedt is de viscositeit. In hoofdstuk 3 wordt daarom het viscositeitsbereik onderzocht dat mogelijkheid biedt tot stabiel en reproduceerbaar elektrospinnen. Tetraethoxysilaan (TEOS) werd geselecteerd als sol-gelprecursor omwille van het veelvuldig gebruik en de reeds bestaande doorgedreven kennis van de precursor en zijn eigenschappen. Daarnaast wordt ook het belang van de manier waarop de viscositeit bereikt wordt besproken. Uiteindelijk wordt de weerstand van deze membranen tegen hoge temperaturen (1000°C) aangetoond en worden de interessante veranderingen van de hydrofiele/hydrofobe eigenschappen toegelicht. Niet enkel de viscositeit van de oplossing heeft een belangrijke invloed op het elektrospinproces, maar ook andere oplossingsparameters zoals de colloïdale deeltjesgrootte, de vernettingsgraad en de ethanolconcentratie bepalen het elektrospinproces en de hieruit geproduceerde nanovezels. Daarom wordt in hoofdstuk 4 bijkomende aandacht gegeven aan het karakteriseren van deze parameters via verschillende technieken. Bovendien wordt ook de productie van de silicananovezels succesvol opgeschaald. In de hierop volgende hoofdstukken wordt het toepassen van gefunctionaliseerde silicananovezelmembranen voor waterbehandeling en kleurveranderende sensoren uitgebreid behandeld.

De unieke eigenschappen van nanovezelmembranen zorgen ervoor dat ze geschikt zijn voor verschillende toepassingen binnen filtratie. Bovendien zijn deze membranen een uitstekende poreuze drager voor het immobiliseren van titaniumdioxide (TiO_2) nanodeeltjes. Deze TiO_2 nanodeeltjes kunnen vele organische (micro)polluenten afbreken. In hoofdstuk 5 worden zowel polyamide 6 als silicananovezels gefunctionaliseerd met TiO_2 nanodeeltjes. Twee functionalisatie

technieken worden vergeleken, namelijk inline functionalisatie en post-functionalisatie via dipcoaten. De fotokatalytische activiteit van deze membranen wordt vergeleken en aangetoond door het ontkleuren van methyleen blauw. De hoge meerwaarde van deze met TiO_2 gefunctionaliseerde membranen voor het verwijderen van micropolluenten wordt bevestigd door volledige verwijdering van het herbicide isoproturon.

De hoge specifieke oppervlakte en de hoge porositeit van nanovezelmembranen kunnen de gevoeligheid en snelheid van sensoren verbeteren. Kleurveranderende polymeernanovezels hebben hun grote meerwaarde reeds aangetoond. Kleurveranderende keramische nanovezels kunnen door hun chemische stabiliteit een nog bredere toepassingsgebied bereiken. In zowel hoofdstuk 6 als hoofdstuk 7 wordt de nadruk gelegd op het produceren van grote, flexibele en herbruikbare colorimetrische sensoren. Opnieuw worden verschillende functionalisatietechnieken vergeleken, zowel fysisch als covalent immobiliseren van de kleurstof komen aan bod. Het covalent binden van een kleurstof in de nanovezelmatrix zorgt ervoor dat migratie van de kleurstof naar de omgeving, wat vaak een probleem is als de kleurstof enkel fysisch gevangen zit in de matrix, voorkomen wordt. Daarom worden de kleurstoffen in deze hoofdstukken covalent gebonden aan een sol-gelprecursor. In hoofdstuk 6 wordt de gevoeligheid voor pH-veranderingen, HCl en NH_3 dampen en biogene amines van kleurvariërende nanovezels getest. Het feit dat enkel de membranen met een covalent gebonden kleurstof bruikbaar zijn in zure waterige oplossing, toont het belang van de covalente binding aan. Alle nanovezelmembranen veranderen wel onmiddellijk van kleur na blootstelling aan HCl en NH_3 dampen. De gevoeligheid van deze membranen voor biogene amines toont bovendien hun veelzijdigheid aan.

In hoofdstuk 7 worden solvatochrome nanovezelsensoren bestudeerd. In dit hoofdstuk worden drie technieken toegepast voor het functionaliseren met de kleurstof, namelijk fysisch inmengen en covalent inmengen van de kleurstof in de nanovezels, en covalent immobiliseren van de kleurstof op de membranen via een coating. De nanovezelmembranen waarbij de kleurstof covalent werd ingemengd, zijn echter niet stabiel in de gebruikte solventen waardoor de kleurstof migreert naar de omgeving. Het coaten van zuivere silicananovezels voorkomt dit probleem en verbreedt de toepasbaarheid naar andere substraten, maar verder onderzoek is nodig.

Ten slotte worden in hoofdstuk 8 de belangrijkste conclusies van dit doctoraat en enkele bedenkingen met betrekking tot toekomstig onderzoek samengevat.

In dit werk wordt een diepgaande studie uitgevoerd over het elektrospinnen van TEOS sols en de invloed van verschillende parameters op dit proces. De reproduceerbaarheid en opschaalbaarheid van het productieproces van silicananovezels wordt aangetoond. Het toepassen van deze kennis voor de productie van membranen die bruikbaar zijn in waterbehandeling en als colorimetrische sensoren tonen het grote potentieel aan van deze membranen voor geavanceerde toepassingen.

Summary – English

Traditonal ceramics, based on clay, have been used for over 25 000 years. Specific properties associated with ceramic materials are brittleness, compressive strength and stability in both harsh chemical and thermal environments. Ceramic materials can be produced via sol-gel technology. The sol-gel process is a low temperature method enabling the production of ceramics with an excellent control of product purity and composition. Developments in advanced ceramics have significantly increased over the last decades. More recently, also the interest in nanotechnology expanded rapidly. Nanofibers, typically having a diameter of less than 500 nm, are known for their unique properties including a large specific surface area, a high porosity and small pore sizes. Ceramic nanofibers can be produced by combining electrospinning and sol-gel technology. The combination of the unique properties of nanofibers with the versatility of the sol-gel process gives the opportunity to produce ceramic nanofibrous membranes usable in various advanced applications.

This PhD explores the production of novel silica nanofibers. These novel nanofibers are produced by applying a preparation procedure different from what is typically used in literature for the production of ceramic nanofibers. In contrast to literature no organic polymer is added to the electrospinning solution, hereby giving the possibility to avoid the heat treatment step typically used to remove the organic polymer after electrospinning. This heat treatment results most of the time in fragile ceramic nanofibrous membranes, that have the tendency to break into little pieces. Avoiding the heat treatment thus avoids a deleterious effect on the nanofibrous membranes themselves as well as the possible destruction of added functionalities. Both the sol-gel process and the electrospinning process allow for easy functionalization of these silica nanofibers offering applicability in various applications. In this PhD focus is given to two application domains being water treatment and colorimetric sensors.

Chapter 1 provides an overview on sol-gel technology, the electrospinning process and the envisioned applications. Subsequently, the materials and methods used throughout this PhD are described in Chapter 2.

When electrospinning of silica nanofibers is carried out without organic polymer addition in the electrospinning solution, proper control of the sols rheology is essential to enable stable and scalable electrospinning. One of the characteristics that highly affects the electrospinning process is the viscosity of a solution. Therefore, in Chapter 3 the viscosity range that enables uniform and reproducible nanofibers is determined. Tetraethyl orthosilicate (TEOS) is selected as sol-gel precursor, since this is the most commonly used and most thoroughly studied sol-gel precursor. The importance of the route to obtain this viscosity is discussed as well. Additionally, the resistance of these membranes to high temperatures (1000°C) is shown and the interesting changes in hydrophilic properties are denoted. It was found that not only the viscosity of the sol has a major influence on the electrospinning process, but also other parameters including colloidal particle sizes, ethanol concentration and degree of crosslinking are determining the electrospinning process and the resulting nanofibers. Therefore, additional attention is given to the characterization of these parameters in Chapter 4 by using multiple characterization techniques. Moreover, successful upscaling of these silica nanofibers was carried out. Subsequently, the following chapters elaborate on the application of functionalized silica nanofibers for water treatment and colorimetric sensors.

The unique properties of nanofibrous membranes makes them ideal for a wide range of filtration applications. Moreover, they show to be an excellent porous support for the immobilization of titanium dioxide (TiO_2) nanoparticles. These TiO_2 nanoparticles are capable of oxidizing many organic (micro)pollutants. In Chapter 5 both polyamide 6 and silica nanofibers are functionalized with TiO_2 nanoparticles. Two techniques for functionalization are compared, namely inline functionalization and post-functionalization via dip-coating. Their high photocatalytic activity is demonstrated and compared by decoloring of Methylene Blue. The high value of TiO_2 functionalized nanofibrous membranes for organic (micro)pollutants removal is shown through complete degradation of isoproturon.

Due to the high specific surface area and high porosity of nanofibrous membranes, the sensitivity and response time of sensors can be improved. Color changing polymer nanofibers have already shown to be highly valuable in previous research. Color changing ceramic nanofibers can be

applied in an even broader application domain due to their chemical resistance. Chapter 6 and 7 both focus on the production of large area, flexible, reusable colorimetric sensors. In line with Chapter 5, different functionalization techniques are compared, including both physical entrapment (dye-doping) and covalent immombilization of the dye within the nanofibrous matrix. Covalent immobilization of a dye significantly improves dye leaching compared to dye-doped membranes. Therefore, color changing dyes are covalently linked to a selected sol-gel precursor in both chapters. In Chapter 6 color-changing nanofibers are tested in their response toward pH-changes in water, hydrochloric acid and ammonia vapors, and biogenic amines. The importance of the covalent linkage is proven, as only the membranes with a covalently link between dye and sol-gel matrix are suitable to be used as pH-sensor in aqueous acidic environments. All nanofibrous membranes showed an immediate and clear color change upon exposure to hydrogen chloride and ammonia vapors. Their sensitivity towards biogenic amines demonstrates the versatility of these membranes.

Chapter 7 focuses on solvatochromic nanofibrous sensor materials. Three functionalization techniques are used, namely dye doping, covalent coupling inside the nanofibers and covalent immobilization on the membranes via coating. A major limitation in Chapter 7 for the inline covalently coupled nanofibrous membranes was, however, their instability in the solvents resulting in insufficient immobilization of the dye giving high dye leaching. Although further studies are still needed it was already clear that coating of pure silica nanofibers overcomes this problem and broadens the applicability on various substrates.

Finally, Chapter 8 summarizes the main conclusions of this PhD and provides an outlook towards possible future work.

In this work an in-depth study is thus carried out on the electrospinning process of TEOS sols and the parameters influencing this process. The reproducibility and scalability of the production of silica nanofibers is demonstrated. The implementation of this knowledge for the production of membranes applicable for water treatment and for color-changing sensor materials shows the major potential for advanced applications.

List of publications

* based on results presented in this PhD

Research papers

E. Schoolaert, P. Ryckx, **J. Geltmeyer**, S. Maji, P.H.M. Van Steenberge, D. R. D'hooge, R. Hoogenboom, and K. De Clerck, "Waterborne electrospinning of poly(n-isopropylacrylamide) toward stable nanofibers", In preparation

*** J. Geltmeyer**, H. Teixido, M. Meire, K. Deventer, L. Balcaen, S. Van Hulle, K. De Buysser, and K. De Clerck, "TiO_2 functionalized nanofibrous membranes for removal of organic (micro)pollutants," Submitted to Separation and Purification Technology, 2016.

JCR IF ^{2015} 3.299 (3.758 5-year), ranking Q1 in Engineering, chemical.

*** J. Geltmeyer**, G. Vancoillie, I. Steyaert; B. Breyne, G. Cousins, K. Lava, R. Hoogenboom, K. De Buysser, and K. De Clerck, "Dye Modification of Nanofibrous Silicon Oxide Membranes for Colorimetric HCl and NH_3 sensing," *Adv. Funct. Mater.*, vol. 26, pp. 5987-5996, 2016. Back cover.

JCR IF ^{2015} 11.382 (11.774 5-year), ranking Q1 in Materials Science, multidisciplinary

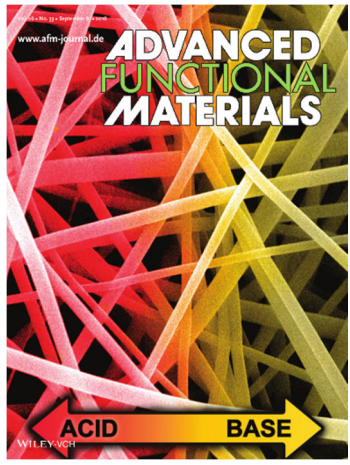

E. Schoolaert, I. Steyaert, G. Vancoillie, **J. Geltmeyer**, K. Lava, R. Hoogenboom, and K. De Clerck, "Blend electrospinning of dye-functionalized chitosan and poly(ε-caprolactone): towards biocompatible pH-sensors," *J. Mater. Chem. B*, vol. 4, pp. 4507-4516, 2016. Front cover.

JCR IF 2015 4.872 (4.879 5-year), ranking Q1 in Materials Science, Biomaterials

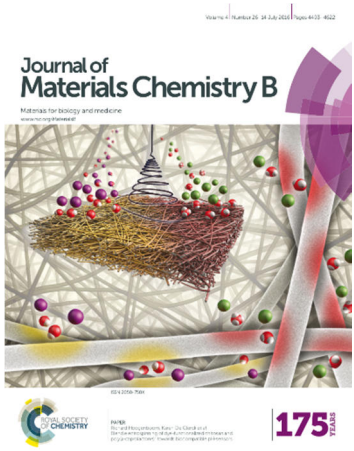

*** J. Geltmeyer**, J. De Roo, F. Van den Broeck, J. C. Martins, K. De Buysser, and K. De Clerck, "The influence of tetraethoxysilane sol preparation on the electrospinning of silica nanofibers," *J. Sol-Gel Sci. Technol.*, vol. 77, no. 2, pp. 453–462, 2016.

JCR IF 2015 1.473 (1.624 5-year), ranking Q2 in Materials Science, ceramics

*** J. Geltmeyer**, L. Van der Schueren, F. Goethals, K. De Buysser, and K. De Clerck, "Optimum sol viscosity for stable electrospinning of silica nanofibres," *J. Sol-Gel Sci. Technol.*, vol. 67, no. 1, pp. 188–195, 2013.

JCR IF 2013 1.547 (1.763 5-year), ranking Q1 in Materials Science, ceramics

Conference proceedings

* K. De Clerck, E. Schoolaert, **J. Geltmeyer**, I. Steyaert, G. Vancoillie, and R. Hoogenboom, "Dye functionalized nanofibers for fast, reversible and easy read-out colorimetric sensor materials," *2nd International Caparica Conference on Chromogenic and Emissive Materials,* Lisbon (Portugal), 5-8 September 2016

*** J. Geltmeyer**, G. Vancoillie, R. Hoogenboom, K. De Buysser, and K. De Clerck, "Colorimetric HCl and NH_3 sensing via dye modified silicon oxide nanofibrous membranes," *4th International Conference on Electrospinning*, Otranto (Italy), 28 June – 1 July 2016.

K. De Clerck, E. Schoolaert, **J. Geltmeyer**, I. Steyaert, G. Vancoillie, and R. Hoogenboom, "Blend electrospinning of dye functionalized polymer nanofibres for colorimetric sensors," *4th International Conference on Electrospinning*, Otranto (Italy), 28 June – 1 July 2016.

* K. De Clerck, E. Schoolaert, **J. Geltmeyer**, G. Vancoillie, I. Steyaert, K. De Buysser, and R. Hoogenboom, "Dye-functionalized electrospun nanofibers for colorimetric sensors," Electrospinning: Science and Application (EMPA workshop), St. Gallen (Switzerland), 16 June 2016.

*** J. Geltmeyer**, K. De Buysser, and K. De Clerck, "The influence of tetraethoxysilane sol preparation on the electrospinning of silica nanofibers, " *3rd International Conference on Electrospinning*, San Francisco (USA), 4-7 August 2014

*** J. Geltmeyer**, K. De Buysser, and K. De Clerck, "Stable electrospinning of silica nanofibres: influence of viscosity", *17th International Sol-Gel Conference*, Madrid (Spain), 25-30 August 2013

*** J. Geltmeyer**, L. Van der Schueren, K. De Buysser, and K. De Clerck, "Stable electrospinning of silica nanofibres: influence of viscosity, " *1st International Conference in Polymers with Special Focus in Early Stage Researchers*, Barcelona (Spain), 3-7 November 2013.

K. De Clerck, **J. Geltmeyer**, I. Steyaert, and L. Van der Schueren, "Halochromic textile materials as innovative pH-sensors, " *23th IFATCC International Congress*, Budapest (Hungary), 8-10 May 2013

*** J. Geltmeyer**, L. Van der Schueren, K. De Buysser, and K. De Clerck, "Stable electrospinning of silica nanofibres: viscosity study," *13th World Textile Conference AUTEX*, Dresden (Germany), 22-24 May 2013

J. Geltmeyer, M. Frances, V.C.E. Mordacque, S. Almuhamed, N. Khenoussi, M. Bonne, B. Lebeau, L. Schacher, J. Brendlé, G. Chaplais, and D.C. Adolphe, "Electrospuns including clay and ordered mesoporous silica materials," *12th World Textile Conference AUTEX*, Zadar (Croatia), 13-15 June 2012.

List of symbols and abbreviations

A

A	Absorbance
AA	Acetic acid
APTES	(3-aminopropyl)triethoxysilane
APTES-MR	Methyl Red functionalized APTES
ATR	Attenuated total reflectance FTIR

B

C

c	Concentration
CTES	Chlorotriethoxysilane
CTES-DR1	Disperse Red 1 functionalized CTES
C-DR	Disperse Red 1 functionalized CTES

D

DC	Dip-coated or dip-coating
DCC	*N,N'*-dicyclohexylcarbodiimide
DCM	Dichloromethane
DIC	*N,N'*-diisopropylcarbodiimide
DMA	Dimethylamine
DR1	C.I. Disperse Red 1
DLS	Dynamic Light Scattering

E

EDC	1-ethyl-3-(3-dimethylaminopropyl)carbodiimide
EtOAc	Ethyl acetate

F

FA	Formic acid
FR	Flow rate
FTIR	Fourier transform infrared

G

H

H	Hydrophilic

I

ICP-OES	Inductively coupled plasma optical emission spectroscopy
IL	Inline
IP	Isoproturon
IR	Infrared

J

K

K-M	Kubelka-Munk

L

LC-MS	Liquid chromatography – mass spectrometry

M

MB	Methylene Blue
MY	Methyl Yellow
MR	Methyl Red

N

NHS	*N*-hydroxysuccinimide
NMR	Nuclear magnetic resonance
n-hex	*N*-hexaan

O

P

PA	Polyamide
PEO	Polyethylene oxide
PFP	Pentafluorophenol
PVA	Polyvinyl alcohol
PVP	Polyvinyl pyrrolidone

Q

R

R	Reflectance
RH	Relative humidity
RPM	Revolutions per minute

S

SEM	Scanning electron microscopy

T

TEOS	Tetraethoxysilane
T	Transmittance
TA/MR	TEOS-APTES nanofibers functionalized with MR via doping
TA-MR	TEOS-APTES nanofibers inline covalently functionalized MR
TCD	Tip-to-collector distance
TC/DR	TEOS-CTES nanofibers functionalized with DR1 via doping
TC-DR	TEOS-CTES nanofibers inline covalently functionalized DR1
TGA	Thermogravimetric analysis
THF	Tetrahydrofuran
TLC	Thin-layer chromatography
TMA	Trimethylamine
T/DR	TEOS sols inline functionalized with DR1
T/MR	TEOS sols inline functionalized with MR

U

UV-Vis	Ultraviolet-visible

V

W

wt%	Weight percent

X

XRD	X-ray diffraction

Y

Z

1

Introduction

Ceramic materials are typically known for their excellent thermal properties and chemical resistance. Nanofibrous membranes have highly unique properties, such as a high porosity, a high surface to volume ratio and small pore sizes. Combining all of these excellent properties makes ceramic nanofibers highly suitable for various applications such as catalysis, electrodes for energy conversion, sensors, filtration, separation, etc. This first chapter provides an introduction to the different subjects essential to understand the production and use of silica nanofibers. An introduction is given on the sol-gel process, the electrospinning technique and different applications aimed for in this PhD. The chapter ends with the objectives and outline of this PhD.

1.1 Silica nanofibers via sol-gel technology

Traditional ceramics, based on clay, have been used for over 25 000 years. Specific properties associated with ceramic materials are brittleness, compressive strength and stability in both harsh chemical and thermal environments. Advanced ceramics have been developed within the last 100 years, having typically superior mechanical properties, corrosion/oxidation resistance, electrical, optical and/or magnetic properties. The sol-gel process is a low temperature method used to produce ceramics with a high purity and homogeneity. It is used commercially in many applications, such as forming coatings on window glass, textiles and wood; production of powders, films and fibers. At the start pure materials are used, which results in an excellent control of product purity and composition. [1]–[3]

The interest in nanotechnology has significantly increased in the last years, because of the enhanced properties compared to the large-scale counterparts. Since it is difficult to imagine how small a nanometer is, the relative comparison can be made between a marble and the earth. If a marble would have a diameter of 1 nm, than the diameter of the earth would be 1 m. Nanofibers have per definition a diameter smaller than 500 nm, but even diameters of a few nanometers have been reported. Their length, on the contrary, is macroscale making these nanofibrous membranes easily manageable. Figure 1.1 shows a human hair on top of a nanofibrous membrane. These nanofibrous membranes have very unique properties due to their small fiber diameters. They have a very large specific surface area, up to 100 m^2/g and even more [4], a very high porosity (90%) [5],[6] and small pore sizes ranging in between 50 to 500 nm [7].

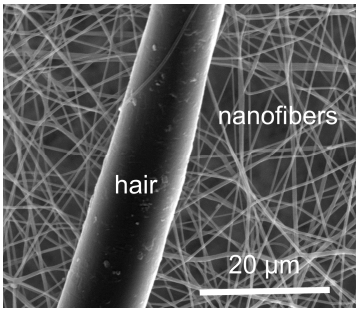

Figure 1.1 A human hair on top of a polymer nanofibrous membrane

The electrospinning process is the only scalable, repeatable process that offers the production of long, continuous nanofibers with control over fiber dimensions [8]. The electrospinning of polymers has been extensively studied the last 10-15 years [9]. The interest in electrospinning of ceramics, using sol-gel technology, is much more recent but is also increasing fast [10]. Typically, ceramic nanofibers are produced using a solution that combines the sol-gel precursors with an organic polymer. The organic polymer is added to ensure good electrospinnabilty and is removed afterwards via a high temperature treatment [10]. This temperature treatment can be deleterious not only to the nanofibrous membrane, but also to the added organic functionalities. Moreover, the use and subsequent polymer removal is an economic and ecological inconvenience. The use of electrospinning solutions consisting of solely sol-gel precursors can thus be highly valuable. The electrospinning of these sols is, however, a big challenge due to hydrolysis and condensation reactions taking place in the sol solution [11]. An in-depth study on the electrospinning of pure sols (without organic polymer) is missing, but is vital for optimizing the electrospinning process and thus ensuring reproducibility and scalability.

The combination of the unique characteristics of nanofibers with the versatility of the sol-process offers the opportunity to produce ceramic nanofibrous membranes usable in various application domains, such as catalysis, sensors, filtration, energy technology, etc. In addition, the sol-gel process as well as the electrospinning process allow for easy functionalization, broadening the application domains for which these membranes can be used and thus enabling the production of highly advanced nanofibrous materials. In this PhD focus is given to two application domains, which can benefit from the adjusted preparation procedure and the advanced properties (chemical and thermal resistance) of silica nanofibers, namely water treatment and colorimetric sensors. In the next sections, the sol-gel process and the electrospinning process will be discussed separately. This is followed by a detailed discussion on the application of the membranes for water treatment and colorimetric sensors.

1.2 The sol-gel process

The sol-gel process is a well-known process in materials science and is typically used to produce various inorganic or even inorganic/organic composite materials such as dense films, dense ceramics, fibers, particles, aerogels, etc. A schematic overview is given in Figure 1.2.

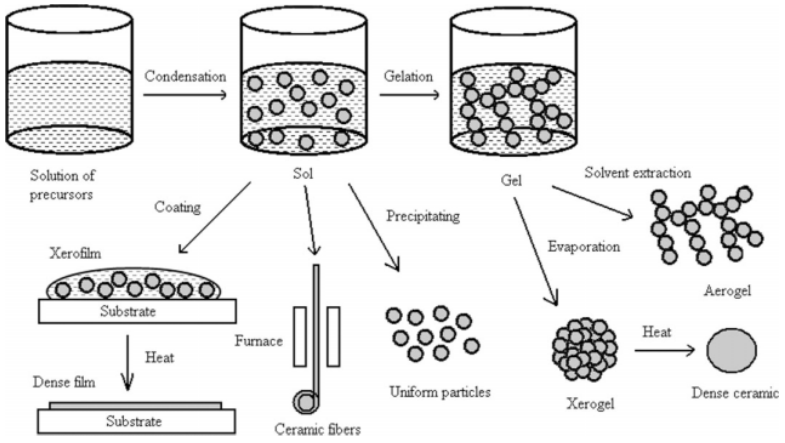

Figure 1.2 Schematic overview of the sol-gel process [12]

1.2.1 Principle

The sol-gel process involves the generation of colloidal suspensions (sols) which are subsequently converted to viscous gels and then to solid materials [12]. The precursors used to prepare these colloidal suspensions consist of a metal or metalloid element surrounded by ligands. The most widely used precursors are metal alkoxides, which have an organic ligand attached to a metal or metalloid atom. The most commonly used and most thoroughly studied metal alkoxide is tetraethyl orthosilicate (TEOS), thus also in this PhD project focus is given to TEOS as sol-gel precursor for the novel production of silica nanofibers (Figure 1.3).

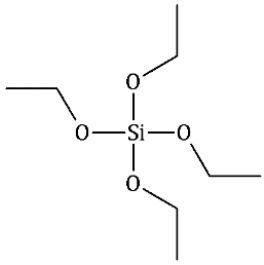

Figure 1.3 Sol-gel precursor: tetraethyl orthosilicate (TEOS)

The sol-gel process is generally described by three reactions, visualized in Figure 1.4. Metal alkoxides are preferably used since they react easily with water (hydrolysis), resulting in a hydroxyl ion becoming attached to the metal atom (Figure 1.4 (1)). It will depend on the amount of water or added catalyst (e.g. a mineral acid HCl or a base NH_3) whether the hydrolysis reaction will go to completion. These (partially) hydrolyzed species will then further link together via condensation reactions producing siloxane bonds (Si-O-Si), releasing water or an alcohol (Figure 1.4 (2)). [3],[13] An alcohol is typically used as a homogenizing agent, since water and alkoxysilanes are immiscible. However, alcohol released during the hydrolysis reactions can be sufficient to homogenize the initially phase separated system, making the addition of an alcohol not a prerequisite [14].

Iler [13] states that the polymerization occurs in three stages (Figure 1.5). First, monomer polymerizes to form particles. Nuclear Magnetic Resonance (NMR) measurements have shown that condensation reactions take place to maximize the number of Si-O-Si bonds and minimize the number of terminal hydroxyl groups via internal condensation [3]. As a result cyclic structures are formed, to which monomers add, resulting in three dimensional particles. Next, these particles can grow to varying sizes depending on the type of catalyst, H_2O:Si molar ratio, pH, etc. Finally, these particles will link to chains and then extending networks resulting in the formation of a gel [3]. In basic solutions, the growth of the particles will continue to much larger sizes.

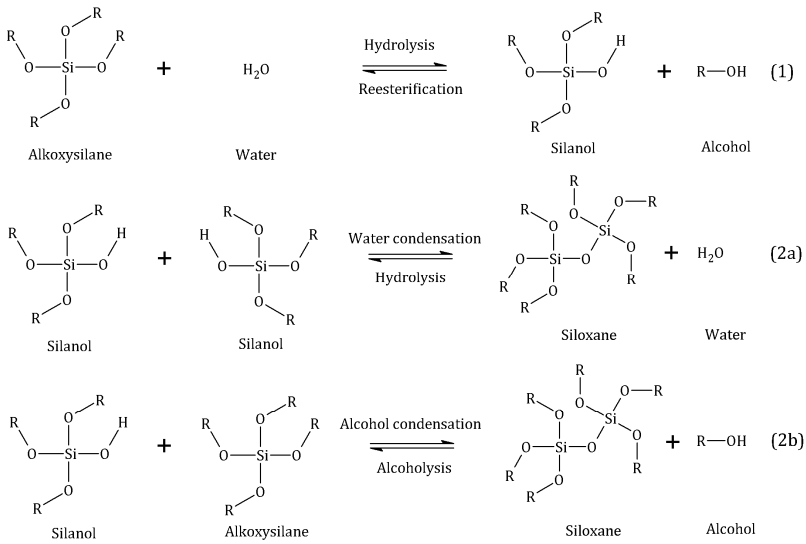

Figure 1.4 Hydrolysis and condensation reactions in the sol-gel process [3]

Depending on the intended end product, such as fibers, films, powders, gels, etc.; varying parameters of the initial solution should be optimized. The type of solvent, H_2O:Si molar ratio *r,* concentration and type of catalyst, pH, temperature, time, aging conditions and drying conditions are all factors which influence the hydrolysis and condensation reactions making it possible to vary the structure and properties of the sol-gel derived materials over a wide range [15]. The H_2O:Si molar ratio *r* and the amount and choice of the catalyst are two essential factors determining the processing possibilities and end characteristics. In acid catalyzed solutions with low *r* values (1 or 2) "polymeric[1]" sols are formed that give viscous, spinnable sols that can be drawn into fibers [16]–[18]. On the contrary, base catalyzed solutions with large *r* values result in highly condensed "particulate" sols, giving the possibility to produce SiO_2 powders [3],[19].

[1] The term polymer is used in sol-gel science to describe an inorganic silicon oxide macromolecule.

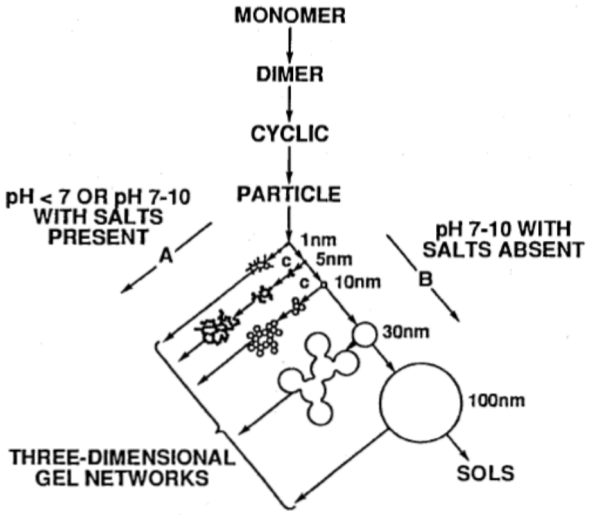

Figure 1.5 Iler's [13] view on the polymerization behavior of aqueous silica. In acid solutions or basic solutions with flocculating salts present, monomers will polymerize into particles, which will then aggregate into three-dimensional gel networks (A). In basic solutions the particles will grow to larger sizes with a decrease in number (B). [3]

1.2.2 Modification of sols

Sols can easily be modified by incorporating particular compounds resulting in new or additional functional properties [2]. Two types of modification can be defined, namely physical and chemical modification.

Physical modification of the sols can be carried out before or after the hydrolysis step. Additives are homogenously incorporated and immobilized in the inorganic network without the formation of covalent bonds. Usually larger molecules are added, such as organic polymers, pigments, biomolecules, etc.

Chemical modification of sols implies the formation of a covalent link between the additive and the inorganic network. Various possibilities exist for a chemical modification. The co-condensation of different types of alkoxides, such as TEOS with other metal alkoxides ($Me(OR)_n$), results in the formation of metal alkoxides with varying ratios of metals. The co-hydrolysis and co-condensation of other types of trialkoxysilanes R'-$Si(OR)_3$ is another approach (Figure 1.6), which may result in various

additional properties for the end applications. It should be noted that the incorporation of these modified precursors can have a significant influence on the reaction kinetics of the hydrolysis and condensation reactions in the sol-gel process [20].

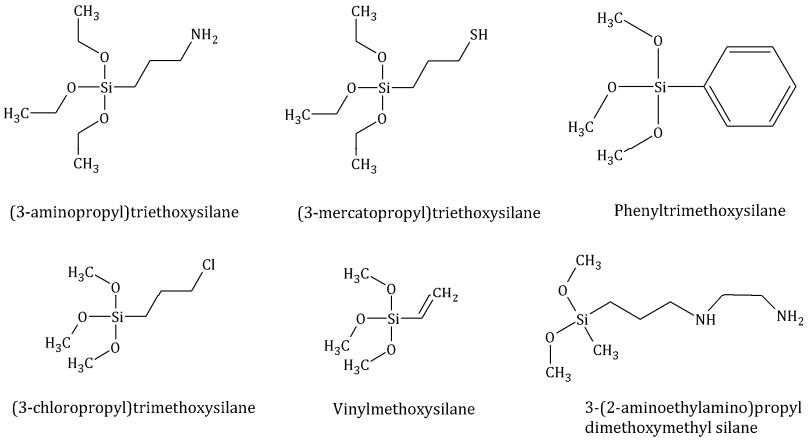

Figure 1.6 Alkoxysilane precurors with varying functional rest R'

1.3 Electrospinning of nanofibers

In the last years nanofibrous structures have gained a lot of scientific, technological and industrial interest. These nanofibrous structures have various application possibilities in multiple fields such as tissue engineering, drug delivery, water and air purification, sensors, photonics, electronics, etc. [21]–[27]. Various techniques can be used to obtain nanofibers, namely self-assembly [28]–[31], drawing [32], template synthesis [33], phase separation [34], melt blowing [35] and electrospinning [8],[36],[37]. The electrospinning process is the only technique that is simple, reproducible, versatile and allows the production of continuous nanofibers on a large scale. Therefore, it offers the potential for industrial upscaling. Moreover, the electrospinning process allows the production of nanofibers from numerous materials including organic polymers, composites, metals and ceramics [36].

1.3.1 The principle of the electrospinning process

In the electrospinning process an electric field is applied between the tip of a nozzle, through which the solution is flowing, and a collector plate. As the high voltage is applied, the pendant drop of the solution will become highly electrified. Under the influence of the electrostatic interactions the solution at the tip of the nozzle deforms from a pendant drop to a conical shape, the Taylor cone. When the electrostatic forces overcome the surface tension of the solution, a liquid jet is ejected. Upon its way to the collector plate, the jet undergoes a stretching and whipping (spiraling) process, resulting in the formation of a long and thin thread. The main forces influencing the jet are the electric force, the Coulomb force, the viscoelastic force and the surface tension. The jet is continuously elongated and the solvent is evaporated. As a consequence, the jets diameter is reduced from hundreds of micrometers to as small as hundreds or even tens of nanometers. Finally, the fiber is deposited as a randomly oriented, non-woven nanofibrous membrane. [36],[37] A schematic illustration of a basic electrospinning set-up is given in Figure 1.7.

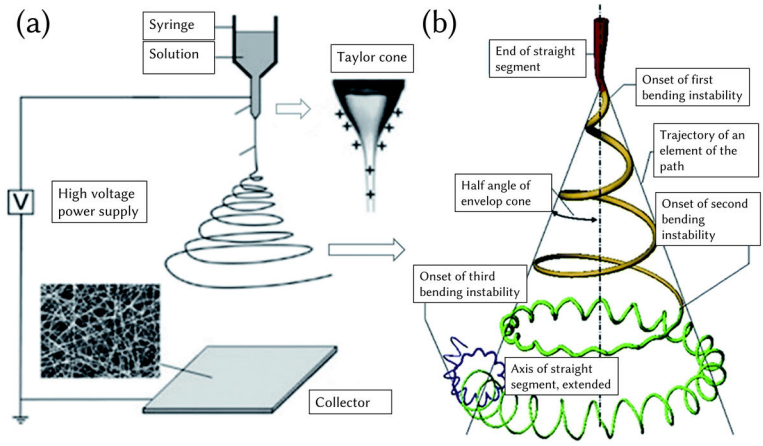

Figure 1.7 Schematic illustration of a basic electrospinning set-up (a) the inset shows a drawing of an electrified Taylor cone. The trajectory of the jet as controlled by the bending instabilities (b) [38]

The basic set-up for electrospinning is very simple and can easily be modified to tailor the structures of the resultant nanofibers [37]. In addition

to a single needle, also parallel needles or coaxial needles can be used in order to electrospin two different solutions simultaneously. Moreover, various collectors can be used, influencing mainly the size of the nanofibrous membrane and the fiber orientation. A conveyor belt makes it possible to collect the fibers as uniform mats [39]. High speed rotating drums allow alignment of the nanofibers (large scale) [39],[40], together with collectors based on a pair of split electrodes (smaller scale) [41],[42]. More complex application-dependent fiber depositions are possible using specialized collector architectures [43]. Finally, the configuration of the set-up can be horizontal (sidewards) or vertical (up or downwards).

Although the electrospinning process is based on a simple principle, the spinning mechanism is rather complicated and various parameters have their influence, including solution parameters, process parameters and ambient parameters. All of these parameters should be optimized to obtain nanofibers with a desired morphology in a stable, reproducible and scalable way.

Below an introduction is given on the electrospinning of ceramic nanofibers, followed by a more in-depth discussion on the various parameters influencing electrospinning of both organic polymers and inorganic sols.

1.3.2 Electrospinning of ceramic nanofibers using sol-gel technology

The typical procedure used to prepare ceramic nanofibers is visualized in Figure 1.8. It consist of following steps: (1) preparation of an inorganic sol or solution containing a sol-gel precursor and an organic polymer, (2) electrospinning of this solution under the appropriate conditions and (3) calcination, sintering, or chemical conversion of the precursor in the desired ceramic at high temperatures, with removal of all the organic components of the precursor fibers. [10],[11]

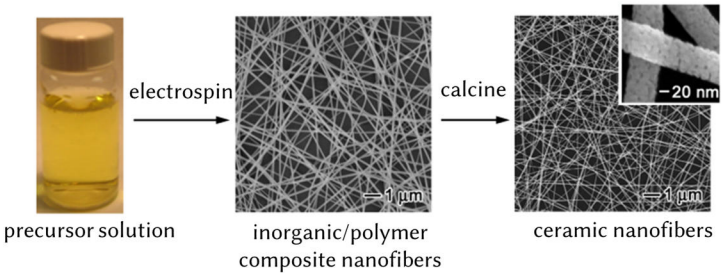

Figure 1.8 Schematic presentation of a typical procedure for preparation of ceramic nanofibers [11].

An essential prerequisite for successful electrospinning of ceramic nanofibers is the preparation of a precursor solution with appropriate rheological conditions. Most of the time, organic polymers such as poly(vinyl pyrrolidone) (PVP), poly(vinyl alcohol) (PVA) or poly(ethylene oxide) (PEO) are added to the precursor solution to adjust the rheological properties of the solution. These solutions are easily prepared by co-dissolving the precursor and polymer in alcohol. Using this strategy multiple oxide-based nanofibers including, for example, TiO_2 [44], CuO [45], Co_3O_4 [46], V_2O_5 [47], $MgTiO_3$ [48], SiO_2 [49], have been prepared for various applications. This strategy is always followed by a heat treatment step, removing all of the organic components. However, removing the polymer may result in poor mechanical properties and eventually loss of the material's coherence [50]. The ceramic nanofibrous membranes become fragile upon heat treatment and have the tendency to break into small pieces [10].

An alternative method, is the electrospinning of inorganic sols without organic polymer addition. Inorganic sols with controllable viscosities prepared by hydrolysis and condensation of the properly chosen metal alkoxides precursors can be electrospun directly [51],[52], but is not well understood yet. As a consequence, depending on the envisaged end application the heat treatment can become redundant. Hereby, preventing not only the deleterious effect on the nanofibrous structure, but it is also an ecological and economic benefit. Additionally, for future application a heat treatment might destroy added organic functionalities and should thus be avoided. Therefore, direct electrospun fibers without addition of organic polymers is the preferred strategy which will be followed and

studied in this PhD. The influence of a heat treatment on these new nanofibers and their morphology will be studied in Chapter 3.

1.3.3 Parameters of the electrospinning process

The principle for the electrospinning of inorganic sols and organic polymers is basically the same. As mentioned in section 1.3.1, various parameters have their influence on the electrospinning process. Therefore, a more in-depth discussion will be carried out on the most important solution, process and ambient parameters influencing the electrospinning process of organic polymers as well as inorganic sols.

1.3.3.1 Solution parameters

Conductivity

To initiate electrospinning the solution must carry sufficient charges so that the repulsive forces overcome the surface tension of the solution [53]. Subsequent stretching of the solution will also depend on the ability of the solution to carry charges. A low conductivity will lead to insufficient stretching and the formation of beads [9]. An increase in conductivity will lead to increased stretching of the solution and results in nanofibers with smaller diameters [54].

Surface tension

The surface tension of the solution has to be overcome to initiate electrospinning. As the jet travels towards the collector, a high surface tension may result in the formation of beads, being more pronounced for low viscosity solutions [53]. The formation of smooth fibers can be enhanced by using solvents with a low surface tension, or by addition of surfactants.

Viscosity

The molecular weight and concentration of an organic polymer will influence the chain entanglements in the solution, and both will thus effect the viscosity. From polymer solutions, continuous uniform nanofibers can thus be electrospun at polymer concentrations allowing sufficient chain entanglements [55]. Organic polymers are thus typically added to precursor solutions of ceramic nanofibers to easily control the rheology

of the solution. When no organic polymer is added the viscosity of the solution will be influenced by the hydrolysis and condensation reactions taking place during sol preparation, and thus the resulting degree of crosslinking. The degree of crosslinking is in turn influenced by several factors such as the temperature, heating time, amount of water and acid, etc.

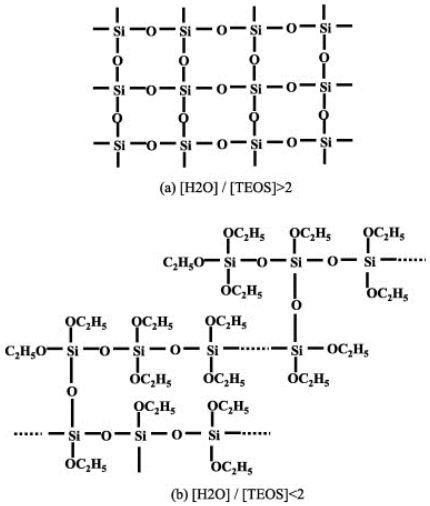

Figure 1.9 Schematic presentation of the silicon oxide network formed with a H_20/TEOS molar ratio exceeding 2 (a) or a H_2O/TEOS molar ratio smaller than 2 (b) [56].

Xu *et al* [57] and Iimura *et al* [56] studied the spinnability of sols, which showed to be determined by the linearity of the structure. As mentioned before, acid catalyzed sols with low *r* ratios are necessary to obtain viscous, spinnable sols, which are defined as "polymeric" sols. They stated that the water to TEOS ratio should be 2 or less to obtain a "linear" spinnable structure (Figure 1.9 b). When the molar ratio of water to TEOS is larger than two, more than three ethoxy groups will be replaced by hydroxyl groups, resulting in a mutually grown network which is not spinnable (Figure 1.9 a). Hydrochloric acid has a catalytic effect on both the hydrolysis as the condensation reaction, a moderate amount of hydrochloric acid is necessary to obtain an appropriate reaction rate.

1.3.3.2 Process parameters

Flow rate

The flow rate is the rate at which the solution is pumped through the needle to replenish the Taylor cone. If the flow rate corresponds to the rate at which the solution is drawn away from the tip, continuous nanofibers with uniform diameters are obtained. For a given voltage, a corresponding flow rate can thus be found resulting in a stable Taylor cone. If the flow rate is increased, larger fiber diameters are noted and beads are often formed.

Tip-to-collector distance (TCD)

The distance between the tip of the needle and the collector plate defines the strength of the electric field as well as the time available for solvent evaporation. A TCD that is too small can lead to 'wet' fibers that fuse on the collector [58]. Since appropriate jet stretching is only obtained when sufficient electrostatic forces are applied to the jet, an increase in TCD will thus demand for higher voltages, or it may even result in drops [59].

Applied voltage

The applied voltage supplies the charges necessary for electrospinning. The voltage should be adjusted to obtain an appropriate field strength, needed to initiate and maintain the stability of the process. With the applied voltage, instability and stretching of the jet increases, resulting generally to smaller nanofiber diameters [55]. However, even increasing fiber diameters have been reported as well, therefore the influence of the applied voltage should always be considered together with other parameters, particularly the flow rate and TCD [55].

1.3.3.3 Ambient parameters

The final group of parameters are the ambient parameters containing the relative humidity, temperature, solvent build up, atmosphere and pressure. Despite that it is known that these ambient parameters can have a substantial effect on the electrospinning process and resulting nanofiber morphology [36],[53], they are still poorly investigated. These parameters will mainly influence the solution parameters and solvent evaporation rate. For example, the relative humidity will influence solvent evaporation for water containing systems, which may influence the resulting fiber

morphology, leading to (controlled) formation of pores on the fiber surface [60]. Moreover, water can act as a plasticizer for several polymer systems and can thus affect the nanofiber diameters [61]. Additionally, temperature will influence the solution viscosity, solvent evaporation, etc.

1.4 Active and sensitive membranes via functionalization of silica nanofibers

The sol-gel process as well as the electrospinning process allow for easy functionalization. Low molar mass components or nanoparticles can be directly added to the electrospinning solution prior to nanofiber formation, i.e. doping or inline functionalization. The sol-gel process allows the use of various sol-gel precursors with varying functional rest. Proper selection of this functional rest allows for a covalent linkage with a specific compound and thus immobilization of this compound in the nanofibrous matrix. The combination of sol-gel and electrospinning thus allows for the production of highly tailored nanofibrous membranes for various end applications. In this PhD, focus is given to both active and sensitive membranes, membranes for water treatment and sensor applications, respectively.

1.4.1 Active membranes: silica nanofibers for water treatment

1.4.1.1 Nanofibrous membranes for water treatment

Nanofibrous membranes have a very high specific surface to volume ratio compared to other non-woven membranes. Moreover, they have a very high porosity (up to 90%) and small pore sizes. The open pore structure and low density of these membranes renders them ideal to be used for a wide range of filtration applications [21],[62],[63]. Figure 1.10 represents the increased filter efficiency for a nanofibrous membrane (right) compared to conventional membranes. Due to the small fiber diameters and high porosity a higher amount of water can pass through the surface or interact with the nanofibrous surface. The filter efficiency, which is closely related to the fiber diameter, is one of the most important concerns for filter performance [63]. In addition, the ease of functionalization allows the

production of membranes with an even broader application domain for water treatment.

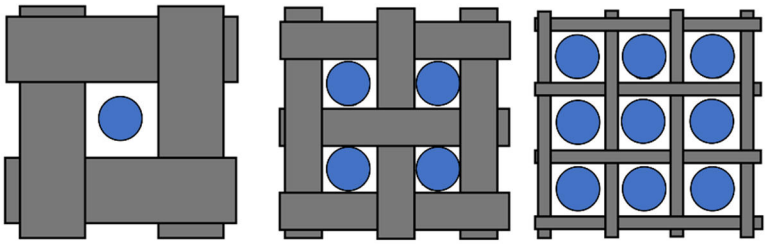

Figure 1.10 Filter efficiency increases with decreasing fiber diameter [63]

1.4.1.2 Functionalization of membranes with TiO_2

Titanium dioxide is a well-known photocatalyst that is widely used because of its great availability, low cost, non-toxicity, chemical and thermal stability [64]. One of the most interesting properties of titanium dioxide is its photocatalytic activity under UV irradiation [65],[66]. This results in many applications such as self-cleaning and anti-fogging surfaces, air purification and water purification [67]–[71]. Since many of the applications rely on surface related phenomena, a high specific surface area is desired as it enhances the performance of the photocatalyst. TiO_2 nanoparticles are thus known to have greater photocatalytic properties compared to their bulk counterpart [72].

The photocatalytic activity of TiO_2 is a result of the absorption of ultraviolet light with an energy corresponding to the band gap energy (usually 3.2 eV (anatase) or 3.0 eV (rutile)) [65],[66],[73]. This results in the generation of an electron-hole pair: a conduction band electron (e^-) and a valence band hole (h^+). The photo-generated holes react with water, resulting in the formation of hydroxyl radicals (•OH). These can promote the oxidation of organic pollutants at the TiO_2 surface. At the same time, the electrons of the conduction band will react with adsorbed molecular oxygen, resulting in the formation of superoxide radical anions ($O_2^{\bullet-}$), which will also contribute to the degradation of the contaminant. A schematic representation of the photocatalytic process is given in Figure 1.11.

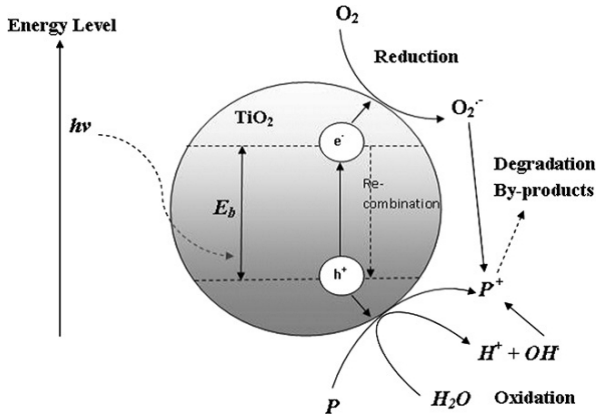

Figure 1.11 Schematic representation of the photo-induced formation of the electron-hole pair in a TiO_2 particle in the presence of a pollutant (P) [73]

Photocatalytic reactor configurations for water treatment can be classified into two types depending on the state of the photocatalyst: reactors with suspended photocatalyst particles (1) and reactors with immobilized photocatalyst particles (2) [73]. A major disadvantage of slurry type reactors (type 1) is the additional post-separation step of the photocatalyst. A growing interest is thus seen in immobilization of these TiO_2 nanoparticles onto an inert carrier. Immobilization of the catalyst has been carried out using mesoporous clays, fibers, nanofibers, nanowires or rods, or even by the production of photocatalytic titania membranes [74]–[81].

Immobilization of titanium dioxide nanoparticles on nanofibrous membranes combines the advantages of both. These nanofibrous membranes can be fabricated into microfiltration (MF), ultrafiltration (UF) or even photocatalytic membranes [73]. The added titanium dioxide results in an additional removal of organic contaminants and promotes anti-fouling. Daels *et al* investigated thoroughly the use of polyamide nanofibrous membranes for water filtration with and without TiO_2 functionalization [82]–[85]. The potential of TiO_2 functionalized nanofibrous membranes as high-flux anti-fouling membranes was shown by the oxidation of humic acids and the deactivation of bacteria [84],[85].

The simplest approach for functionalization with TiO_2 nanoparticles is the addition of a chosen amount to the solution prior to electrospinning, namely inline functionalization. An alternative method is post-

functionalization, where the membranes are functionalized with TiO_2 after production. Both functionalization methods have their advantages and disadvantages. Inline functionalization is an easy and straightforward, one-step functionalization method, resulting in TiO_2 nanoparticles which are distributed inside the nanofibers (Figure 1.12 right). Dip-coating, on the contrary, is a two-step process resulting in the presence of the nanoparticles on the surface of the nanofibers and making them more accessible to the pollutants (Figure 1.12 left). Three challenges are encountered during surface modification, being uniformity, coating without affecting the pore sizes and possibility for industrial upscaling [86]. Moreover, the accessibility of the TiO_2 nanoparticles by the UV light and thus consequently their photocatalytic activity may be influenced as well by the functionalization procedure.

Figure 1.12 Functionalization of nanofibers via inline functionalization (right) and post-functionalization (left).

1.4.2 Sensitive membranes: silica nanofibers for colorimetric sensors

1.4.2.1 Color and reversible chromic phenomena

The color of species is based on their ability to absorb electromagnetic radiation in the range of wavelengths between 380 and 780 nm (visible light). This energy is used to promote electrons to higher energy levels. The observed color will be complementary to the color of the absorbed wavelength. A dye is colored due to the presence of a linear or cyclic system of conjugated bonds (chromophore). In addition, most dyes also contain electron donors and/or acceptors (auxochromes), their presence will shift the color or may influence the dye solubility. A color is typically characterized by the wavelength at maximum absorbance (λ_{max}) and by the extinction coefficient (ε_{max}) at λ_{max}.

Halochromism

Halochromism refers to the reversible change of color of a material under pH-changes. Due to protonation or deprotonation of a dye the electron

configuration of the conjugated system may change, a different part of the electromagnetic spectrum will be absorbed, resulting in a change of λ_{max} and ε_{max},, and thus a color change. This color shift can be a visual color shift from one color to another, from colorless to colored [87], or it can even be a varying fluorescence as pH changes [88],[89]. In this PhD focus is given to dyes that result in a color change in the visual range. The main dye classes showing pH-sensitivity are phtalides, triarylmethanes, fluorans and azo dyes [87].

Azo dyes are, in general, the most important dye class accounting for over 50% of all commercial dyes [90]. Therefore, they have been studied extensively and they are known to undergo tautomerism. Halochromic azo dyes typically have amino groups in the 4-position. As a consequence, they can undergo protonation at either the terminal nitrogen atom (ammonium tautomer) or at the β-nitrogen of the azo group resulting in a resonance stabilized azonium tautomer [90] (Figure 1.13). Which tautomer is stabilized depends on the electron withdrawing or donating nature of the R_1 group [87]. The tautomeric forms each have their own λ_{max} and ε_{max}, different from the neutral dye, making pH-sensing possible.

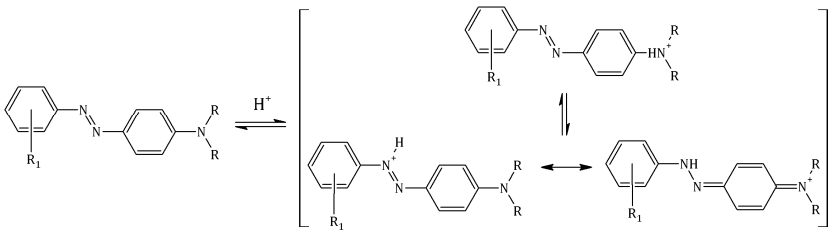

Figure 1.13 Azo dyes with an amino group in the 4-position can undergo protonation resulting in an ammonium tautomer or a resonance stabilized azonium tautomer.

In this PhD work, Methyl Yellow (MY), Methyl Red (MR) and C.I. Disperse Red 1 (DR1) azo dyes were selected for functionalization of the sols (Figure 1.14). In paragraph 1.4.2.3 the importance of covalent immobilization of dyes to prevent dye leaching will be discussed. In this work, Methyl Red and C.I. Disperse Red 1 were selected for their carboxyl group and hydroxyl group, respectively. The carboxylgroup of MR allows for covalent bonding to the amino group of the sol-gel precursor (3-aminopropyl)triethoxysilane (APTES), similarly the terminal hydroxylgroup of DR1 allows for covalent linking with the sol-gel

precursor chlorotriethoxysilane (CTES). On the other hand the absence of a functional group on Methyl Yellow does not allow covalent linking to the silicon oxide nanofibers. Moreover, DR1 was not only selected for its halochromic behavior, but also for its solvatochromic properties.

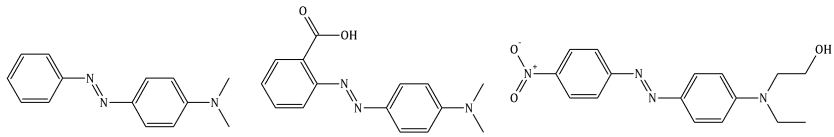

Figure 1.14 Methyl Yellow (left), Methyl Red (center) and C.I. Disperse Red 1 (right).

Solvatochromism

Solvatochromism refers to the reversible color change when a compound is immersed in different solvents. As explained, absorption of visible light causes electronic transitions. In solvatochromism, color shifts are observed due to differences in solvation energies of the ground state and the excited state, when the polarity of the solvent is changed [87]. When the excited state is more polar than the ground state, the excited state will be stabilized by more polar solvents, the transition energy will decrease and a bathochromic shift (to longer wavelength, positive solvatochromism) in the spectrum will be seen. Vice versa, when the ground state is more polar, the opposite will be seen, giving a hypsochromic shift (to shorter wavelength, negative solvatochromism).

DR1 belongs to the group of push-pull azobenzenes, containing an electron-donating group in one benzene ring and an electron-withdrawing group in the other benzene ring [91]. These push-pull azobenzenes have a permanent dipole moment, which becomes even larger after excitation of the molecule to the ππ* excited state. The permanent dipole moment of the ground state together with the charge transfer character of the transition, will result in positive solvatochromism [91].

1.4.2.2 Sol-gel technology for optical sensor applications

Sensor materials that result in a change in optical properties, which are detectable with the naked eye (visual) or inexpensive equipment such as a portable spectrophotometer (optical), can be used for the detection of various parameters (pH, temperature) or compounds (gases, solvents,

ionic species). Due to its simplicity and versatility, the sol-gel process has been used for the development of optical sensors. Typically, optical bulk glass or thin films are used for these sensor applications. A component sensitive to the analyzed parameter or compound should be added to the sensor material, being typically analyte-sensitive dyes. Most of the reported sol-gel based optical sensors are related to pH-measurements [92]–[98]. In medicine, environmental sciences, safety, agriculture and food science, pH-measurements are of significant importance [99]. Optical sensors for the detection of gases have also been considered to be very attractive and the developments of optical gas sensors using sol-gel thin films is becoming increasingly more important [92],[100]–[102]. In addition, optical sensors that enable the continuous monitoring of solvents, with applications in chemical, food industries and environmental control have gained significant interest as well [103]–[106].

The combination of sol-gel technology and textiles has shown to be promising for the production of halochromic textiles. Moreover, the combination of sol-gel and textiles would be highly promising for the detection of gases and solvents as well. Van der Schueren *et al* applied a dye functionalized sol-gel coating on conventional polyamide 6 and cotton fibers [107]. This resulted in large area, flexible halochromic sensor materials. Combining sol-gel and textiles can thus result in sensor materials with highly promising characteristics, such as lightweight, flexibility, reusability, breathability and mechanical stability. Moreover, a local easy-to-interpret signal can be obtained while monitoring a large area. However, the sensitivity of these membranes should be improved and this can be carried out by diminishing their fiber diameters. Due to their small pore sizes, high porosity and large surface area, nanofibrous membranes will result in an improved sensor sensitivity and response time, highly desired for sensor applications.

1.4.2.3 Colorimetric nanofibrous sensors

pH-sensitive organic polymer nanofibers have been successfully produced [108]–[112]. Immobilization of the dyes in the nanofibers is essential to obtain a reusable sensor material. Different strategies can be followed for dye immobilization. Doping or inline functionalization is the most frequently used strategy for nanofiber functionalization. This is an easy, flexible and fast way to incorporate the dye in the nanofibers [108],[111],[113],[114]. A major disadvantage of dye doping is however dye

leaching, which will not only affect the long term sensitivity and stability of the nanofibrous membranes, but also the toxicity of the leached dye is a major concern. Polymeric complexing agents have been added to the electrospinning solution to reduce the dye mobility [108],[112], but this strategy cannot be used with every dye class. Covalent immobilization of the dye in the matrix is the preferred functionalization method, since a covalent link between dye and matrix is the most efficient manner to inhibit dye migration [115]–[118] (Figure 1.15). Also for pH optical sensors based on sol-gel the importance of the covalent link has been demonstrated [93]. A disadvantage of organic polymer nanofibers is their low temperature resistance and their low resistance to strong acidic and/or basic environments making them less suitable in colorimetric sensor applications under harsh conditions. The use of ceramic nanofibrous membranes would be highly valuable for these harsh environments. A major challenge in obtaining these nanofibers is combining the knowledge on dye immobilization with the electrospinning process of sols, without compromising the processing of the electrospinning itself nor the resulting nanofiber morphology nor the dye sensing performance.

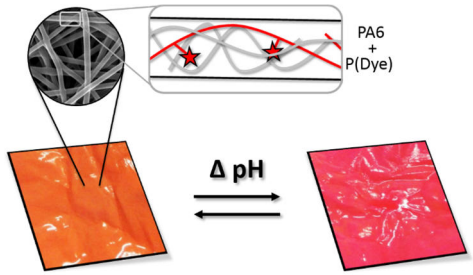

Figure 1.15 Covalent bonding of a pH-sensitive dye to an organic polymer backbone, and subsequent blend electrospinning, creates usable nanofibers for sensor materials [118]

1.5 Objectives and outline

It is described in this first chapter that the combination of sol-gel technology and electrospinning offers the potential to produce ceramic nanofibers with excellent properties for various applications. Typically organic polymers are added to the precursor solutions to enable electrospinning of sols, which results in the subsequent removal of the

polymer by a heat treatment to obtain pure ceramic membranes. To fully exploit the potential of the produced membranes, it is preferred to electrospin these membranes without added polymer. The electrospinning of these pure sols is not as straightforward, which makes an in-depth characterization of these sols an essential prerequisite and a first major objective of this PhD. Additionally, the combination of the sol-gel process and the electrospinning process allow for easy functionalization, a second objective of this PhD. Two application domains are aimed at: water treatment and colorimetric sensors.

Nanofibrous membranes are highly valuable for filtration applications due to their unique properties. The high chemical resistance of silica nanofibers allows their use in harsh environments where organic polymers are no longer usable. Addition of titanium dioxide gives the possibility to even further enhance their properties making the degradation of organic compounds present in effluents possible. Silica nanofibrous membranes will be functionalized with titanium dioxide nanoparticles with the production of membranes for micro pollutant removal as goal.

Colorimetric sensors for monitoring or visual reporting of acidic environments both in water and air, or for the detection of solvents; are highly valuable in various fields, such as safety, defense and technical textiles. A fast, clearly visual signal upon exposure to toxic substances can be lifesaving. Until now, the majority of these sol-gel sensors are optical bulk glass or thin films. The combination of sol-gel and nanofibers makes it possible to obtain a large area, flexible, reusable sensor. Color changing dyes will be incorporated in the silica nanofibrous membranes aiming for applications such as personal protective equipment and clothes.

To reach the set objectives in this PhD, the development and upscaling of the electrospinning process of silica nanofibrous membranes without the use of an organic polymer is tackled first. The viscosity of a solution is known to be a highly important parameter influencing the electrospinning process. Therefore, a first study of the TEOS sols is carried out in Chapter 3 by studying the optimum viscosity necessary for stable electrospinning. In addition, the high temperature resistance and the hydrophilic properties of these membranes are examined. Next, a more in-depth characterization of multiple sol parameters is carried out using various characterization techniques being ^{29}Si NMR, ^{1}H NMR, ATR-FTIR and DLS

in Chapter 4. The reproducibility of the preparation procedure of these silica nanofibrous membranes and their successful up-scaling is reported.

To account for the second key objective the potential of these nanofibrous membranes for water treatment and colorimetric sensor applications is demonstrated. Chapter 5 studies the comparison between polymeric nanofibrous membranes and silica nanofibrous membranes, both functionalized with TiO_2 via inline and post-functionalization. The production of these functionalized membranes is optimized and the degradation of the herbicide isoproturon by these photocatalytic membranes is studied. Chapter 6 and Chapter 7 focus on colorimetric sensors by functionalizing the silicon oxide sols with dyes. The dyes are added by both dye doping and covalent immobilization. The sensitivity of these membranes towards pH changes in water, HCl and NH_3 vapors, and biogenic amines is reported in Chapter 6. Solvatochromic sensors are aimed at in Chapter 7.

References

[1] C. Barry Carter and M. Grant Norton, *Ceramic materials: Science and Engineering*. New York: Springer Science + Business Media, 2007.

[2] B. Mahltig and T. Textor, *Nanosols and Textiles*. Singapore: World Scientific, 2008.

[3] C. J. Brinker and G. W. Scherer, *Sol-Gel Science: The Physics and Chemistry of Sol-Gel Processing*. 1990.

[4] S. De Vrieze, P. Westbroek, T. Van Camp, and L. Van Langenhove, "Electrospinning of chitosan nanofibrous structures: Feasibility study," *J. Mater. Sci.*, vol. 42, no. 19, pp. 8029–8034, 2007.

[5] H. Na, Y. Zhao, X. Liu, C. Zhao, and X. Yuan, "Structure and properties of electrospun poly(vinylidene fluoride)/polycarbonate membranes after hot press," *J. Appl. Polym. Sci.*, vol. 122, pp. 774–781, 2011.

[6] A. M. Bazargan, M. Keyanpour-rad, F. A. Hesari, and M. E. Ganji, "A study on the microfiltration behavior of self-supporting electrospun nanofibrous membrane in water using an optical particle counter," *Desalination*, vol. 265, no. 1–3, pp. 148–152, 2011.

[7] S. de Vrieze, B. De Schoenmaker, and K. De Clerck, "Morphologic study of steady state electrospun polyamide 6 nanofibres," *J. Appl. Polym. Sci.*, vol. 119, no. 7, pp. 2984–2990, 2011.

[8] S. Ramakrishna, K. Fujihara, W. E. Teo, T.-C. Lim, and Z. Ma, *An introduction to electrospinning and nanofibers*. 2005.

[9] A. Greiner and J. H. Wendorff, "Electrospinning: A fascinating method for the preparation of ultrathin fibers," *Angew. Chemie - Int. Ed.*, vol. 46, no. 30, pp. 5670–5703, 2007.

[10] Y. Dai, W. Liu, E. Formo, Y. Sun, and Y. Xia, "Ceramic nanofibers fabricated by electrospinning and their applications in catalysis, environmental science, and energy technology," *Polym. Adv. Technol.*, vol. 22, no. 3, pp. 326–338, 2011.

[11] D. Li, J. T. McCann, Y. Xia, and M. Marquez, "Electrospinning: A simple and versatile technique for producing ceramic nanofibers and nanotubes," *J. Am. Ceram. Soc.*, vol. 89, no. 6, pp. 1861–1869, 2006.

[12] J. D. Wright and N. A. J. M. Sommerdijk, *Sol-Gel Materials: Chemistry and Applications*. Boca Raton, Florida: CRC Press, 2001.

[13] R. K. Iler, *The chemistry of silica: solubility, polymerization, colloid and surface properties and biochemistry of silica.* New York: Wiley, 1979.

[14] D. Avnir and V. R. Kaufman, "Alcohol is an unnecessary additive in the silicon alkoxide sol-gel process," *J. Non. Cryst. Solids*, vol. 92, no. 1, pp. 180–182, 1987.

[15] N. K. Chaudhury, R. Gupta, and S. Gulia, "Sol-gel technology for sensor applications," *Def. Sci. J.*, vol. 57, no. 3, pp. 241–253, 2007.

[16] S. Sakka and H. Kozuka, "Rheology of sols and fiber drawing," *J. Non. Cryst. Solids*, vol. 100, pp. 142–153, 1988.

[17] S. Sakka and T. Yoko, "Fibers from gels," *J. Non Cryst. Solids*, vol. 148, pp. 394–403, 1992.

[18] H. Kozuka, H. Kuroki, and S. Sakka, "Flow characteristics and spinnability of sols prepared from silicon alkoxide solution," *J. Non. Cryst. Solids*, vol. 100, pp. 226–230, 1988.

[19] W. Stöber, A. Fink, and E. Bohn, "Controlled growth of monodisperse silica spheres in the micron size range," *J. Colloid Interface Sci.*, vol. 26, no. 1, pp. 62–69, 1968.

[20] B. Tan and S. E. Rankin, "Study of the effects of progressive changes in alkoxysilane structure on sol-gel reactivity," *J. Phys. Chem. B*, vol. 110, no. 45, pp. 22353–22364, 2006.

[21] R. Gopal, S. Kaur, Z. Ma, C. Chan, S. Ramakrishna, and T. Matsuura, "Electrospun nanofibrous filtration membrane," *J. Memb. Sci.*, vol. 281, no. 1–2, pp. 581–586, 2006.

[22] I. Steyaert, H. Rahier, and K. D. E. Clerck, "Nanofibre-based sensors for visual and optical monitoring," in *Electrospinning for High Performance Sensors*, A. Macagnano, E. Zampetti, and E. Kny, Eds. 2015, pp. 157–177.

[23] H. S. Koh, T. Yong, C. K. Chan, and S. Ramakrishna, "Enhancement of neurite outgrowth using nano-structured scaffolds coupled with laminin," *Biomaterials*, vol. 29, no. 26, pp. 3574–3582, 2008.

[24] D. Grafahrend, K.-H. Heffels, M. V Beer, P. Gasteier, M. Möller, G. Boehm, P. D. Dalton, and J. Groll, "Degradable polyester scaffolds with controlled surface chemistry combining minimal protein adsorption with specific bioactivation," *Nat. Mater.*, vol. 10, no. 1, pp. 67–73, 2010.

[25] T. Okuda, K. Tominaga, and S. Kidoaki, "Time-programmed dual release formulation by multilayered drug-loaded nanofiber meshes," *J. Control. Release*, vol. 143, no. 2, pp. 258–264, 2010.

[26] Y. Hong, X. Chen, X. Jing, H. Fan, B. Guo, Z. Gu, and X. Zhang, "Preparation, bioactivity, and drug release of hierarchical nanoporous bioactive glass ultrathin fibers," *Adv. Mater.*, vol. 22, no. 6, pp. 754–758, 2010.

[27] P. Gibson, H. Schreuder-Gibson, and D. Rivin, "Transport properties of

porous membranes based on electrospun nanofibers," *Colloids Surfaces A Physicochem. Eng. Asp.*, vol. 187–188, pp. 469–481, 2001.

[28] G. Liu, L. Qiao, and A. Guo, "Diblock Copolymer Nanofibers," *Macromolecules*, vol. 29, no. 16, pp. 5508–5510, 1996.

[29] X. Yan, G. Liu, F. Liu, and B. Tang, "Superparamagnetic triblock copolymer/Fe2O3 hybrid nanofibers," *Angew. Chem. Int. Ed. Engl.*, vol. 40, no. 19, pp. 3593–3596, 2001.

[30] K. De Moel, G. O. R. Alberda van Ekenstein, H. Nijland, E. Polushkin, G. Ten Brinke, R. Mäki-Ontto, and O. Ikkala, "Polymeric nanofibers prepared from self-organized supramolecules," *Chem. Mater.*, vol. 13, no. 12, pp. 4580–4583, 2001.

[31] J. D. Hartgerink, "Self-Assembly and Mineralization of Peptide-Amphiphile Nanofibers," *Science*, vol. 294, no. 5547, pp. 1684–1688, 2001.

[32] T. Ondarçuhu and C. Joachim, "Drawing a single nanofibre over hundreds of microns," *Europhys. Lett.*, vol. 42, no. 2, pp. 215–220, 1998.

[33] L. Feng, S. Li, H. Li, J. Zhai, Y. Song, L. Jiang, and D. Zhu, "Super-Hydrophobic Surface of Aligned Polyacrilonitrile Nanofibers," *Angew. Chem., Int. Ed.*, vol. 41, no. 7, pp. 1221–1223, 2002.

[34] P. X. Ma and R. Zhang, "Synthetic nano-scale fibrous extracellular matrix," *J. Biomed. Mater. Res.*, vol. 46, no. 1, pp. 60–72, 1999.

[35] C. J. Ellison, A. Phatak, D. W. Giles, C. W. Macosko, and F. S. Bates, "Melt blown nanofibers: Fiber diameter distributions and onset of fiber breakup," *Polymer*, vol. 48, no. 11, pp. 3306–3316, 2007.

[36] J. H. Wendorff, S. Agarwal, and A. Greiner, *Electrospinning: Materials, Processing and Applications*. 2012.

[37] D. Li and Y. Xia, "Electrospinning of nanofibers: Reinventing the wheel?," *Adv. Mater.*, vol. 16, no. 14, pp. 1151–1170, 2004.

[38] P. Ke, X.-N. Jiao, X.-H. Ge, W.-M. Xiao, and B. Yu, "From macro to micro: structural biomimetic materials by electrospinning," *RSC Adv.*, vol. 4, no. 75, pp. 39704–39724, 2014.

[39] J. Kim and D. H. Reneker, "Polybenzimidazole nanofiber produced by electrospinning," *Polym. Eng. Sci.*, vol. 39, no. 5, pp. 849–854, 1999.

[40] J. Kameoka and H. G. Craighead, "Fabrication of oriented polymeric nanofibers on planar surfaces by electrospinning," *Appl. Phys. Lett.*, vol. 83, no. 2, pp. 371–373, 2003.

[41] D. Li, Y. Wang, and Y. Xia, "Electrospinning of polymeric and ceramic nanofibers as uniaxially aligned arrays," *Nano Lett.*, vol. 3, no. 8, pp. 1167–

1171, 2003.

[42] D. Li, Y. Wang, Y. Xia, D. Li, Y. Wang, Y. Wang, Y. Xia, and Y. Xia, "Electrospinning Nanofibers as Uniaxially Aligned Arrays and Layer-by-Layer Stacked Films," *Adv. Mater.*, vol. 16, no. 4, pp. 361–366, 2004.

[43] D. Pisignano, *Polymer nanofibers: building blocks for nanotechnology*. Cambridge: RSC Publishing, 2013.

[44] D. Li and Y. Xia, "Fabrication of titania nanofibers by electrospinning," *Nano Lett.*, vol. 3, no. 4, pp. 555–560, 2003.

[45] H. Guan, C. Shao, B. Chen, J. Gong, and X. Yang, "A novel method for making CuO superfine fibres via an electrospinning technique," *Inorg. Chem. Commun.*, vol. 6, no. 11, pp. 1409–1411, 2003.

[46] H. Guan, C. Shao, S. Wen, B. Chen, J. Gong, and X. Yang, "A novel method for preparing Co3O4 nanofibers by using electrospun PVA/cobalt acetate composite fibers as precursor," *Mater. Chem. Phys.*, vol. 82, no. 3, pp. 1002–1006, 2003.

[47] P. Viswanathamurthi, N. Bhattarai, H. Y. Kim, and D. R. Lee, "Vanadium pentoxide nanofibers by electrospinning," *Scr. Mater.*, vol. 49, no. 6, pp. 577–581, 2003.

[48] N. Dharmaraj, H. C. Park, B. M. Lee, P. Viswanathamurthi, H. Y. Kim, and D. R. Lee, "Preparation and morphology of magnesium titanate nanofibres via electrospinning," *Inorg. Chem. Commun.*, vol. 7, no. 3, pp. 431–433, 2004.

[49] C. Shao, H. Y. Kim, J. Gong, B. Ding, D. R. Lee, and S. J. Park, "Fiber mats of poly(vinyl alcohol)/silica composite via electrospinning," *Mater. Lett.*, vol. 57, no. 9–10, pp. 1579–1584, 2003.

[50] S. W. Lee, Y. U. Kim, S. S. Choi, T. Y. Park, Y. L. Joo, and S. G. Lee, "Preparation of SiO2/TiO2 composite fibers by sol-gel reaction and electrospinning," *Mater. Lett.*, vol. 61, no. 3, pp. 889–893, 2007.

[51] S. Choi and S. G. O. O. Lee, "Silica nanofibers from electrospinning / sol-gel process," *J. Mater. Sci. Lett.*, vol. 22, pp. 891–893, 2003.

[52] S. Choi, "Titania-Doped Silica Fibers Prepared by Electrospinning and Sol-Gel Process," *J. Sol-Gel Sci. Technol.*, vol. 30, pp. 215–221, 2004.

[53] S. Ramakrishna, K. Fujihara, W. E. Teo, T. C. Lim, and Z. Ma, *An Introduction to Electrospinning And Nanofibers*. Singapore: World Scientific, 2005.

[54] X. Zong, K. Kim, D. Fang, S. Ran, B. S. Hsiao, and B. Chu, "Structure and process relationship of electrospun bioabsorbable nanofiber membranes," *Polymer (Guildf).*, vol. 43, no. 16, pp. 4403–4412, 2002.

[55] L. A. Andrady, *Science and Technology of Polymer Nanofibers*. 2008.

[56] K. Iimura, T. Oi, M. Suzuki, and M. Hirota, "Preparation of silica fibers and non-woven cloth by electrospinning," *Adv. Powder Technol.*, vol. 21, no. 1, pp. 64–68, Jan. 2010.

[57] Y. Xu, W. Zhou, L. Zhang, and L. Cheng, "Spinnability and crystallizability of silica glass fiber by the sol-gel method," *J. Mater. Process. Technol.*, vol. 101, pp. 46–48, 2000.

[58] C. M. Hsu and S. Shivkumar, "Nano-sized beads and porous fiber constructs of Poly(ε-caprolactone) produced by electrospinning," *J. Mater. Sci.*, vol. 39, no. 9, pp. 3003–3013, 2004.

[59] S. Megelski, J. S. Stephens, D. Bruce Chase, and J. F. Rabolt, "Micro- and nanostructured surface morphology on electrospun polymer fibers," *Macromolecules*, vol. 35, no. 22, pp. 8456–8466, 2002.

[60] C. L. Casper and J. S. Stephens, "Controlling Surface Morphology of Electrospun Polysterene Fibers: Effect of Humidity and Molecular Weight in Electrospinning Process," *Macromolecules*, vol. 37, pp. 573–578, 2004.

[61] B. De Schoenmaker, L. Van Der Schueren, R. Zugle, A. Goethals, P. Westbroek, P. Kiekens, T. Nyokong, and K. De Clerck, "Effect of the relative humidity on the fibre morphology of polyamide 4.6 and polyamide 6.9 nanofibres," *J. Mater. Sci.*, vol. 48, no. 4, pp. 1746–1754, 2013.

[62] R. S. Barhate, C. K. Loong, and S. Ramakrishna, "Preparation and characterization of nanofibrous filtering media," *J. Memb. Sci.*, vol. 283, no. 1–2, pp. 209–218, 2006.

[63] Z. M. Huang, Y. Z. Zhang, M. Kotaki, and S. Ramakrishna, "A review on polymer nanofibers by electrospinning and their applications in nanocomposites," *Compos. Sci. Technol.*, vol. 63, no. 15, pp. 2223–2253, 2003.

[64] X. Chen and S. S. Mao, "Titanium dioxide nanomaterials: Synthesis, properties, modifications and applications," *Chem. Rev.*, vol. 107, no. 7, pp. 2891–2959, 2007.

[65] K. Hashimoto, H. Irie, and A. Fujishima, "TiO2 Photocatalyis: A Historical Overview and Future Prospects," *Jpn. J. Appl. Phys.*, vol. 44, no. 12, pp. 8269–8285, 2005.

[66] A. Fujishima, T. N. Rao, and D. a. Tryk, "Titanium dioxide photocatalysis," *J. Photochem. Photobiol. C Photochem. Rev.*, vol. 1, no. 1, pp. 1–21, 2000.

[67] N. Van De Velde, M. Arin, P. Lommens, D. Poelman, and I. Van Driessche, "Characterization of the aqueous peroxomethod for the synthesis of transparent TiO2 thin films," *Thin Solid Films*, vol. 519, no. 11, pp. 3475–3479, 2011.

[68] J. M. Herrmann, "Heterogeneous photocatalysis: State of the art and present applications," *Top. Catal.*, vol. 34, no. 1–4, pp. 49–65, 2005.

[69] J. Watté, P. Lommens, G. Pollefeyt, M. Meire, K. De Buysser, and I. Van Driessche, "Highly Crystalline Nanoparticle Suspensions for Low-Temperature Processing of TiO 2 Thin Films," *ACS Appl. Mater. Interfaces*, p. acsami.6b01684, 2016.

[70] N. Savage and M. S. Diallo, "Nanomaterials and water purification: Opportunities and challenges," *J. Nanoparticle Res.*, vol. 7, no. 4–5, pp. 331–342, 2005.

[71] J. Mo, Y. Zhang, Q. Xu, J. J. Lamson, and R. Zhao, "Photocatalytic purification of volatile organic compounds in indoor air: A literature review," *Atmos. Environ.*, vol. 43, no. 14, pp. 2229–2246, 2009.

[72] Z. Zhang, C.-C. Wang, R. Zakaria, and J. Y. Ying, "Role of Particle Size in Nanocrystalline TiO2-Based Photocatalysts," *J. Phys. Chem. B*, vol. 102, no. 52, pp. 10871–10878, 1998.

[73] M. N. Chong, B. Jin, C. W. K. Chow, and C. Saint, "Recent developments in photocatalytic water treatment technology: A review," *Water Res.*, vol. 44, no. 10, pp. 2997–3027, 2010.

[74] M. N. Chong, V. Vimonses, S. Lei, B. Jin, C. Chow, and C. Saint, "Synthesis and characterisation of novel titania impregnated kaolinite nano-photocatalyst," *Microporous Mesoporous Mater.*, vol. 117, no. 1–2, pp. 233–242, 2009.

[75] Z. Sun, Y. Chen, Q. Ke, Y. Yang, and J. Yuan, "Photocatalytic degradation of cationic azo dye by TiO2/bentonite nanocomposite," *J. Photochem. Photobiol. A Chem.*, vol. 149, no. 1–3, pp. 169–174, 2002.

[76] X. Zhang, J. H. Pan, A. J. Du, W. Fu, D. D. Sun, and J. O. Leckie, "Combination of one-dimensional TiO2 nanowire photocatalytic oxidation with microfiltration for water treatment," *Water Res.*, vol. 43, no. 5, pp. 1179–1186, 2009.

[77] F. Bosc, A. Ayral, and C. Guizard, "Mesoporous anatase coatings for coupling membrane separation and photocatalyzed reactions," *J. Memb. Sci.*, vol. 265, no. 1–2, pp. 13–19, 2005.

[78] H. Zhang, X. Quan, S. Chen, H. Zhao, and Y. Zhao, "The removal of sodium dodecylbenzene sulfonate surfactant from water using silica/titania nanorods/nanotubes composite membrane with photocatalytic capability," *Appl. Surf. Sci.*, vol. 252, no. 24, pp. 8598–8604, 2006.

[79] S. H. Kim, S. Y. Kwak, B. H. Sohn, and T. H. Park, "Design of TiO2 nanoparticle self-assembled aromatic polyamide thin-film-composite (TFC) membrane as an approach to solve biofouling problem," *J. Memb. Sci.*, vol. 211, no. 1, pp. 157–165, 2003.

[80] I. R. Bellobono, F. Morazzoni, R. Bianchi, E. S. Mangone, R. Stanescu, C. Costache, and P. M. Tozzi, "Solar energy driven photocatalytic membrane modules for water reuse in agricultural and food industries. Pre-industrial experience using s-triazines as model molecules," *Int. J. Photoenergy*, vol. 7, no. 2, pp. 87–94, 2005.

[81] S. P. Albu, A. Ghicov, J. M. Macak, R. Hahn, and P. Schmuki, "Nanotube Membrane for Flow-through Photocatalytic Applications," pp. 5–8, 2007.

[82] D. Bjorge, N. Daels, S. de Vrieze, P. Dejans, T. van Camp, W. Audenaert, P. Westbroek, K. de Clerck, C. Boeckaert, and S. W. H. van Hulle, "Initial testing of electrospun nanofibre filters in water filtration applications," *Water SA*, vol. 36, no. 1, pp. 151–156, 2010.

[83] D. Bjorge, N. Daels, S. De Vrieze, P. Dejans, T. Van Camp, W. Audenaert, J. Hogie, P. Westbroek, K. De Clerck, and S. W. H. Van Hulle, "Performance assessment of electrospun nanofibers for filter applications," *Desalination*, vol. 249, no. 3, pp. 942–948, 2009.

[84] N. Daels, M. Radoicic, M. Radetic, K. De Clerck, and S. W. H. Van Hulle, "Electrospun nanofibre membranes functionalised with TiO2 nanoparticles: Evaluation of humic acid and bacterial removal from polluted water," *Sep. Purif. Technol.*, vol. 149, pp. 488–494, 2015.

[85] N. Daels, M. Radoicic, M. Radetic, S. W. H. Van Hulle, and K. De Clerck, "Functionalisation of electrospun polymer nanofibre membranes with TiO2 nanoparticles in view of dissolved organic matter photodegradation," *Sep. Purif. Technol.*, vol. 133, pp. 282–290, 2014.

[86] R. S. Barhate and S. Ramakrishna, "Nanofibrous filtering media: Filtration problems and solutions from tiny materials," *J. Memb. Sci.*, vol. 296, no. 1–2, pp. 1–8, 2007.

[87] P. Bamfield, *Chromic phenomena: Technological applications of colour chemistry*. Cambridge: The Royal Society of Chemistry, 2001.

[88] J. Griffiths and J. Mama, "pH-dependent absorption and fluorescence spectra of hydroxyaryl-squarylium dyes," *Dye. Pigment.*, vol. 44, no. 1, pp. 9–17, 1999.

[89] R. M. El-Shishtawy and P. Almeida, "A new Vilsmeier-type reaction for one-pot synthesis of pH sensitive fluorescent cyanine dyes," *Tetrahedron*, vol. 62, no. 33, pp. 7793–7798, 2006.

[90] A. D. Broadbent, *Basic principles of textile coloration*. Bradford: Society of Dyers and Colourists, 2001.

[91] M. Poprawa-Smoluch, J. Baggerman, H. Zhang, H. P. A. Maas, L. De Cola, and A. M. Brouwer, "Photoisomerization of disperse red 1 studied with transient absorption spectroscopy and quantum chemical calculations," *J. Phys. Chem. A*, vol. 110, no. 43, pp. 11926–11937, 2006.

[92] P. C. a Jerónimo, A. N. Araújo, and M. C. B. S. M. Montenegro, "Optical sensors and biosensors based on sol-gel films," *Talanta*, vol. 72, pp. 13–27, 2007.

[93] A. Lobnik, I. Oehme, I. Murkovic, and O. S. Wolfbeis, "pH optical sensors based on sol–gels: Chemical doping versus covalent immobilization," *Anal. Chim. Acta*, vol. 367, no. 1–3, pp. 159–165, Jul. 1998.

[94] F. R. Zaggout, N. M. El-Ashgar, S. M. Zourab, I. M. El-Nahhal, and H. Motaweh, "Encapsulation of methyl orange pH-indicator into a sol-gel matrix," *Mater. Lett.*, vol. 59, no. 23, pp. 2928–2931, 2005.

[95] E. Wang, K.-F. Chow, V. Kwan, T. Chin, C. Wong, and A. Bocarsly, "Fast and long term optical sensors for pH based on sol-gels," *Anal. Chim. Acta*, vol. 495, pp. 45–50, 2003.

[96] E. Wang, K.-F. Chow, W. Wang, C. Wong, C. Yee, A. Persad, J. Mann, and A. Bocarsly, "Optical sensing of HCl with phenol red doped sol-gels," *Anal. Chim. Acta*, vol. 534, pp. 301–306, 2005.

[97] R. Makote and M. M. Collinson, "Organically modified silicate films for stable pH sensors," *Anal. Chim. Acta*, vol. 394, no. 2–3, pp. 195–200, 1999.

[98] C. Rottman, M. Ottolenghi, R. Zusman, O. Lev, M. Smith, G. Gong, M. L. Kagan, and D. Avnir, "Doped sol-gel glasses as pH sensors," *Mater. Lett.*, vol. 13, no. 6, pp. 293–298, 1992.

[99] I. M. El-Nahhal, J. Livage, S. M. Zourab, F. S. Kodeh, and A. Al swearky, "Entrapment of phenol red (PR) pH indicator into sol–gel matrix in presence of some surfactants," *J. Sol-Gel Sci. Technol.*, vol. 75, no. 2, pp. 313–322, 2015.

[100] D. A. Nivens, M. V Schiza, and S. M. Angel, "Multilayer sol-gel membranes for optical sensing applications : single layer pH and dual layer CO2 and NH3 sensors," *Talanta*, vol. 58, pp. 543–550, 2002.

[101] C. Malins and B. D. MacCraith, "Dye-doped organically modified silica glass for fluorescence based carbon dioxide gas detection," *Analyst*, vol. 123, pp. 2373–2376, 1998.

[102] H. Segawa, E. Ohnishi, Y. Arai, and K. Yoshida, "Sensitivity of fiber-optic carbon dioxide sensors utilizing indicator dye," *Sensors Actuators, B Chem.*, vol. 94, no. 3, pp. 276–281, 2003.

[103] P. C. a Jerónimo, A. N. Araújo, and M. Conceição B S M Montenegro, "Optical sensors and biosensors based on sol-gel films.," *Talanta*, vol. 72, no. 1, pp. 13–27, 2007.

[104] D. N. Simon, R. Czolk, and H. J. Ache, "Doped sol-gel films for the development of optochemical ethanol sensors," *Thin Solid Films*, vol. 260, no. 1, pp. 107–110, 1995.

[105] P. J. Skrdla, S. B. Mendes, N. R. Armstrong, and S. S. Saavedra, "Planar integrated optical waveguide sensor for isopropyl alcohol in aqueous media," *J. Sol-Gel Sci. Technol.*, vol. 24, no. 2, pp. 167–173, 2002.

[106] S. A. Wallington, C. Pilon, and J. D. Wright, "Sol-Gel Composites for Optical Sensing of Solvents," *J. Sol-Gel Sci. Technol.*, vol. 8, pp. 1127–1132, 1997.

[107] L. Van der Schueren, K. De Clerck, G. Brancatelli, G. Rosace, E. Van Damme, and W. De Vos, "Novel cellulose and polyamide halochromic textile sensors based on the encapsulation of Methyl Red into a sol–gel matrix," *Sensors Actuators B Chem.*, vol. 162, no. 1, pp. 27–34, Feb. 2012.

[108] L. Van Der Schueren, T. Mollet, Ö. Ceylan, and K. De Clerck, "The development of polyamide 6.6 nanofibres with a pH-sensitive function by electrospinning," *Eur. Polym. J.*, vol. 46, no. 12, pp. 2229–2239, 2010.

[109] A. Camposeo, F. Di Benedetto, R. Stabile, R. Cingolani, and D. Pisignano, "Electrospun dye-doped polymer nanofibers emitting in the near infrared," *Appl. Phys. Lett.*, vol. 90, no. 2007, p. 143115, 2007.

[110] F. Di Benedetto, E. Mele, A. Camposeo, A. Athanassiou, R. Cingolani, and D. Pisignano, "Photoswitchable organic nanofibers," *Adv. Mater.*, vol. 20, pp. 314–318, 2008.

[111] A. Agarwal, A. Raheja, T. S. Natarajan, and T. S. Chandra, "Development of universal pH sensing electrospun nanofibers," *Sensors Actuators, B Chem.*, vol. 161, pp. 1097–1101, 2012.

[112] L. Van der Schueren, T. De Meyer, I. Steyaert, Ö. Ceylan, and K. Hemelsoet, "Polycaprolactone and polycaprolactone/chitosan nanofibres functionalised with the pH-sensitive dye Nitrazine Yellow," *Carbohydr. Polym.*, vol. 91, pp. 284–293, 2013.

[113] D. Fantini and L. Costa, "Dye, fluorophores and pigment coloration of nanofibers produced by electrospinning," *Polym. Adv. Technol.*, vol. 20, no. 2, pp. 111–121, 2009.

[114] L. Van Der Schueren, K. Hemelsoet, V. Van Speybroeck, and K. De Clerck, "The influence of a polyamide matrix on the halochromic behaviour of the pH-sensitive azo dye Nitrazine Yellow," *Dye. Pigment.*, vol. 94, no. 3, pp. 443–451, 2012.

[115] C. Rottman, A. Turniansky, and D. Avnir, "Sol-gel physical and covalent entrapment of three methyl red indicators: a comparative study," *J. Sol-Gel Sci. Technol.*, vol. 13, pp. 17–25, 1998.

[116] S. Trupp, M. Alberti, T. Carofiglio, E. Lubian, H. Lehmann, R. Heuermann, E. Yacoub-George, K. Bock, and G. J. Mohr, "Development of pH-sensitive indicator dyes for the preparation of micro-patterned optical sensor layers," *Sensors Actuators, B Chem.*, vol. 150, no. 1, pp. 206–210, 2010.

[117] G. J. Mohr, H. Müller, B. Bussemer, A. Stark, T. Carofiglio, S. Trupp, R. Heuermann, T. Henkel, D. Escudero, and L. González, "Design of acidochromic dyes for facile preparation of pH sensor layers," *Anal. Bioanal. Chem.*, vol. 392, no. 7–8, pp. 1411–1418, 2008.

[118] I. Steyaert, G. Vancoillie, R. Hoogenboom, and K. De Clerck, "Dye immobilization in halochromic nanofibers through blend electrospinning of a dye-containing copolymer and polyamide-6," *Polym. Chem.*, 2015.

[119] S. Ramakrishna, R. Jose, P. S. Archana, A. S. Nair, R. Balamurugan, J. Venugopal, and W. E. Teo, "Science and engineering of electrospun nanofibers for advances in clean energy, water filtration, and regenerative medicine," *J. Mater. Sci.*, vol. 45, no. 23, pp. 6283–6312, 2010.

[120] J. Kim and B. Van Der Bruggen, "The use of nanoparticles in polymeric and ceramic membrane structures: Review of manufacturing procedures and performance improvement for water treatment," *Environ. Pollut.*, vol. 158, no. 7, pp. 2335–2349, 2010.

[121] F. R. Zaggout, "Entrapment of phenol red pH indicator into a sol–gel matrix," *Mater. Lett.*, vol. 60, no. 8, pp. 1026–1030, 2006.

2

Materials and Methods

This chapter gives an overview of the generic materials and methods used for the research in this PhD. Materials and methods dedicated to a specific chapter are discussed within the relevant chapters.

2.1 Materials

The **sol-gel precursors** tetraethyl orthosilicate (TEOS, reagent grade 98%), (3-aminopropyl)triethoxysilane (APTES, ≥ 98%) and chlorotriethoxysilane (CTES, 98%) were all provided by Sigma-Aldrich and used as received (Figure 2.1, 2.2 and 2.3).

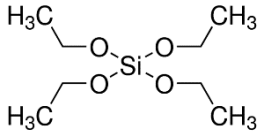

Figure 2.1 Tetraethyl orthosilicate (TEOS)

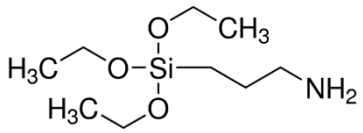

Figure 2.2 (3-aminopropyl)triethoxysilane (APTES)

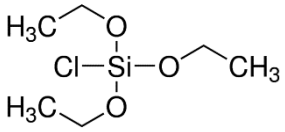

Figure 2.3 Chlorotriethoxysilane (CTES)

The **solvent** ethanol absolute used for sol preparation was obtained from Fiers. Hydrochloric acid (HCl, 37%) used as catalyst and for the preparation of the pH-baths as well as the vapor experiments was supplied by Sigma-Aldrich. Sodium hydroxide used for the preparation of the pH-baths and ammonium hydroxide solution (ACS reagent, 28-30% NH_3 basis) were also obtained from Sigma-Aldrich. Deionized water (Type III) was used throughout this PhD.

All the **additives** used for functionalization throughout this PhD were supplied by Sigma-Aldrich. These include the indicator dyes Methyl Yellow, Methyl Red and C.I. Disperse Red 1. These dyes were used to dope the electrospinning solutions, or to functionalize the precursors APTES and CTES. Titanium (IV) oxide (Degussa P25) was obtained from Sigma Aldrich. It is a standard material in the field of photocatalytic reactions,

having a primary particle size of 21 nm and a specific surface area of 35-65 m^2/g.

2.2 Electrospinning

2.2.1 Sol preparation

Three different systems, one open and two closed set-up(s), were used for the preparation of the sols (Figure 2.4). In every chapter the used set-up(s) will be mentioned in the materials and methods section. The first steps of the preparation procedure were similar for all set-ups. All sols were prepared from a mixture of TEOS, ethanol, water and HCl with a molar ratio of respectively 1:2:2:0.01. Firstly, TEOS and ethanol were mixed. Secondly, aqueous HCl was added to the solution under vigorous stirring with a magnetic stir bar. After completion of the hydrolysis reactions (exothermic reaction) the sols were heated under stirring at 80°C.

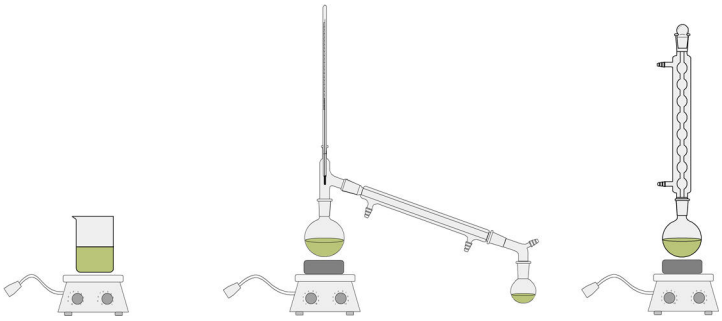

Figure 2.4 Schematic representation of the systems used for sol preparation: open set-up (left), Liebig set-up (center) and Allihn set-up (right)

In the open system, sols were heated and stirred in a beaker, in contact with the atmosphere. The volume of the sols decreased to around 3/8 of the initial volume when attaining the optimum viscosity. When the desired viscosity was reached, the solution was cooled down to room temperature.

In the Liebig set-up, evaporated ethanol was condensed via a Liebig cooler and collected in a round bottom flask. The evaporation of ethanol was

monitored by weighing the condensed ethanol after fixed time periods. The reaction was allowed to continue until the solution reached the desired viscosity. Finally, the solution was cooled down to room temperature.

In the Allihn set-up, ethanol was refluxing and could not escape from the system. The reaction was allowed to continue for fixed time periods of 30 min, 2 h, 6 h, 12 h, 24 h and 48 h. Next, a rotary evaporator was used to evaporate ethanol until a desired viscosity was reached.

2.2.2 Characterization of the electrospinning solutions

The viscosity of the solutions was measured prior to electrospinning using a Brookfield viscometer LVDV-II. A volume of 7 mL was used, and all viscosities were measured at room temperature (21 ± 1 °C). Conductivity measurements were carried out using a CDM210 conductivity meter (Radiometer Analytical).

2.2.3 Electrospinning equipment

Two types of electrospinning set-ups were used throughout the PhD. A mono nozzle set-up was used to evaluate and optimize the stability of the electrospinning process of the sols. Upscaling was carried out using a rotating drum set-up (Figure 2.5).

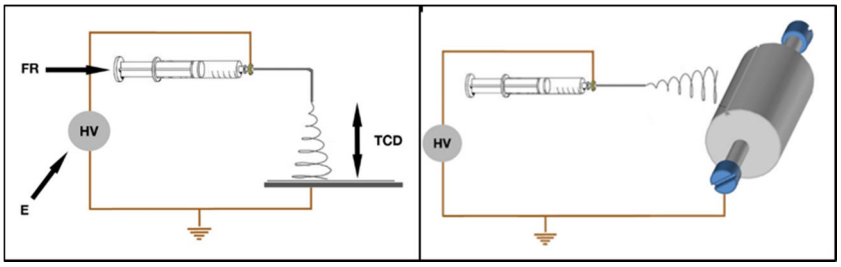

Figure 2.5 Schematic representation of the electrospinning set-ups: mono-nozzle (left) and rotating drum set-up (right)

A **mono-nozzle** electrospinning set-up was used to obtain small size nanofibrous structures (Figure 2.5 left). The sols were loaded in a 20 mL

syringe equipped with a stainless steel 316 syringe needle with an inner diameter of 1.024 mm and a pipetting blunt tip of 90° (Sigma-Aldrich). A Glassman High Voltage Series EH 30P3 was used to apply the voltage and the flow rate was fixed at 1 $mL.h^{-1}$ with a syringe KD Scientific Pump Series 100. The tip-to-collector distance was fixed at 15 cm. The nanofibers were collected on a grounded aluminum foil.

A **rotating drum** set-up uses one needle, that is moved or fixed along the axis of the rotating drum collector, while electrospinning sideways (Figure 2.5 right). The speed (RPM) of the rotating drum collector can be adjusted. Random nanofibrous membranes are obtained at low RPM, aligned nanofibers can be obtained at high RPM. Thick stand-alone membranes can be obtained for both by spinning for prolonged times. All other components of the set-up are identical to the mono-nozzle set-up. Again aluminum foil was fixed on the rotating drum collector for sample collection.

All experiments were performed at room temperature (22 ± 2°C) and room humidity (33 ± 10% RH). The stability of the electrospinning process was evaluated visually by the stability of the Taylor cone in time and by verifying the absence of droplets and beads on the SEM images.

2.3 Characterization techniques

2.3.1 Scanning electron microscopy

The morphology of the fibers was examined using a FEI Quanta 200 F SEM at an accelerating voltage of 20 kV. Prior to SEM analysis a gold coating was applied using a gold sputter coater (Balzers Union SKD 030). The nanofiber diameters were determined using Cell D (Olympus) or ImageJ software. The average fiber diameters and their standard deviations are based on 50 measurements for each sample.

2.3.2 Infrared spectroscopy

A Fourier Transform Infrared (FTIR) spectrometer with Attenuated Total Reflectance (ATR) accessory (diamond crystal) from Thermo Scientific was used to record the spectra, of both the sols and nanofibers. Spectra

were recorded from 4000 to 400 cm^{-1} with a resolution of 4 cm^{-1}, 32 scans were taken for each experiment.

2.3.3 Contact angle measurements

The contact angles of the nanofibrous membranes were characterized via contact angle measurements with a drop shape analyzer (DSA 30 Krüss GmbH). Deionized water was used as solvent.

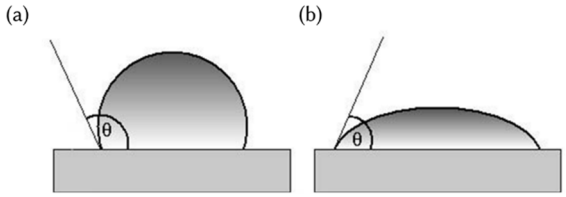

Figure 2.6 Contact angle θ of a surface with a low wettability (a) and high wettability (b)

2.3.4 Color measurement

UV Vis spectra were recorded using a Perkin-Elmer Lambda 900 spectrophotometer. 1 cm matched quartz cells were used for the transmission spectra of solutions and an integrated sphere (Spectralon Labsphere 150 mm) was used for the reflection measurements on the membranes. The spectra were recorded from 380 nm to 780 nm with a data interval of 1 nm for transmission and 4 nm for reflection. Transmission and reflection measurements were converted to absorbance (Eq. 2.1) and Kubelka-Munk (Eq. 2.2), respectively. These conversions are made due to their correlation with dye concentration.

$$A = \log\left(\frac{1}{T}\right) = a.l.c \qquad \text{[Eq. 2.1]}$$

with A = *absorbance*
T = *transmission*
a = *extinction coefficient (dependent of wavelength)*
l = *path length (= 1 cm)*
c = *dye concentration in solution*

$$K - M = \frac{K}{S} = \frac{(1-R)^2}{2R} \sim c \qquad \text{[Eq. 2.2]}$$

with *K-M = Kubelka-Munk value*
K = light absorption coefficient
S = light scattering coefficient
R = reflectance
c = dye concentration in solid material

These physical spectra do not take into account the observer (human eye) and the incident light. To quantify the actual color observed, different systems were developed which take all three parameters into account (sample, observer and illuminant). The most widely adopted system for color description is the CIE system (Commission International de l'Eclairage). It is based on the fact that light reflected from any colored surface can be visually matched by an additive mixture of red, green and blue light [1]. The CIE color description is thus derived from the reflectance spectra R(λ), the energy distribution of the light in which the color is viewed E(λ) and the standard observer response curves x(λ), y(λ) and z(λ). The tristimulus values can be determined using Eq. 2.3 [1],[2].

$$X = \int_{380}^{780} R(\lambda).E(\lambda).x(\lambda)d\lambda \qquad \text{[Eq. 2.3]}$$

$$Y = \int_{380}^{780} R(\lambda).E(\lambda).y(\lambda)d\lambda$$

$$Z = \int_{380}^{780} R(\lambda).E(\lambda).z(\lambda)d\lambda$$

with *X, Y, Z = tristimulus values for the sample*
R = reflectance
E = spectral energy distribution illuminant (D65)
x, y, z = color matching functions observer (10°)
λ = wavelength [nm]

These tristimulus values can be further used to calculate L, a, b values (Eq. 2.4). The CIELab system takes into account the hue (the color attributes), saturation (absence of white, grey or black) and lightness [3], represented in Figure 2.7. The coordinates L*, a* and b* of the CIELab system represent, respectively, lightness (perfect black is 0 and perfect white is 100), red-green and yellow-blue color variations (Figure 2.7). Using this

system, every color can thus be given a unique description. In practice, Lab values are calculated using OptLab-SPX (10° observer, D65 illuminant) from Ascanis and are based on Eq. 2.3 and Eq. 2.4.

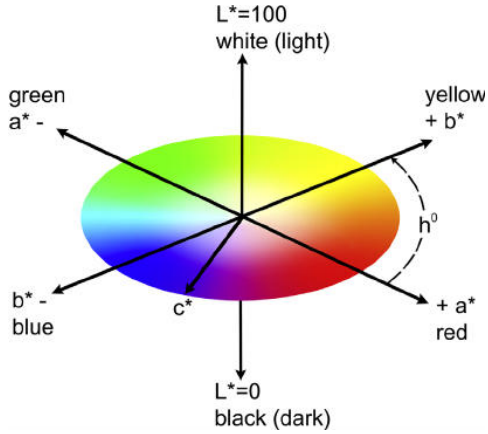

Figure 2.7 CIELab color space, illustrating Lab coordinates and linked hue (h) and chroma (c*)

$$L^* = 166\,(Y/Y_n)^{1/3} - 16$$

$$a^* = 500\,(X/X_n)^{1/3} - 500\,(Y/Y_n)^{1/3}$$

$$b^* = 200\,(Y/Y_n)^{1/3} - 200\,(Z/Z_n)^{1/3}$$

$$\text{if} \quad \left.\begin{matrix} X/X_n \\ Y/Y_n \\ Z/Z_n \end{matrix}\right\} > 0.008856 \qquad \text{[Eq. 2.4]}$$

with
X, Y, Z = tristimulus values for the sample
R = reflectance
E = spectral energy distribution illuminant (D65)
x, y, z = color matching functions observer (10°)
λ = wavelength [nm]

Furthermore, this system is suited to calculate color differences ΔE (Eq. 2.5). ΔE values higher than one represent a visual noticeable color difference. The higher the ΔE value, the more pronounced the difference in color.

$$\Delta E = \sqrt{\Delta L^{*2} + \Delta a^{*2} + \Delta b^{*2}} \qquad \text{[Eq. 2.5]}$$

with
ΔE = color difference between 2 samples
ΔL^* = difference in lightness between 2 samples
Δa^* = red/green difference between 2 samples
Δb^* = yellow/blue difference between 2 samples

2.3.5 Halochromic behavior, solvatochromic behavior and dye leaching

The pH of aqueous solutions was measured with a combined reference and glass electrode (SympHony Meters VMR). Hydrochloric acid and sodium hydroxide were used to adjust the pH. Via a drop of deionized water the pH of the direct environment of the nanofibrous membranes was measured using a flat pH-electrode (FlaTrode, Hamilton).

The dye leaching was evaluated by immersing 5 mg of fabric in 5 mL of the pH baths or the solvents, for 24 hours. The dye migration was then determined by UV-Vis spectroscopy. The amount of leached dye was calculated as a percentage of the total dye present in a 5 mg sample. Both the normalized and non-normalized UV-Vis spectra were used to evaluate the halochromic and solvatochromic behavior. To visualize the halochromic color shift, the normalized absorbance and Kubelka-Munk spectra were plotted at the acidic and alkaline peak maximum as a function of pH.

The vapor induced halochromic behavior of the samples was evaluated by placing a sample in a 1 cm matched quartz cell. The cell was closed using a septum and varying amounts of HCl and NH_3 vapors were inserted. The spectra were recorded in reflection. The vapor pressure of the vapors was determined via titration.

The pK_a values of the dyes were calculated based on absorbance spectra using Eq. 2.6. A_x is the absorbance obtained at a certain pH and A_a and A_b are the absorbance of the acid form and the base form of the dye, respectively.

$$pK_a = pH - \log\frac{A_x - A_a}{A_b - A_x} \qquad \text{[Eq. 2.6]}$$

2.3.6 Band gap energy determination via Tauc plot

Diffuse reflectance spectra of titanium dioxide functionalized samples were collected with a Lambda 900 UV-Vis spectrophotometer (Perkin-Elmer) using an integrating sphere (Spectralon Labsphere 150 mm). Non-functionalized nanofibrous samples were used as background. The optical absorption data near the band edge can be used to determine the optical band gap of a crystalline semiconductor using Eq. 2.7:

$$\alpha h\nu = A\,(h\nu - E_g)^n \qquad \text{[Eq. 2.7]}$$

with
α = absorption coefficient
h = Planck's constant [J.s]
ν = light frequency [s^{-1}]
A = a proportionality constant
E_g = band gap energy

The value of n is determined by the characteristics of the transition in the semi-conductor, with n= ½ for direct allowed, n = 2 for indirect allowed, n = 3/2 for forbidden direct and n = 3 for forbidden indirect transitions. The Kubelka-Munk method (K-M or F(R)) (Eq. 2.2) can be used for the determination of the band gap energy, since F(R) is proportional to the absorption coefficient (α):

$$F\,(R)\cdot h\nu \approx A\,(h\nu - E_g)^n \qquad \text{[Eq. 2.8]}$$

The values of the band gap energy can be determined by the construction of the Tauc plot by plotting $(F(R)*h\nu)^{1/n}$ as a function of hν (photon energy) [4]. The band gap energy is then determined by extrapolating the straightest line to the hν axis intercept. For commercial Degussa P25 TiO_2 nanoparticles, the use of equation Eq. 2.8 with n = 2 for indirect allowed transitions is suggested [5].

References

[1] H. Zollinger, *Color Chemistry: Syntheses, Properties and Applications of Organic Dyes and Pigments*, 2nd ed. VCH, 1991.

[2] A. D. Broadbent, *Basic principles of textile coloration*. Society of Dyers and Colourists, 2001.

[3] P. Bamfield, *Chromic phenomena: Technological applications of colour chemistry*. Cambridge: The Royal Society of Chemistry, 2001.

[4] J. Tauc, R. Grigorovici, and A. Vancu, "Optical properties and electronic structure of amorphous germanium," *Phys. Status Solidi B*, vol. 15, no. 2, pp. 627–637, 1966.

[5] R. López and R. Gómez, "Band-gap energy estimation from diffuse reflectance measurements on sol-gel and commercial TiO2: A comparative study," *J. Sol-Gel Sci. Technol.*, vol. 61, no. 1, pp. 1–7, 2012.

3

Electrospinning of TEOS sols without organic polymer addition

This chapter studies the feasibility of the electrospinning of pure TEOS sols without the addition of an organic polymer. First, the influence of the viscosity on the stability of the electrospinning process is studied and an optimum viscosity range is determined. Secondly, sols having too high viscosities are diluted to viscosities in the optimum range. The influence hereof on the electrospinning process and resulting nanofibers is characterized. Finally, the high temperature resistance of the nanofibrous membranes is evaluated.

Parts of this chapter are published in:

J. Geltmeyer, L. Van der Schueren, F. Goethals, K. De Buysser, and K. De Clerck, "Optimum sol viscosity for stable electrospinning of silica nanofibres," *J. Sol-Gel Sci. Technol.*, vol. 67, no. 1, pp. 188–195, 2013.

3.1 Introduction

The electrospinning of pure alkoxide precursors (without organic polymer) is not well understood yet, with only a few recent published studies [1]–[5]. No detailed literature on the influence of the sol properties on the resulting ceramic nanofibers is available. In addition, no attention has been given to the stability of the electrospinning process. This knowledge, however, showed to be a crucial prerequisite for polymeric nanofibers and is thus essential for future practice of silica nanofibers as well. One of the characteristics that highly affects the electrospinning process is the viscosity. This viscosity is, as explained in Chapter 1, among others caused by the concentration of the components and the degree of crosslinking which is in its turn influenced by several factors such as heating time, temperature, the amount of water and acid. By selecting one precursor (TEOS) a constant reactivity of the siloxane precursor is ensured and the influence hereof on the viscosity and the spinnability is thus excluded. Additionally, also a fixed amount of water and acid were selected. As described in more detail in Chapter 1, it is known that acid catalyzed sols with low TEOS:H_2O ratios are necessary to obtain viscous, spinnable sols. Therefore, a molar ratio of TEOS:H_2O:Ethanol:HCl of 1:2:2:0.01 was chosen in line with literature [3].

In this chapter, the viscosity range that yields uniform and reproducible nanofibers is determined, followed by an analysis of the fiber morphology. Next, the influence of dilution of the sol, to a desired viscosity, on the electrospinning process and thus the resulting nanofibers is established, to determine whether only the viscosity or also the way to obtain this viscosity has an influence. Since no research has been carried out on the stability of the electrospinning process of TEOS, the stability of the Taylor cone will be evaluated in this first chapter as a first step towards a stable and reproducible electrospinning process. Moreover, the resistance of these nanofibrous membranes to high temperatures (1000°C) is evaluated and their hydrophobic/hydrophilic properties are discussed.

3.2 Materials and Methods

A detailed description of the general materials and methods used in this PhD work can be found in Chapter 2. All sols studied in this chapter were

prepared in an open set-up. The open set-up was chosen since it is the most simple and practical set-up. The initial amount of TEOS used for sol preparation was 40 g. This resulted in sols with an initial volume of ± 72 mL. After evaporation of the solvent the volume decreased to around 3/8 of the initial volume for sols with a viscosity in the optimum range (see section 3.3). Dilution of the sols as discussed in section 3.4 was done by adding in between 1 mL and 4.5 mL of ethanol absolute to the prepared sols, having a volume of 20-25 mL prior to dilution. The amount of solvent added was selected based on the initial viscosity before dilution and the viscosity aimed for after dilution. The nanofibrous membranes were produced on a mononozzle set-up with a grounded aluminum foil as collector.

Nanofibrous membranes were heat treated for 3 hours at 1000°C in an oven (Nabertherm, P330 controller), a heating rate of 10°C per minute was used.

Porosimetry measurements were carried out on a TriStar 3000 automated gas adsorption analyzer from Micromeritics.

3.3 Electrospinnable viscosity range study of TEOS sols

The viscosity plays a dominant role when analyzing the electrospinnability of solutions [6]–[8]. A key prerequisite for obtaining reproducible electrospun nanofibrous non-wovens, is the presence of a stable Taylor cone [6]. In this chapter sols with different viscosities were attempted to electrospin and were visually evaluated on the presence of a stable Taylor cone. Sols with varying viscosities were obtained by changing the heating time of the sols at 80°C. During the heating process, the ethanol evaporates and the TEOS started to crosslink due to hydrolysis and condensation, thus increasing the viscosity of the solution. It should be noted that the evaporation of ethanol will not only cause a change in viscosity, but also the relative concentrations of the components will change. However, the viscosity is chosen as a first parameter to characterize the sols after preparation. Chapter 4 will focus on a more in-depth characterization of the sols degree of crosslinking, colloidal particles sizes and ethanol concentration.

Different viscosities were obtained by varying the heating time of the sols in the open system. These different viscosities showed to have varying spinnabilities. Electrospinning was not possible for sols with viscosities lower than 65 mPa·s and only droplets were deposited on the collector plate. Nanofibers were collected starting from a viscosity of 65 mPa·s up to a viscosity of around 1000 mPa·s. When the viscosity was lower than 110 mPa·s beads and droplets were still clearly visible in the SEM images of the samples (Figure 3.1 a,b) and stable electrospinning was not possible. For viscosities above ±110 mPa·s the most stable electrospinning was noted and uniform, beadless nanofibers were obtained (Figure 3.1 c-g). It should, however, be noted that the stable electrospinning of silica nanofibers showed to be more difficult compared to the electrospinning of certain polymer nanofibers, where a stable Taylor cone in time could be obtained. Instabilities of the Taylor cone were always noticed during electrospinning of the silica nanofibers. These instabilities shown by the Taylor cone are visualized in Figure 3.2.

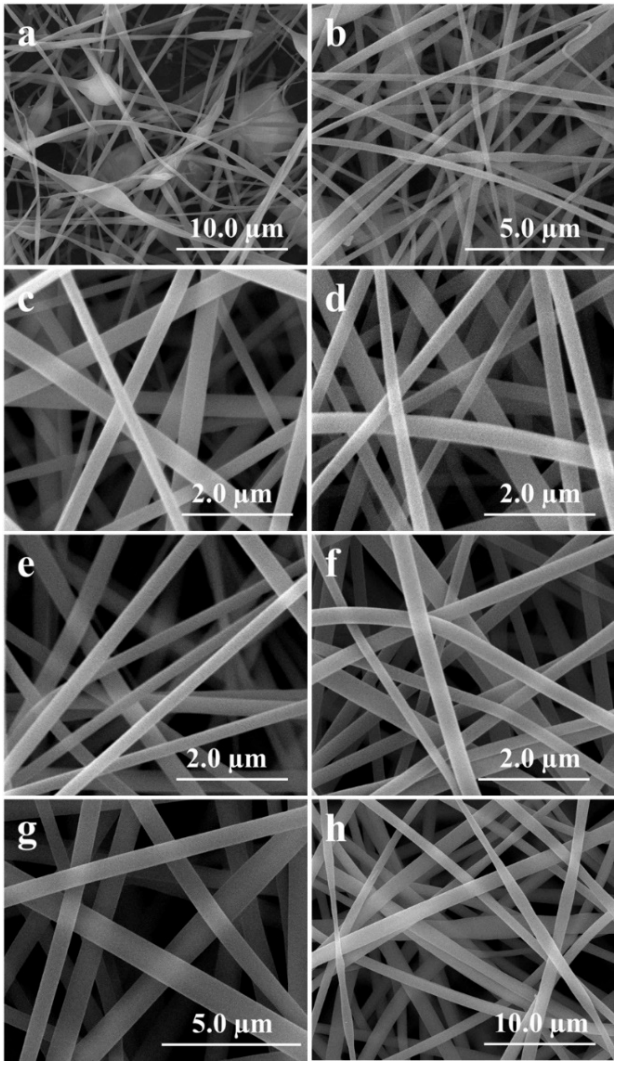

Figure 3.1 SEM images electrospun silica nanofibers (a: 65 mPa·s, b:102 mPa·s, c:110 mPa·s, d:125 mPa·s, e:145 mPa·s, f:198 mPa·s, g:398 mPa·s, h:981 mPa·s)

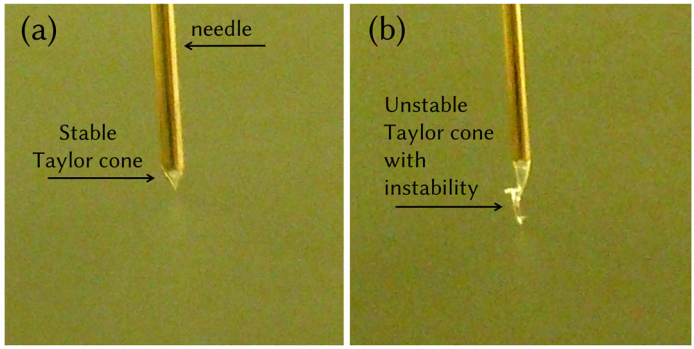

Figure 3.2 Stable Taylor cone (a) and unstable Taylor cone (b)

However, most important, for viscosities in the range of 110-200 mPa·s the unstable Taylor cone recovered after removal of the solidified piece and thus became stable again. The Taylor cone was noted to be stable up to 1 minute or longer. This instability of the Taylor cone within this optimum viscosity range did not have an influence on the stability of the produced nanofibers, nor on the continuity of the electrospinning process as it recovered automatically. These sols are thus usable when aiming for future upscaling. For viscosities above 200 mPa·s instabilities are seen within seconds and the unstable Taylor cone grows substantially larger before recovering or needle blocking. The unstable Taylor cone did thus not always recover due to too fast gelation of the sol at the needle tip, finally resulting in blocking of the needle. When looking at future upscaling these sols can thus not be used since electrospinning is not possible for time periods exceeding 30 minutes. The optimum viscosity range for the most stable electrospinning of silica nanofibers possible for longer time periods and resulting in uniform, beadless nanofibers is defined within a viscosity range of 110-200 mPa·s.

Additionally, the stability of the viscosity in time was determined (Figure 3.3) for sols having a viscosity close to this optimum range. The viscosity of three sols, which were all kept both at room temperature (RT) and cooled in the fridge (4°C), was followed in time. An acceptable viscosity increase was found for sols cooled and non-cooled, and they showed to be usable for electrospinning for at least 3-4 hours (Figure 3.3 a). This allows electrospinning for longer time periods and thus upscaling of the electrospinning process, discussed in Chapter 4. Following the viscosity increase for 24 hours (Figure 3.3 b), it was noticed that the viscosity of the sols which were not cooled increased exponentially in time. Resulting in a

viscosity over 800 mPa·s and thus largely exceeding the stability region. The viscosity of the sols which were cooled in the fridge, increased as expected much slower and even after 20 hours the viscosity was slightly higher than 200 mPa·s, the border of the stable viscosity window.

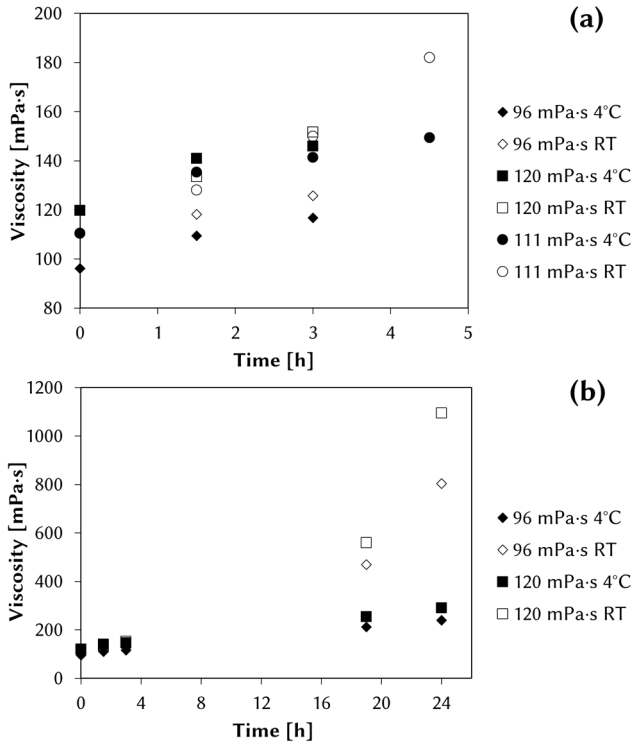

Figure 3.3 Viscosity increase as a function of time for sols held at both room temperature and at 4°C: 0-4.5 h (a) and 0-24 h (b)

A clear influence of the viscosity on the nanofiber diameters can be noticed, Figure 3.4. A minimum viscosity is necessary to obtain a stable Taylor cone and uniform, beadless nanofibers. On the other hand too high viscosities may lead to needle blocking. Within the optimum viscosity range (110 – 200 mPa·s) the lowest mean nanofiber diameters are obtained, with a nearly constant diameter in between 210 nm and 310 nm. At viscosities above the optimal range, an increase in nanofiber diameter is observed with an increase in solution viscosity. The fiber diameter increases from 260 ± 70 nm at a viscosity of 136 mPa·s to 670 ± 200 nm at a viscosity of 398 mPa·s. This is in line with electrospinning of polymer solutions, where an increase in viscosity also results in an increasing fiber

diameter [7],[9]. When the viscosity of a solution rises, a higher resistance of the jet to the bending instability and a faster solidification of the jet, indeed leads to thicker fibers [10],[11]. Typical variation coefficients are between 20% and 30%. These are again in line with variation coefficients of polymer nanofibers found in literature [11]–[13]. The reproducibility within the stable electrospinning region was guaranteed, as demonstrated by the constant diameter of two samples with the same viscosity (135 mPa·s and 136 mPa·s). The samples showed a diameter of 270 ± 70 nm and 260 ± 70 nm.

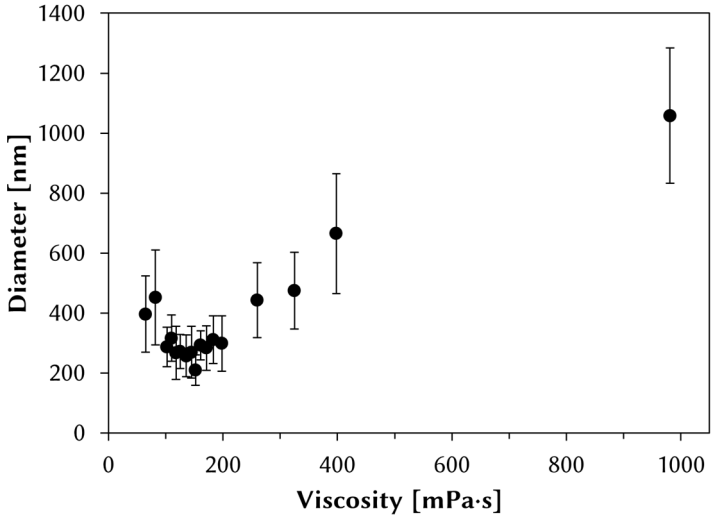

Figure 3.4 Diameters of silica nanofibers as a function of the viscosity of the sol

3.4 Effect of diluting the sol to the desired viscosity

Preparation of a sol via the open system does not allow for a straightforward control of the sols viscosity. Dilution of a sol having a viscosity that exceeds the optimum viscosity window may aid to an easy sample preparation since a specific viscosity and thus a specific fiber diameter can be easily obtained. However, the initial degree of crosslinking may very well have an influence. To analyze this, TEOS sols were prepared with a higher viscosity than the desired one. These sols were diluted with ethanol to obtain viscosities around the optimal

viscosities being 110-200 mPa·s. Ethanol was chosen as a solvent to dilute the sols in order to minimize the influence of this dilution on the reactions proceeding in the sol. An overview of the samples obtained with this method are summarized in Table 3.1.

Table 3.1 Overview of samples obtained by dilution of fresh sols

Sample n°	Viscosity (mPa·s)	Viscosity original TEOS sol (mPa·s)
1	92	371
2	100	358
3	105	1025
4	110	137
5	114	1340
6	115	562
7	131	372
8	138	969
9	160	200

First of all, it was noted that all samples were electrospinnable, but the Taylor cone was less stable (for only seconds) compared to the electrospinning of freshly prepared sols. This might be attributed to a too high degree of crosslinking. Indeed, due to heating, ethanol evaporates, the relative concentrations of the components change and the sol starts to crosslink, thus increasing the viscosity. Once a certain degree of crosslinking is obtained, dilution of the sol with ethanol reduces the viscosity, but the degree of crosslinking is probably not affected, causing unstable electrospinning.

Focus is given to one example. Sample 8 and 9 with viscosities of respectively 138 mPa·s and 160 mPa·s, thus in the stable electrospinning range, are prepared by diluting sols with viscosities of respectively 969 mPa·s and 200 mPa·s. However, as mentioned above the electrospinning was less stable compared to fresh sols. At a high magnification (Figure 3.5 a,c) uniform nanofibers are visible for both samples. However, when the magnification is decreased (Figure 3.5 b,d) it is clearly visible that many beads are noticed for sample 8 prepared at a higher viscosity while these are absent in sample 9. This confirms the clear influence and importance of the viscosity of the original sol as well as the initial degree of crosslinking of the sol, influencing both the stability of the electrospinning process as well as the uniformity and reproducibility of the nanofibers.

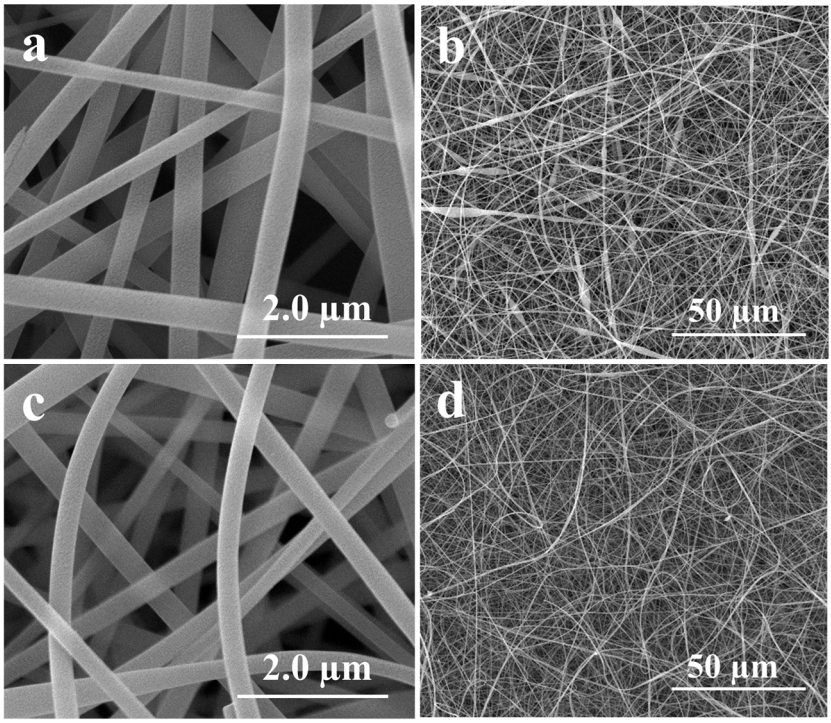

Figure 3.5 SEM images of silica nanofibers obtained from diluted sols (a and b:138 mPa·s diluted from 969 mPa·s , c and d:160 mPa·s diluted from 200 mPa·s)

The diameters of the nanofibers obtained from the diluted sols are more or less in the same range as those from the fresh sols as can be seen in Figure 3.6. A small increase in nanofiber diameter can, however, be noticed. Coefficient of variations are typically between 20% and 30%, analogous to the coefficients of variation for nanofibers prepared from fresh sols, but beads were not taken into account for nanofiber diameter determination. Electrospinning of diluted sols is thus possible, however, not as stable as electrospinning of fresh sols. In the stable region beadless and uniform nanofibers can be obtained if the viscosity of the original sol falls within the desired viscosity range. In conclusion, dilution of sols is not advised as it significantly reduces the reproducibility of both the electrospinning process and the resulting nanofibrous membranes. These results hint that the degree of crosslinking is indeed an important parameter probably influencing the electrospinning process. Chapter 4 focuses more in-depth on the characterization of this degree of crosslinking.

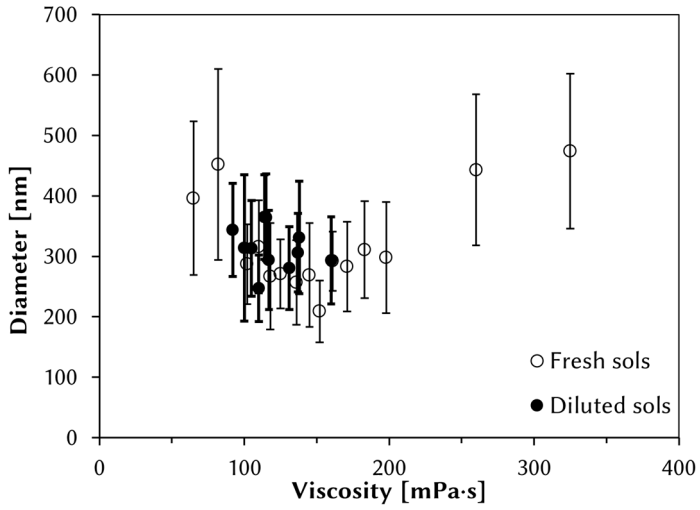

Figure 3.6 Fiber diameters of silica nanofibers obtained from fresh and diluted sols as a function of the sol viscosity

3.5 Hydrophobic/hydrophilic properties and high temperature resistance

As explained in Chapter 1, ceramic nanofibers are most of the time produced by combining sol-gel precursors and organic polymers in the electrospinning solution. The organic polymer is afterwards removed via a thermal treatment [14],[15], which may be deleterious to the nanofibers [16] and result in poor mechanical properties and loss of material's coherence. The method used in this work makes the thermal treatment redundant. However, it should be tested if the produced membranes are still resistant to high temperatures and if they maintain their cohesion. In addition, it was noticed that the hydrophobic properties of the produced membranes changed in time, going from highly hydrophobic immediately after electrospinning to highly hydrophilic after aging at room temperature for 3 months. Afterwards this hydrophilic behavior remained stable in time. Therefore, two samples were selected: a freshly electrospun sample (1 week old) and a sample that had aged for 1 year at room temperature and room humidity. The resistance of these nanofibrous membranes to high temperatures was evaluated by heating at 1000°C for 3 hours. The influence hereof on their fiber morphology and composition was

evaluated via SEM (Figure 3.7) and ATR-FTIR (Figure 3.8), respectively. Their hydrophobic/hydrophilic properties were characterized by contact angle measurements (Table 3.3).

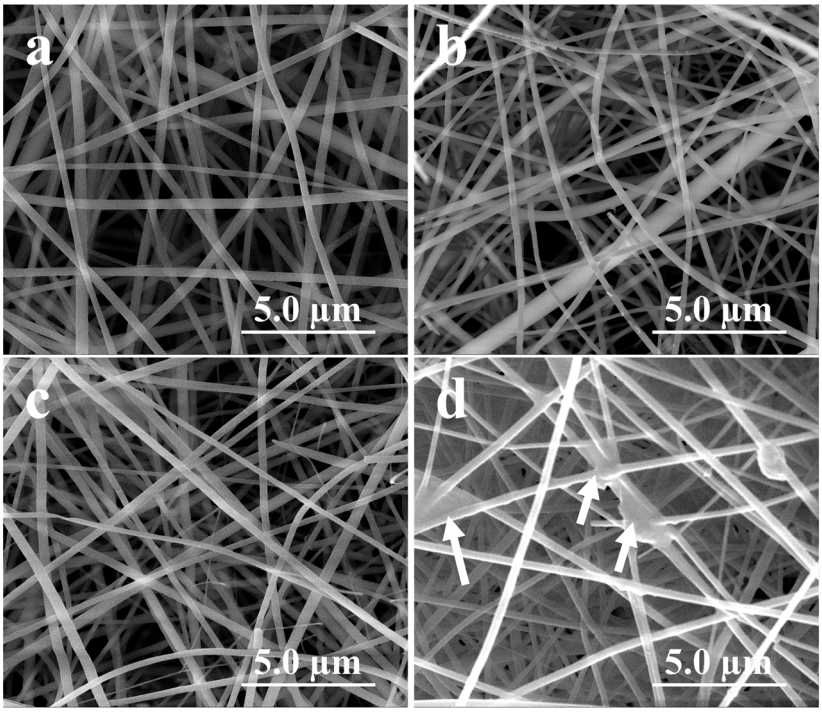

Figure 3.7 SEM images of new nanofibrous sample before (a) and after (b) heat treatment; SEM images of 1 year old nanofibrous sample before (c) and after (d) heat treatment.

SEM images (Figure 3.7) showed only a minor change in morphology of the nanofibrous samples before and after the heat treatment. The freshly electrospun sample showed less uniform nanofibers after the heat treatment and thus a higher standard deviation of the nanofiber diameters. The mean nanofiber diameter remained unchanged upon heat treating, namely 290 ± 60 nm and 295 ± 205 nm for the non-heat treated and heat treated sample, respectively. Some more profound changes in morphology were seen for the sample that had aged for 1 year. Upon heat treating the nanofibers seemed to fuse slightly together. A similar nanofiber diameter before and after heat treatment was noted (within the standard deviation), namely 275 ± 110 nm and 305 ± 85 nm for the non-heat treated and heat treated sample, respectively.

ATR-FTIR spectra of the two membranes, before and after the heat treatment are compared (Figure 3.8). An overview of the assignment of the different peaks is given in Table 3.2 [17]–[19]. First, a broadening of the OH peak (3300 cm^{-1}) was seen upon aging of the samples together with the disappearance of alkyl groups (2974 cm^{-1} , 2894 cm^{-1} and 1383 cm^{-1}). The last might be attributed to evaporation of the solvent ethanol and the disappearance of ethoxy groups within the sol-gel network due to further crosslinking. The heat treatment at 1000°C resulted in the same spectrum for both samples. As expected, all peaks non-related to pure silica disappeared and thus only three peaks at 1064 cm^{-1} (Si-O-Si asymm stretch), 802 cm^{-1} (Si-O-Si symm stretch) and 454 cm^{-1} (Si-O-Si bend) remained.

The contact angles of the samples are given in Table 3.3. Upon aging the samples go from highly hydrophobic to hydrophilic. These changes with time might be attributed to the disappearance of the hydrophobic alkyl groups or surface water build up on the nanofibrous membranes. The heat treated membranes were hydrophilic and immediate wetting of the samples was seen (contact angle of 0°C). Hydrophilic properties of silica are typically ascribed to silanol (Si-OH) groups present on the surface [20]. These silanol groups are, however, no longer visible on the ATR-FTIR spectra of the heat treated samples (Figure 3.8). The heat treated samples seem to be composed of solely siloxane groups (Si-O-Si) which are hydrophobic [21]. Therefore, their hydrophilic properties are assumed to be due to the capillary effect inherent to the nanofibrous structure. Capillarity is known as the tendency of a liquid to be drawn into a small passage such as a tube of small cross-sectional area, like the space in between the nanofibers. It is a result of the balance between the cohesive forces within the water and the adhesive forces between water and the surface of the fibers.

Porosimetry analysis of non-heat treated samples, aged samples and heat treated samples did not show significant changes in average pore size, pore volume or surface area. It should be noted that the changes in hydrophilic properties upon aging or heat treatment were highly reproducible. It is therefore suggested that the initial hydrophobic properties of the as-spun membranes might be linked to their chemical structure assuming that alkyl groups are present at the nanofibrous surface, but further research is necessary.

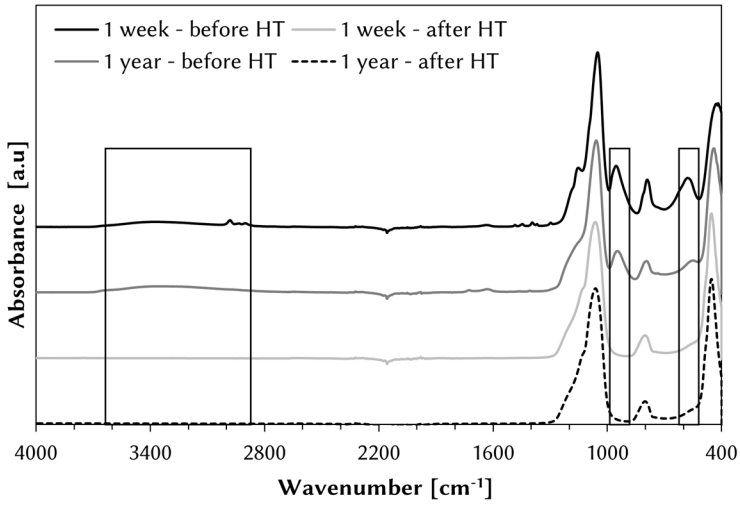

Figure 3.8 ATR-FTIR spectra of fresh (1 week old) and old (1 year old) silica nanofibers before and after heat treatment (HT) at 1000°C.

Table 3.2 Peak assignment of ATR-FTIR spectra [17]-[19]

Wavenumber (cm^{-1})	Assignment
3324	OH stretch
2974	CH_3CH_2
2894	CH_3CH_2
1383	CH_3 bend/OH bend
1154	Si–O–C/C–O–C/CH_3
1076	Si–O–Si Asymm stretch
1044	C–C–O Asymm stretch
966	Silanol Si–OH stretch
880	C–C–O Symm stretch
795	Si–O–Si Symm stretch
582	OH out of plane bend
431	Si–O–Si bend

Table 3.3 Contact angles on new, aged and heat treated silica nanofibrous membranes

	Contact angle	
Sample age	Before heat treatment	After heat treatment
1 week	136° ± 6°	0°
1 year	0°	0°

3.6 Conclusion

In this chapter, successful and reproducible electrospinning was established of TEOS sols without organic polymer addition. A novel and indispensable insight in the optimum viscosity range for electrospinning of these pure sols was established, which is essential for future upscaling and functionalization. The electrospinning of TEOS sols with different viscosities was evaluated. A clear viscosity region could be noticed for which the electrospinning of TEOS sols was most stable, namely between 110 and 200 mPa·s. Furthermore, electrospinning of sols having viscosities in this region resulted in nanofibers with the finest mean nanofiber diameter. Higher viscosities resulted in needle blocking, lower viscosities resulted in droplets and beads in the final nanofibers. To obtain the desired viscosities dilution of sols with ethanol was possible as well. To this end, the electrospinning of freshly prepared TEOS sols was compared to the electrospinning of diluted sols, which were obtained from fresh sols with higher viscosities than the stable viscosity region. The electrospinning process of the diluted sols was less stable, probably caused by the high degree of crosslinking of the original sol. The optimum viscosity for stable electrospinning was thus ideally obtained by preparing a new sol. We can thus conclude that not only the viscosity and the relative concentrations determine the spinnability of the siloxane sols, but the degree of crosslinking has a major influence as well. An in-depth study hereof via various characterization techniques will be carried out in the following chapter. Additionally, the resistance of these silica nanofibers to high temperatures (up to 1000°C) was confirmed and their interesting changes from hydrophobic to hydrophilic upon heat treatment and aging were reported.

References

[1] T. Yamaguchi, S. Sakai, and K. Kawakami, "Application of silicate electrospun nanofibers for cell culture," *J. Sol-Gel Sci. Technol.*, vol. 48, no. 3, pp. 350–355, 2008.

[2] K. Iimura, T. Oi, M. Suzuki, and M. Hirota, "Preparation of silica fibers and non-woven cloth by electrospinning," *Adv. Powder Technol.*, vol. 21, no. 1, pp. 64–68, Jan. 2010.

[3] S. Choi and S. G. O. O. Lee, "Silica nanofibers from electrospinning / sol-gel process," *J. Mater. Sci. Lett.*, vol. 22, pp. 891–893, 2003.

[4] S. Choi, "Titania-Doped Silica Fibers Prepared by Electrospinning and Sol-Gel Process," *J. Sol-Gel Sci. Technol.*, vol. 30, pp. 215–221, 2004.

[5] Y. Xu, W. Zhou, L. Zhang, and L. Cheng, "Spinnability and crystallizability of silica glass fiber by the sol-gel method," *J. Mater. Process. Technol.*, vol. 101, pp. 46–48, 2000.

[6] S. Ramakrishna, K. Fujihara, W. E. Teo, T.-C. Lim, and Z. Ma, *An introduction to electrospinning and nanofibers*. 2005.

[7] Z. M. Huang, Y. Z. Zhang, M. Kotaki, and S. Ramakrishna, "A review on polymer nanofibers by electrospinning and their applications in nanocomposites," *Compos. Sci. Technol.*, vol. 63, no. 15, pp. 2223–2253, 2003.

[8] J. H. Wendorff, S. Agarwal, and A. Greiner, *Electrospinning: Materials, Processing and Applications*. 2012.

[9] C. Mit-uppatham, M. Nithitanakul, and P. Supaphol, "Ultrafine electrospun polyamide-6 fibers: Effect of solution conditions on morphology and average fiber diameter," *Macromol. Chem. Phys.*, vol. 205, no. 17, pp. 2327–2338, 2004.

[10] S. De Vrieze, P. Westbroek, T. Van Camp, and K. De Clerck, "Solvent system for steady state electrospinning of polyamide 6.6," *J. Appl. Polym. Sci.*, vol. 115, pp. 837–842, 2010.

[11] V. Jacobs, R. Anandjiwala, and M. Maaza, "The influence of electrospinning parameters on the structural morphology and diameter of electrospun nanofibers," *J. Appl. Polym. Sci.*, vol. 115, pp. 3130–3136, 2010.

[12] L. Van Der Schueren, B. De Schoenmaker, Ö. I. Kalaoglu, and K. De Clerck, "An alternative solvent system for the steady state electrospinning of polycaprolactone," *Eur. Polym. J.*, vol. 47, no. 6, pp. 1256–1263, 2011.

[13] B. De Schoenmaker, L. Van Der Schueren, Ö. Ceylan, and K. De Clerck, "Electrospun polyamide 4.6 nanofibrous nonwovens: Parameter study

and characterization," *J. Nanomater.*, vol. 2012, 2012.

[14] D. Li, J. T. McCann, Y. Xia, and M. Marquez, "Electrospinning: A simple and versatile technique for producing ceramic nanofibers and nanotubes," *J. Am. Ceram. Soc.*, vol. 89, no. 6, pp. 1861–1869, 2006.

[15] Y. Dai, W. Liu, E. Formo, Y. Sun, and Y. Xia, "Ceramic nanofibers fabricated by electrospinning and their applications in catalysis, environmental science, and energy technology," *Polym. Adv. Technol.*, vol. 22, no. 3, pp. 326–338, 2011.

[16] S. W. Lee, Y. U. Kim, S. S. Choi, T. Y. Park, Y. L. Joo, and S. G. Lee, "Preparation of SiO2/TiO2 composite fibers by sol-gel reaction and electrospinning," *Mater. Lett.*, vol. 61, no. 3, pp. 889–893, 2007.

[17] B. Smith, *Infrared spectral interpretation: a systematic approach*. Boca Raton, Florida: CRC Press, 1999.

[18] T. Pirzada, S. a. Arvidson, C. D. Saquing, S. S. Shah, and S. a. Khan, "Hybrid silica-PVA nanofibers via sol-gel electrospinning," *Langmuir*, vol. 28, no. 13, pp. 5834–5844, 2012.

[19] P. Innocenzi, "Infrared spectroscopy of sol-gel derived silica-based films: A spectra-microstructure overview," *J. Non. Cryst. Solids*, vol. 316, no. 2–3, pp. 309–319, 2003.

[20] B. Siboulet, B. Coasne, J.-F. Dufrêche, and P. Turcq, "Hydrophobic transition in porous amorphous silica," *J. Phys. Chem. B.*, vol. 115, pp. 7881-7886, 2011.

[21] J. Laskowski and J. a. Kitchener, "The hydrophilic—hydrophobic transition on silica," *J. Colloid Interface Sci.*, vol. 29, no. 4, pp. 670–679, 1969.

4

In-depth study of critical sol preparation parameters influencing electrospinning

The previous chapter suggested the impact of the degree of crosslinking on the electrospinning process of TEOS sols. Therefore, this chapter focuses on a more in-depth characterization of the critical sol parameters influencing electrospinning. The optimum degree of crosslinking, amount of ethanol and size of the colloidal species in the sols necessary for stable electrospinning are determined using ^{1}H NMR, ^{29}Si NMR, ATR-FTIR and DLS.

Parts of this chapter are published in:

J. Geltmeyer, J. De Roo, F. Van den Broeck, J. C. Martins, K. De Buysser, and K. De Clerck, "The influence of tetraethoxysilane sol preparation on the electrospinning of silica nanofibers," *J. Sol-Gel Sci. Technol.*, vol. 77, no. 2, pp. 453–462, 2016.

4.1 Introduction

Chapter 3 demonstrated that uniform silica nanofibers can be produced in a stable and reproducible manner without the use of an organic polymer. It was also established that the preparation procedure of the sol influences the electrospinning process. This indicates that other critical parameters, such as the concentration of ethanol, the size of colloidal species and the degree of crosslinking, influence the viscosity and thus the stability of the electrospinning process (Figure 4.1).

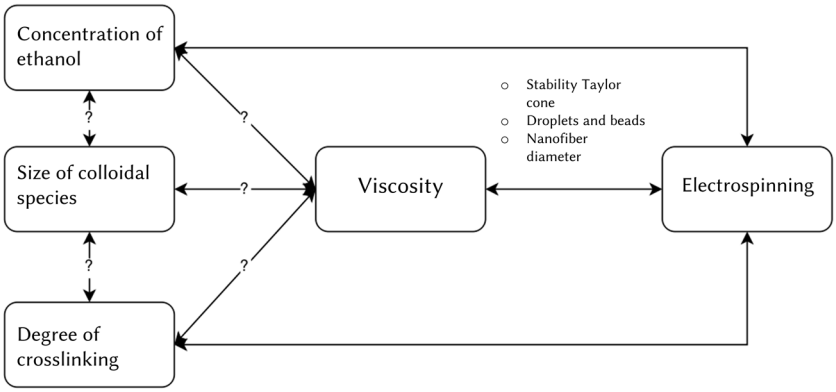

Figure 4.1 Schematic overview of the sol parameters influencing the viscosity and the electrospinning process

To clearly separate the contributions of the critical parameters, three different sol preparation set-ups are compared in this chapter (Figure 2.4, see Chapter 2). An open system was used in Chapter 3 and is the most practical set-up. However, in this set-up the influence of the degree of crosslinking and the concentration of ethanol on the electrospinning process cannot be separated. The closed system with a Liebig cooler (a distillation set-up) is similar to the open system since the crosslinking and ethanol evaporation occur at the same time, both resulting in an increased sol viscosity. However, in contrast to the open system, the evaporation of ethanol during sol preparation can be monitored. A closed system with a reflux condenser or Allihn set-up, keeps the ethanol in the system. Ethanol is removed afterwards via a rotary evaporator to obtain a viscous sol necessary for electrospinning. In this way both parameters, degree of crosslinking and ethanol concentration, can be examined separately. By controlling the reaction conditions, the rheological properties of the sol

can be controlled, allowing electrospinning without addition of an organic polymer.

To evaluate these different critical parameters multiple characterization techniques are used, namely Nuclear Magnetic Resonance spectroscopy (both ^{1}H NMR and ^{29}Si NMR), Attenuated Total Reflectance - Fourier Transform Infrared spectroscopy (ATR-FTIR) and Dynamic Light Scattering (DLS). The degree of crosslinking of the sols will be studied in-depth via ATR-FTIR and ^{29}Si NMR. Previously, multiple research groups [1]–[8] performed ^{29}Si NMR studies on sols with varying compositions and H_2O/Si molar ratios *r*. Brinker *et al* [1] conducted ^{29}Si NMR measurements on silica sols for conventional fiber drawing. Malay *et al* [7] and Sadasivan *et al* [8] combined ^{29}Si NMR and DLS for a detailed study of the effect of the solvent on silica synthesis. An in-depth study, however, on pure sols (without organic polymer) used for electrospinning is still missing. In addition to the degree of crosslinking, both the amount of ethanol evaporated from the sols as well as the concentration of ethanol still present in the sols after evaporation is monitored. Using the Liebig set-up, the former is determined from the collected volume of ethanol, while the latter is determined via ^{1}H NMR of the remaining sol. Finally, the size of the colloidal species in the sols is studied using DLS. By combining the results of the three different set-ups studied via DLS, ^{29}Si NMR, ^{1}H NMR and ATR-FTIR the influence of the critical parameters on the viscosity and thus the electrospinning process is thoroughly characterized, which is vital for fully exploiting the potential of these nanofibrous membranes.

4.2 Materials and Methods

Three different systems, one open and two closed, were used for the preparation of the sols (Section 2.2.1, Chapter 2). Samples prepared via the open system, via the Liebig set-up, via the Allihn set-up before ethanol evaporation or via the Allihn set-up after ethanol evaporation will be denoted respectively with the letters O, L, A or Ae followed by the viscosity of the sol or the reaction time.

For the Nuclear Magnetic Resonance (NMR) measurements, the sols were diluted with 10% D_2O for locking purposes and 600 µL was put in a 5mm NMR tube. All measurements were recorded on a Bruker Avance III Spectrometer equipped with a BBI-Z probe and operating at a ^{1}H and ^{29}Si

frequency of 500.13 MHz and 99.36 MHz respectively. The sample temperature was set to 298.2 K. One dimensional (1D) ^{29}Si quantitative spectra were acquired with inverse gated 1H decoupling using a zggpseig pulse spin-echo sequence. This sequence was chosen in order to maximize signal intensities and avoid residual background ^{29}Si signal from the glass of the NMR tube. Throughout all measurements, 29840 data points were sampled with the spectral width set to 450 ppm around a carrier frequency of 0 ppm and a relaxation delay of 60 sec. The number of scans was set to 200 and the number of dummy scans to 4. This results in a total measuring time of 3.5 h, which gave a good signal to noise ratio without giving the samples sufficient time to gelate. For the quantitative 1D ^{1}H measurements, 64k data points were sampled with the spectral width set to 16 ppm and a relaxation delay of 30 sec. Concentrations were obtained using the Digital ERETIC method. Deconvolution of the ^{29}Si spectra was achieved by fitting an appropriate number of Gaussians to the spectra with IGOR pro. ^{1}H NMR and ^{29}Si NMR spectroscopy and detailed data analysis were performed by the NMR and Structure Analysis group at the Department of Organic and Macromolecular Chemistry.

For Dynamic Light Scattering (DLS) a Malvern Nano ZS was used in backscattering mode (173°).

4.3 Characterization of TEOS sols

A thorough study of the amount of ethanol, size of colloidal species and degree of crosslinking is one of the goals of the present chapter. As introduced above, three different sol preparation set-ups are compared to clearly separate the contributions of the critical parameters. An overview of the advantages and disadvantages of the three different set-ups is given in Table 4.1.

Table 4.1 Advantages and disadvantages of the different set-ups

Open system	Closed systems	
	Liebig set-up	**Allihn set-up**
+ fast	+ fast	– slow
– no control	+ control	+ control
– evaporation of ethanol and crosslinking at the same time	– evaporation of ethanol and crosslinking at the same time	+ separate evaporation of ethanol and crosslinking
+ simple and practical	+ similar to the open system	– additional ethanol evaporation step needed

4.3.1 Degree of crosslinking

Via ATR-FTIR and ^{29}Si NMR spectroscopy the degree of crosslinking in the sols and the influence on viscosity is investigated. An overview of the assignment of the different peaks for ATR-FTIR spectra is given in Table 4.2 [9]–[11].

Table 4.2 Peak assignment ATR-FTIR spectra [9]-[11]

Wavenumber (cm^{-1})	Assignment
3324	OH stretch
2974	CH_3CH_2
2894	CH_3CH_2
1383	CH_3 bend/OH bend
1154	Si–O–C/C–O–C/CH_3
1076	Si–O–Si Asymm stretch
1044	C–C–O Asymm stretch
966	Silanol Si–OH stretch
880	C–C–O Symm stretch
795	Si–O–Si Symm stretch
582	OH out of plane bend
431	Si–O–Si bend

To describe a Si network Q^n notation is typically used, where *n* is the number of bridging oxygen atoms per Si atom. The ^{29}Si NMR spectra of the sols show resonances in three different regions: Q^2 species from –90 ppm to –97 ppm, Q^3 species from –98 ppm to –105 ppm and Q^4 species from –105 to –115 ppm [12],[13]. When the sum of two spectra of the same sample is taken the noise on the spectrum diminishes (higher resolution), but the

small peaks on top of the larger, broader peaks are still visible and they can thus be attributed to slightly different Q species (Figure 4.2 a,c). In this PhD ^{29}Si NMR is used to focus on the changes in relative ratios of Q^2, Q^3 and Q^4 species. More details on the detailed assignments of these different Q species can be found in literature [6],[13],[14]. Most importantly, the reproducibility of all sols via the three set-ups is confirmed by both ATR-FTIR and ^{29}Si NMR (Figure 4.2).

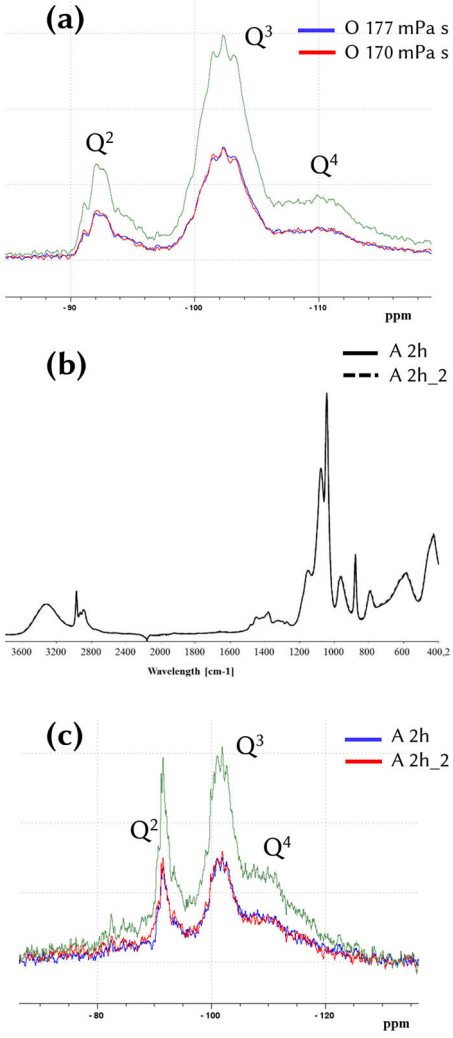

Figure 4.2 The ^{29}Si NMR spectra of two sols having a viscosity of 177 and 170 mPa·s prepared via the open system coincide (a), spectra of two sols with a

reaction time of 2 h prepared in the Allihn set-up coincide as well: ATR-FTIR spectra (b) and ^{29}Si NMR spectra (c). The green spectrum represents the sum of the red and blue spectrum (a) and (c).

4.3.1.1 Open system and Liebig set-up

ATR-FTIR spectra of sols prepared in the open system with varying viscosities are compared, as illustrated in Figure 4.3 for the 10 mPa·s and the 170 mPa·s samples. Clear differences in peak height can be seen for the sols with different viscosities. At 431 cm^{-1}, corresponding with the Si–O–Si bend, an increase in peak height is seen with increasing viscosity. This points to increased crosslinking. The differences in peak heights in the region 1200-700 cm^{-1} can be ascribed to a different degree of crosslinking or to a difference in ethanol concentration. Indeed, the peaks of Si–O–Si at 1076 cm^{-1} and of C–C–O at 1044 cm^{-1} overlap. Additionally, the broad peak at 3324 cm^{-1} originating from the O-H stretch decreases with increasing viscosity. This might be due to the evaporation of ethanol or by the condensation of Si–OH in Si-O-Si, and thus higher crosslinking. ATR-FTIR hints at an increased crosslinking with increasing viscosity, but other techniques are necessary to draw unambiguous conclusions.

Therefore, the same sols were investigated via solution ^{29}Si NMR, see Figure 4.3 b. The amount of Q^3 and Q^4 species increases with an increased sol viscosity, thus confirming the increased degree of crosslinking with increasing viscosity. Figure 4.4 a illustrates the trend for the Liebig set-up to be similar to the open system; again a higher viscosity leads to more Q^3 and Q^4 species.

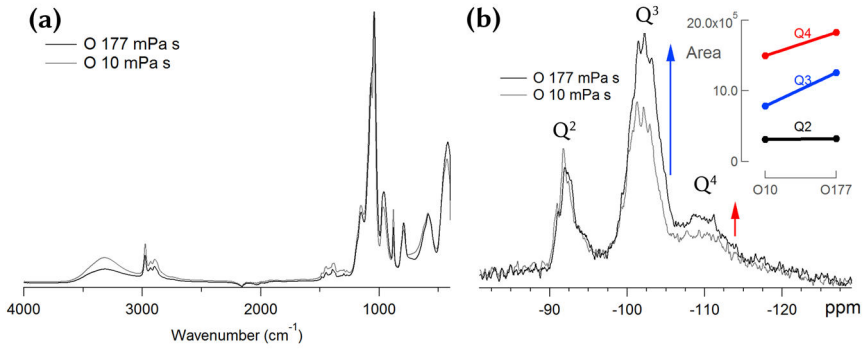

Figure 4.3 ATR-FTIR (a) and ^{29}Si NMR spectra of sols with a viscosity of 10 mPa s (reaction time (RT): 87 min) and 177 mPa·s (RT: 110 min and c_{EtOH}: 8.7 M) prepared in the open system, inset: area of fitted Gaussian curves (b)

It is observed that when a sol with a viscosity that is too high is diluted to an optimum viscosity, the electrospinning results are different than for sols that have the correct viscosity from the start (Chapter 3). The spectrum of a sample with a reference viscosity of 158 mPa·s (stable region) is compared to a sample with a viscosity of 682 mPa·s diluted to this reference viscosity, Figure 4.4 b. The diluted sample has more Q^4 and therefore a higher degree of crosslinking. Therefore, it can be concluded that a dilution with ethanol can decrease the viscosity but the crosslinking of the sols remains intact.

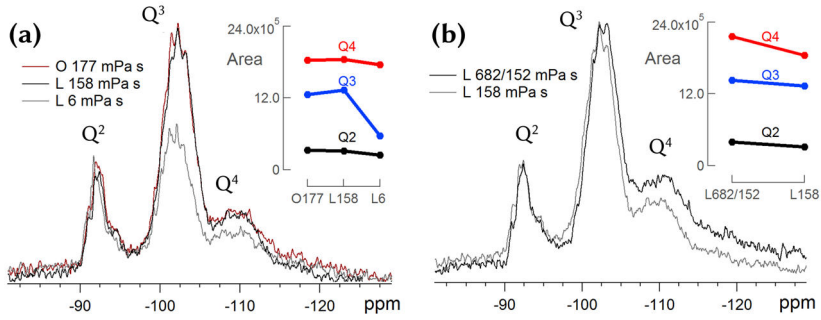

Figure 4.4 ^{29}Si NMR spectra of sols prepared in the open system (177 mPa·s, reaction time (RT): 110 min and c_{EtOH}: 8.7 M) and Liebig set-up (6 mPa s, RT: 110 min, c_{EtOH}: 11.5 M; 158 mPa s, RT: 180 min, c_{EtOH}: 9.3 M) , inset: area of fitted Gaussian curves (a), and ^{29}Si NMR spectra of diluted (682 mPa s diluted to 152 mPa s, RT: 180 min, c_{EtOH}: 9,1 M) and undiluted sol (158 mPa s, RT: 180 min, c_{EtOH}: 9,3 M) prepared in the Liebig set-up, inset: area of fitted Gaussian curves (b)

4.3.1.2 Allihn set-up

ATR-FTIR provides more reliable information for the sols prepared via the Allihn set-up since all samples have the same concentration of ethanol. With an increasing reaction time (RT) the peaks at 980 cm^{-1} (Si-OH bonds, Table 4.2) show a clear decrease, which may be ascribed to an increasing degree of crosslinking, Figure 4.5 a.

A complementary characterization of the degree of crosslinking and the Q species present in the sols is executed via ^{29}Si NMR. When comparing sols prepared in the Allihn set-up with increasing reaction times important changes in crosslinking degree are determined (Figure 4.5 b). Firstly, the amount of Q^2 species decreases drastically when the reaction time is increased from 30 min to 24 h. Secondly, the amount of Q^3 species stays practically constant, but a shift in the Q^3 peak is seen. With increasing

reaction time different Q^3 species seem to be formed and the amount of Q^4 increases as well. In conclusion, the increased crosslinking degree with increased viscosity or increased reaction time is confirmed for all set-ups. The influence hereof on the electrospinning process and resulting nanofibers is discussed later.

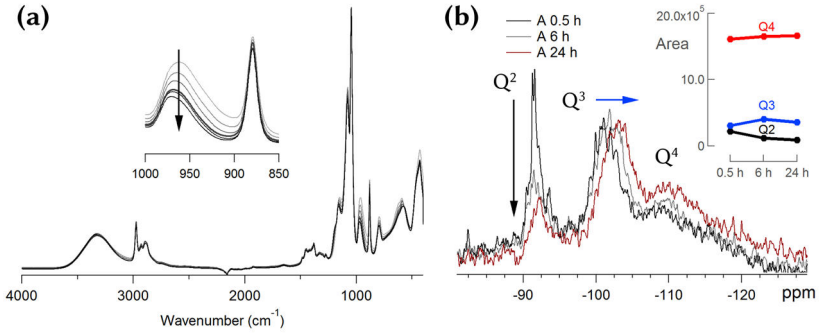

Figure 4.5 ATR-FTIR spectra of sols prepared in the Allihn set-up with increasing reaction times (a), ^{29}Si NMR spectra of Allihn sols with increasing reaction time (RT: 0.5 h, c_{EtOH}: 13.4 M; RT: 6 h, c_{EtOH}: 13.1 M ; RT: 24 h, c_{EtOH}: 13.3 M), inset: area of fitted Gaussian curves (b)

4.3.2 Evaporation of ethanol

Both the amount of solvent evaporated and the amount of ethanol still present in the sols after evaporation are determined. When preparing sols via the open system it was clearly visible that the volume of the solution diminishes, due to the evaporation of the solvent. Using the Liebig set-up the evaporated solvent was collected and monitored in time. Both the reaction time and the amount of solvent evaporated were studied as a function of the viscosity of the sols prepared in the Liebig set-up (Figure 4.6). A slow increase in viscosity is seen with increasing reaction time until a viscosity of around 180 mPa·s is attained, followed by a very sharp increase on further heating. Together with this, evaporation of the solvent commences from the start of the reaction with an almost linear increase of the amount of condensate. However, once a reaction time of 150 min or a viscosity around 80 mPa·s is attained the evaporation of solvent slows down. The initial stage of the viscosity increase of the sols can thus be attributed to the evaporation of ethanol. Once a critical amount of ethanol is evaporated and ethanol evaporation stagnates, further increases in sol

viscosity may be attributed to crosslinking. To obtain a sol with an optimum viscosity for electrospinning the amount of solvent evaporated has to be 37 ± 1 g, if started with a ± 72 mL solution.

Using the Allihn set-up it was possible to keep the ethanol in the system. Different reaction times of the sols were evaluated, namely 0.5 h, 2 h, 6 h, 12 h, 24 h and 48 h. For these samples a constant viscosity of 2-3 mPa·s was measured. To obtain electrospinnable sols from the Allihn set-up, a certain critical amount of ethanol has to be evaporated using a rotary evaporator.

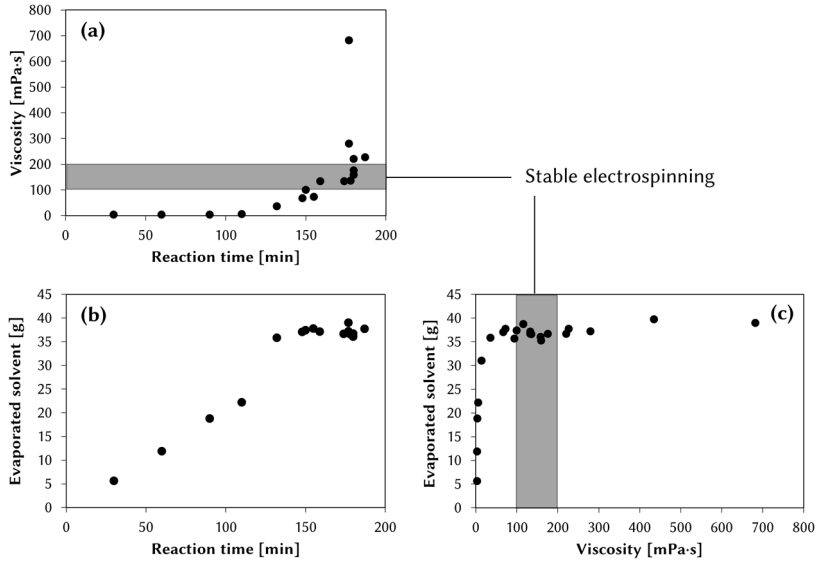

Figure 4.6 Viscosity increase Liebig sols as a function of reaction time (a) and amount of solvent evaporated as a function of reaction time (b) and viscosity of the sols (c)

The amount of ethanol still present in the sols after evaporation of the solvent was measured via ^{1}H NMR for the sols prepared via all three set-ups. The sols prepared via the Allihn set-up have a constant amount of ethanol; 13.3 $\pm$ 0.2 mol.L^{-1}, which corresponds to the initial ethanol concentration, after hydrolysis, at 13.4 mol.L^{-1}. In addition, a sol prepared using the Liebig set-up with a reaction time of 30 min also shows an ethanol concentration of 13.4 mol.L^{-1}. This is expected since almost no ethanol is evaporated after 30 min. The electrospinnable sols, which includes sols prepared via the open system, Liebig set-up and Allihn set-

up after evaporation via the rotary evaporator, all had a concentration of ethanol around 9 mol L^{-1}. To conclude, an optimum amount of solvent has to be evaporated to obtain viscous electrospinnable sols. Moreover, for all three systems the same threshold concentration of ethanol, 9 mol.L^{-1}, was found to obtain electrospinnable sols.

4.3.3 Size of colloidal species

Additional information on the size of colloidal species in the sols is obtained using DLS. Both for the Liebig and Allihn set-up a clear growth in colloidal particle size with increasing reaction time is seen, Figure 4.7. These results are in line with the general theory of polymerization of silica proposed by Iler [15],[16] and described in Chapter 1. In acidic solutions particles are formed, which then aggregate into three dimensional networks which leads to a viscosity increase.

The particle size in Liebig sols increases faster due to simultaneous ethanol evaporation (Figure 4.7 a). The particle size in sols prepared via the Allihn condenser raises slower (Figure 4.7 b). The particle size increases from around 2.5 nm for a sol with a reaction time of 30 min to a particle size of around 7.0 nm for the sol with a reaction time of 48 h. Both the degree of crosslinking (see above) and the size of the particles increase with reaction time. Moreover, the size of the colloidal particles after ethanol evaporation remains mostly unaltered (Figure 4.7 b). It can thus be stated that there is little or no influence of ethanol evaporation using a rotavapor on the final sols.

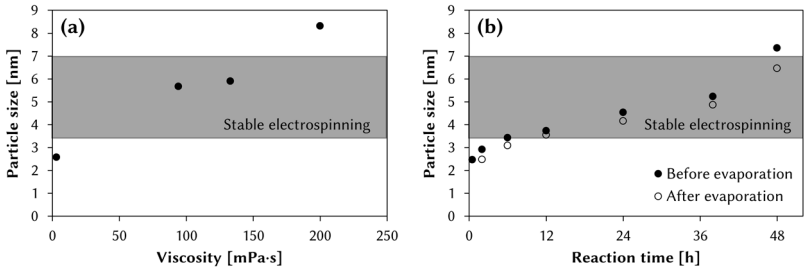

Figure 4.7 Colloidal particle size in the sols prepared via the Liebig set-up (a) and Allihn set-up (b)

4.4 Influence of critical parameters on morphology and stability in time of the nanofibers

A profound view on the degree of crosslinking, size of the colloidal species and amount of ethanol in the sols prepared via three different set-ups was obtained. All of these parameters show to have an influence on the electrospinning process. An overview on the electrospinning stability of the sols prepared with the open system, Liebig set-up and Allihn set-up is provided in Table 4.3. For the Allihn set-up we make a distinction between the sols before (A1, A2, …) and after (A1e, A2e, …) evaporation of ethanol. Based on their electrospinning stability and the resulting nanofibers the sols are divided in four different zones: --, ++, + and -. Figure 4.8 gives an overview of the links between the critical parameters and their optimum values.

The first zone, indicated with --, corresponds with sols which were not electrospinnable, only drops were deposited on the collector plate. These sols all have a viscosity that is too low, below 50 mPa·s, for electrospinning. Even the samples with a high degree of crosslinking (A5-A12) and sizes of colloidal species ranging in between 3 and 7 nm, were not electrospinnable when the viscosity was too low.

A second zone, indicated by +, corresponds with a highly stable Taylor cone in time, however, further crosslinking of the nanofibers took place after deposition of the nanofibers on the collector plate (Figure 4.9 a,b). These sols, A3e-A6e, prepared in the Allihn set-up with a reaction time between 2 and 6 hours have a high amount of Q^2 species and a lower amount of Q^3/Q^4 species compared to sols with a higher reaction time (Figure 4.5 b). In addition, particle sizes in between 2 and 3.5 nm are recorded. A high amount of Q^2 species and small particle sizes thus results in highly stable electrospinning. But, it results in further crosslinking of the nanofibers after deposition on the collector plate, which is negative for the stability of the fibrous web.

Table 4.3 Electrospinning stability of sols prepared via the Allihn, Liebig set-up and open system

Allihn set-up							**Liebig set-up**			**Open system**		
	Reaction time (h)	**ES⁺**		**Reaction time (h)**	**η^***	**ES⁺**		**η^***	**ES⁺**		**η^***	**ES⁺**
A1	0.5	--	A1e	0.5	3	--	L1	3	--	O1	17	--
A2	2	--	A2e	2	37	--	L2	36	--	O2	65	-
A3	2	--	A3e	2	61	+	L3	73	-	O3	82	-
A4	2	--	A4e	2	122	+	L4	100	++	O4	118	++
A5	6	--	A5e	6	59	+	L5	116	++	O5	136	++
A6	6	--	A6e	6	294	+	L6	133	++	O6	152	++
A7	12	--	A7e	12	75	++	L7	136	++	O7	161	++
A8	12	--	A8e	12	104	++	L8	153	++	O8	183	++
A9	24	--	A9e	24	50	++	L9	158	++	O9	198	++
A10	24	--	A10e	24	61	++	L10	160	++	O10	260	-
A11	24	--	A11e	24	165	++	L11	280	-	O11	398	-
A12	48	--	A12e	48	102	-	L12	435	-	O12	981	-

*unit η [mPa·s] ⁺ ES = electrospinning stability

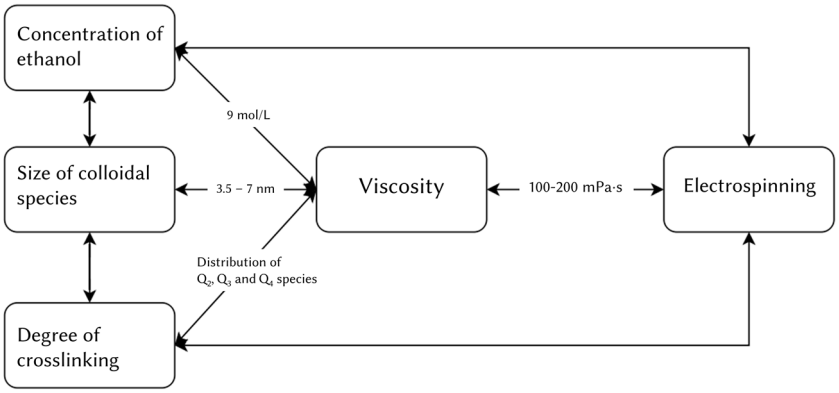

Figure 4.8 Parameters influencing the electrospinning process and their optimum values necessary for stable electrospinning resulting in uniform, beadless nanofibers stable in time.

The sols in zone ++ had a less stable electrospinning behavior compared to zone +. However, the nanofibers showed to be stable in time, with no further crosslinking taking place. The sols prepared in the Allihn set-up with a reaction time of 12 and 24 hours and the sols prepared in the Liebig set-up and open system having a viscosity in between 100 and 200 mPa·s can be classified in this zone. Via ^{29}Si-NMR and DLS a higher degree of crosslinking and increased particles sizes, in between 3.5 nm and 7 nm, were observed (Figure 4.3 b, 4.5 b and 4.7). These reduced the electrospinning stability of the sols, but optimized the stability in time of the resulting nanofibers.

The samples prepared via the Liebig set-up L4-L9 were electrospinnable in the same viscosity range as the sols prepared via the open system, 100-200 mPa·s. The electrospinning of these sols resulted in uniform, beadless nanofibers (Figure 4.10 c). The same trends are seen for sols prepared via the Allihn set-up (A3e-A12e), uniform and beadless nanofibers are obtained for viscosities above 100 mPa·s (Figure 4.9 c). Due to the stable electrospinning and high stability in time of the resulting nanofibers, this zone is seen as the optimum for the electrospinning of silica nanofibers. The sols in this zone were used for further upscaling of the electrospinning process. Continuous electrospinning during 3 hours on a large rotating drum resulted in large, uniform and flexible silica nanofibrous nonwovens, Figure 4.11.

In the last zone, -, electrospinning stability was less stable and beaded fibers or thicker fibers were obtained. Samples prepared in the Liebig set-up and Allihn set-up with a viscosity higher than 200 mPa·s or a high degree of crosslinking and thus a particle size exceeding 7 nm show this reduced electrospinning stability. Also the electrospinning of sols with viscosities lower than 100 mPa·s (L2, L3) was less stable, with sometimes drop formation. Moreover, the electrospinning resulted in beaded nanofibers (Figure 4.10 a,b).

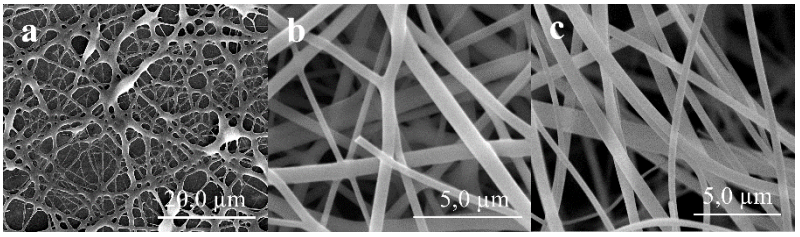

Figure 4.9 SEM images of nanofibers prepared from sols produced via the set-up with Allihn condenser a: 2h 122 mPa·s, b: 6h 294 mPa·s, c: 24h 165 mPa·s

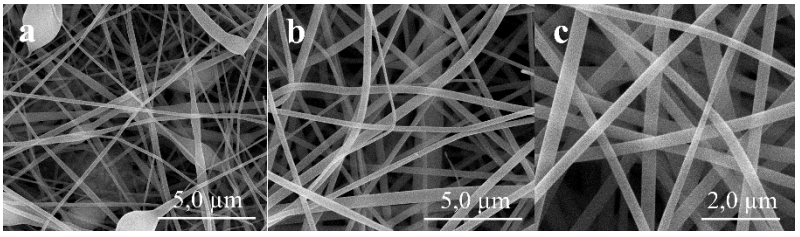

Figure 4.10 SEM images of nanofibers prepared from sols produced via the Liebig set-up a: 36 mPa·s, b: 73 mPa·s, c: 158 mPa·s.

Alongside its influence on the electrospinning stability, the viscosity also has a big influence on the resulting nanofibers and nanofiber diameters. The nanofiber diameters of Liebig and Allihn sols are evaluated and compared to the open system (Figure 4.12). In general, the same trends are observed for nanofibers obtained via all three set-ups. Nanofibers obtained from sols having a viscosity in between 100 and 200 mPa·s have nanofiber diameters around 200-300 nm. The nanofibers obtained from sols with viscosities below 100 mPa·s deviate more due to beads and non-uniformity's present. Above 200 mPa·s an increasing diameter is seen with an increase in viscosity. It is known that solution viscosity has a great effect on the nanofiber diameters, initiating droplet shape and jet instability [17],[18].

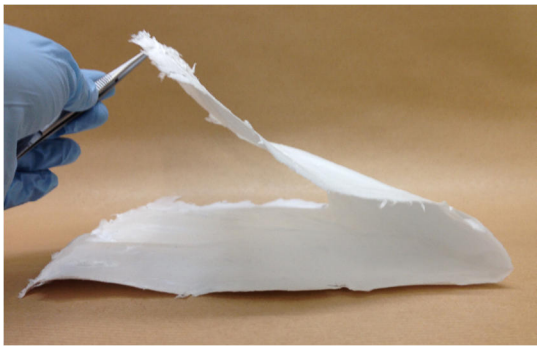

Figure 4.11 Picture of large (30x20 cm) flexible silica nanofibrous sample

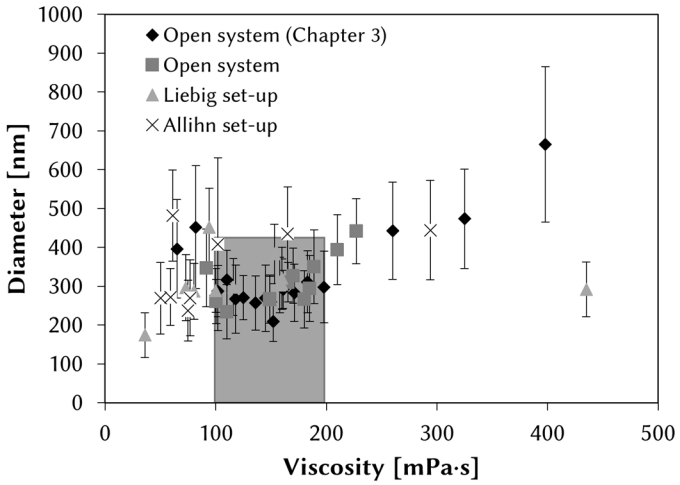

Figure 4.12 Nanofiber diameters as a function of the viscosity for sols prepared via the three set-ups, focus (frame) is given to the samples prepared in the stable viscosity region.

Thus these results indicate that apart from the viscosity, both the degree of crosslinking and the size of colloidal particles have an influence on the electrospinning behavior. Moreover, both parameters seem to be closely related. The higher the amount of Q^2 species and the smaller the colloidal particles, the more stable electrospinning is seen. But a certain degree of crosslinking is necessary to obtain uniform nanofibers which are stable after deposition. The viscosity seems to be the critical parameter determining the nanofiber diameters. Via all three set-ups it was thus possible to produce uniform, beadless nanofibers when all parameters (viscosity, degree of crosslinking, particle size and ethanol concentration)

are within the appropriate boundaries. Moreover, the feasibility of upscaling of the process was confirmed.

4.5 Conclusion

A more detailed characterization of the sol parameters influencing the electrospinning process was carried out in this chapter. All parameters: colloidal particle sizes, solvent concentration, degree of crosslinking and viscosity show to have an influence on the electrospinning process. Starting from a viscosity of 50 mPa·s nanofibers could be obtained, however the optimum viscosity stays in between 100 and 200 mPa·s for all sols, which is in line with the results in Chapter 3. A concentration of ethanol of 9 $mol.L^{-1}$ in the sols seems to be optimal for electrospinning. Additionally, the degree of crosslinking and the particle size have an important influence on the stability of the electrospinning process. Moreover, both parameters seemed to be related. The most stable electrospinning processes are achieved when the particles are small (<3.5 nm) and a high amount of Q^2 species is available. With increasing particle sizes and increasing crosslinking (thus decreasing Q^2 species) electrospinning becomes less stable. However, a certain degree of crosslinking and size of colloidal particles is necessary to obtain no further linking of the nanofibers after deposition. As a consequence, an optimum degree of crosslinking and particle size (3.5-7 nm) exists resulting in a stable electrospinning process and uniform, beadless nanofibers which stay stable in time. Further increasing the viscosity and particle sizes resulted in less stable electrospinning behavior. Moreover, all set-ups used for sol preparation allow for reproducible electrospinning, with the open set-up being most preferred as it is easy, practical and the fastest in use.

In conclusion, by controlling all parameters successful electrospinning was carried out of pure TEOS sols. This enabled upscaling, which resulted in the production of larger, flexible silica nanofibrous membranes. As a consequence these sols can now be further used and evaluated for various end applications, with a focus on active and sensitive membranes in this PhD. TEOS sols and silica nanofibers will be functionalized with TiO_2 nanoparticles and their value for water treatment applications is studied in Chapter 5. Functionalization with dyes is carried out in Chapter 6 and Chapter 7, aiming at the production of colorimetric sensor materials.

References

[1] C. J. Brinker and R. a Assink, "Spinnability of silica sols: structural and rheological criteria," vol. 111, pp. 48–54, 1989.

[2] S. Sakka and T. Yoko, "Fibers from gels," *J. Non Cryst. Solids*, vol. 148, pp. 394–403, 1992.

[3] S. Sakka and H. Kozuka, "Rheology of sols and fiber drawing," *J. Non. Cryst. Solids*, vol. 100, pp. 142–153, 1988.

[4] J. C. Pouxviel, J. P. Boilot, J. C. Beloeil, and J. Y. Lallemand, "NMR study of the sol/gel polymerization," *J. Non. Cryst. Solids*, vol. 89, pp. 345–360, 1987.

[5] A. Depla, E. Verheyen, A. Veyfeyken, M. Van Houteghem, K. Houthoofd, V. Van Speybroeck, M. Waroquier, C. E. a Kirschhock, and J. a. Martens, "UV-Raman and 29Si NMR spectroscopy investigation of the nature of silicate oligomers formed by acid catalyzed hydrolysis and polycondensation of tetramethylorthosilicate," *J. Phys. Chem. C*, vol. 115, no. 22, pp. 11077–11088, 2011.

[6] A. Depla and D. Lesthaeghe, "29Si NMR and UV– Raman Investigation of Initial Oligomerization Reaction Pathways in Acid-Catalyzed Silica Sol–Gel Chemistry," *J. Phys. Chem. C*, vol. 115, pp. 3562–3571, 2011.

[7] O. Malay, I. Yilgor, and Y. Z. Menceloglu, "Effects of solvent on TEOS hydrolysis kinetics and silica particle size under basic conditions," *J. Sol-Gel Sci. Technol.*, vol. 67, no. 2, pp. 351–361, 2013.

[8] S. Sadasivan, A. K. Dubey, Y. Li, and D. H. Rasmussen, "Alcoholic solvent effect on silica synthesis - NMR and DLS investigation," *J. Sol-Gel Sci. Technol.*, vol. 12, no. 1, pp. 5–14, 1998.

[9] T. Pirzada, S. a. Arvidson, C. D. Saquing, S. S. Shah, and S. a. Khan, "Hybrid silica-PVA nanofibers via sol-gel electrospinning," *Langmuir*, vol. 28, no. 13, pp. 5834–5844, 2012.

[10] B. Smith, *Infrared spectral interpretation: a systematic approach*. Boca Raton, Florida: CRC Press, 1999.

[11] P. Innocenzi, "Infrared spectroscopy of sol-gel derived silica-based films: A spectra-microstructure overview," *J. Non. Cryst. Solids*, vol. 316, no. 2–3, pp. 309–319, 2003.

[12] E. K. F. Bahlmann, R. K. Harris, and B. J. Say, "Method for the Quantification of Silicon-29 NMR Spectra , Developed for Viscous Silicate Solutions," *Magn. Reson. Chem.*, vol. 31, pp. 266–267, 1993.

[13] J. A. Schwarz and C. I. Contescu, *Surfaces of nanoparticles and porous*

materials. New York: Marcel Dekker, 1999.

[14] A. V McCormick, A. T. Bell, and C. J. Radke, "Quantitative determination of siliceous species in sodium silicate solutions by silicon-29 NMR spectroscopy," vol. 7, no. 3, pp. 183–190, 1987.

[15] C. J. Brinker and G. W. Scherer, *Sol-Gel Science: The Physics and Chemistry of Sol-Gel Processing*. 1990.

[16] R. K. Iler, *The chemistry of silica: solubility, polymerization, colloid and surface properties and biochemistry of silica.* New York: Wiley, 1979.

[17] A. Greiner and J. H. Wendorff, "Electrospinning: A fascinating method for the preparation of ultrathin fibers," *Angew. Chemie - Int. Ed.*, vol. 46, no. 30, pp. 5670–5703, 2007.

[18] J. H. He, Y. Liu, L. F. Mo, Y. Q. Wan, and L. Xu, *Electrospun nanofibers and their applications*. Shawbury, UK: Smithers Rapra Technology, 2008.

5

Active membranes: TiO_2 functionalized nanofibers for water treatment

Immobilization of titanium dioxide nanoparticles on a porous support such as a nanofibrous membrane can be highly valuable for water treatment. The removal of micro pollutants, such as the herbicide isoproturon, is an actual concern in water treatment today. In this chapter, widely available commercial TiO_2 nanoparticles are immobilized on both polyamide 6 and silica nanofibrous membranes via two techniques, namely inline functionalization and dip-coating. The TiO_2 loading is quantified and the photocatalytic activity is characterized by decoloring of Methylene Blue. The high value of TiO_2 functionalized nanofibrous membranes for organic (micro)pollutants removal is shown through a complete degradation of isoproturon.

Parts of this chapter are published in:

J. Geltmeyer, H. Teixido, M. Meire, K. Deventer, L. Balcaen, S. Van Hulle, K. De Buysser, and K. De Clerck, "TiO_2 functionalized nanofibrous membranes for removal of organic (micro)pollutants," Submitted to Separation and Purification Technology, 2016

5.1 Introduction

Titanium dioxide is widely used because of its great availability, low cost, non-toxicity, chemical and thermal stability [1]. One of the most interesting properties of TiO_2 is its photocatalytic activity under UV irradiation, producing highly oxidative hydroxyl radicals capable of oxidizing many organic (micro)pollutants [2],[3]. Phenylurea herbicides are generally applied for agricultural applications. Isoproturon is one of the most used herbicides in Europe and due to its water solubility, low chemical and biological degradation it contaminates surface and ground water [4],[5]. Heterogenous photocatalysis using TiO_2 has been considered as highly promising for waste water treatment and degradation of these herbicides [6]. Additionally, removal of organic components present in industrial, highly acidic effluents remains a major issue as well, which can also be tackled using TiO_2. As described in Chapter 1 an increased interest is thus seen in immobilizing the TiO_2 nanoparticles on a porous, inert support [7]–[10].

The unique properties of nanofibrous membranes makes them ideal for a wide range of filtration applications [11]–[14]. Moreover, they show to be an ideal highly porous support for immobilization of TiO_2 nanoparticles. Polymer nanofibrous membranes functionalized with TiO_2 nanoparticles have already shown to be promising for photodegradation of dissolved organic matter, humic acids and bacteria [15]–[17]. Ceramic membranes, although less exploited so far, have many advantages over polymeric membranes for filtration applications, since they have typically superior thermal properties, and a better resistance against corrosion and chemicals [18]. These membranes can thus be used for highly acidic effluents. Silica nanofibers have recently shown their added value for removal of heavy metal ions and dyes via sorption [19]–[21]. So far they have not yet been exploited to study the removal of micro pollutants. Functionalization of these nanofibrous membranes with TiO_2 nanoparticles results in an added functionality for removal/degradation of organic components. Additionally, functionalization with TiO_2 prevents fouling of the membranes, which is a major concern in membrane use for water treatment [18],[22].

In this chapter commercial Degussa P25 TiO_2 nanoparticles are immobilized in and on a porous nanofibrous support. Commercial Degussa P25 TiO_2 nanoparticles have already proven their value as

photocatalyst for water treatment, but proper immobilization remains vital as it increases the applicability of these nanoparticles. Therefore, both polymeric (polyamide 6) and ceramic (silica) nanofibrous membranes are functionalized with these TiO_2 nanoparticles. First, the TiO_2 loading of inline and dip-coated nanofibrous membranes are quantified using TGA, XRD and ICP-OES. Next, the photocatalytic behavior is tested by decoloring of Methylene Blue, an ideal test compound for a first screening of the produced membranes and their degradation efficiency. Finally, the true degradation potential of micro pollutants is tested on isoproturon using a basic set-up. Both UV-Vis spectroscopy and LC-MS are used for evaluation of the degradation of the pollutants. The removal of isoproturon is a real concern in water treatment today in view of discharge to the environment and has not yet been solved adequately. It is believed that commercial TiO_2 nanoparticles may be highly valuable when immobilized on porous polyamide or silica nanofibrous membranes for removal of various organic (micro)pollutants. Moreover, these membranes are applicable in various water treatment set-ups such as contact reactors or membrane separation reactors.

5.2 Materials and methods

5.2.1 Materials

Polyamide 6 (PA 6) pellets were provided by Sigma-Aldrich and used as received. The solvents formic acid (98 v%) and acetic acid (99.8 v%) were supplied by Sigma-Aldrich. The dye Methylene Blue (MB) and the herbicide isoproturon were also provided by Sigma-Aldrich.

5.2.2 Electrospinning

Polyamide solutions for electrospinning were prepared by dissolving 13 wt% and 16 wt% of PA 6 in a 50:50 v% formic acid:acetic acid solvent mixture [23],[24]. The sols were prepared using the methodology described in Chapter 2 (Allihn set-up, reaction time of 16 hours).

The electrospinning experiments were executed on a mononozzle set-up with a rotating drum collector. For the electrospinning of the 16 wt%

polyamide solutions a tip-to-collector distance (TCD) of 6 cm was used, a flow rate of 2 mL h^{-1} and a voltage in between 21 and 25 kV. The electrospinning of the 13 wt% PA 6 solution was carried out with a TCD of 10 cm, flow rate of 0.5 ml h^{-1} and a voltage in between 20 and 25 kV to obtain a stable process. For the electrospinning of the silicon oxide sols the TCD was fixed at 15 cm, the flow rate at 1 mL h^{-1} and the voltage was adjusted in between 20 and 24 kV to obtain a stable electrospinning process. All the experiments were executed at a relative humidity of 34% RH ± 10% of and a room temperature of 22°C ± 2°C. Nanofibrous membranes with a density of ± 10 g/m^2 were obtained.

5.2.3 Functionalization methods

Inline (IL) functionalization was carried out by adding varying amounts of TiO_2 nanoparticles to the electrospinning solutions prior to electrospinning. For the lower TiO_2 loadings (0.2 wt% - 5 wt%), TiO_2 powder was added after preparation of the electrospinning solutions, the solutions were stirred with a magnetic stirrer during 0.5 h and next ultrasonicated for 0.5 h, resulting in a homogenous dispersion of the nanoparticles. These low TiO_2 loadings had no influence on the electrospinning process. Electrospinning of a higher TiO_2 load (35 wt%) was only possible when the amount of PA 6 in the formic acid/acetic acid solutions was lowered from 16 wt% to 13 wt% PA 6. To prepare the 35 wt% TiO_2 inline functionalized PA 6 solution, the TiO_2 nanoparticles were first homogenously mixed in the solvent mixture by ultrasonication, after which the polymer pellets were added and the solution was stirred for 6 hours. The electrospinning parameters were optimized as described above. The amount of TiO_2 added is expressed as a weight percentage relative to the total weight of polyamide 6 and TiO_2, or silica and TiO_2. To indicate the relative amounts of TiO_2 added to the silica nanofibers it was assumed that complete crosslinking of the TEOS took place resulting in a SiO_2 network. To denote the samples, the amount of TiO_2 added is expressed as wt% for IL samples

Post-functionalization of the nanofibrous membranes via **dip-coating** (DC) (Figure 5.1) was carried out in a clean room facility (class 100 000/1000). Aqueous TiO_2 nanoparticle suspensions (0.12 mol L^{-1}, 0.34 mol L^{-1} and 0.5 mol L^{-1}) were dip-coated on the nanofibrous membranes at room temperature and at a coating speed of 102.8

mm/min, using a computer controlled dip-coating unit (KSV Instruments). Samples dip-coated (DC) with a 0.12 mol L^{-1} and 0.5 mol L^{-1} TiO_2 aqueous suspension were immersed for 3 min. Samples dip-coated with a 0.34 mol L^{-1} TiO_2 aqueous suspension were immersed for 10 min. Both hydrophobic as well as hydrophilic silica nanofibrous membranes were dip-coated. Hydrophilic membranes functionalized via dip-coating are denoted with a H. The as-coated membranes were first dried at room temperature for 24h, after which the samples were cured during 30 min at 100°C. To denote the DC samples the concentration of TiO_2 in the coating solution is denoted in M (mol L^{-1}).

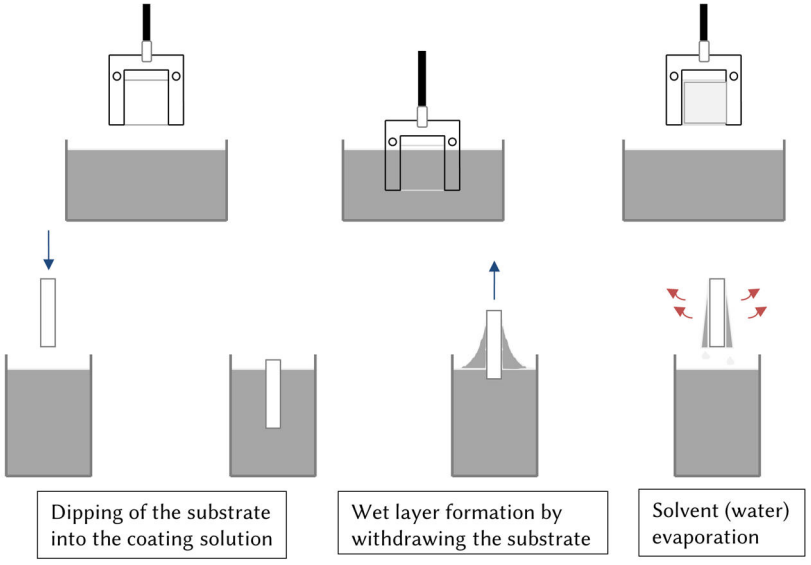

Figure 5.1 Schema of the dip-coating process used for post-functionalization of the nanofibrous membranes

5.2.4 Characterization of nanofibrous membranes

Thermogravimetric analysis (TGA) of the TiO_2 functionalized PA 6 membranes were performed on a Netzsch STA449 FR Jupiter set-up. The samples were heated at a rate of 10°C min^{-1} from room temperature to 800°C under air. The weight fraction remaining at 800°C can be attributed

to TiO_2 as all PA6 was burned out. Based on the amount of TiO_2 the Ti content could be determined.

Inductively Coupled Plasma Optical Emission Spectroscopy (ICP-OES) was carried out to quantify the amount of titanium present in or on the membranes. To ± 10 mg of TiO_2 functionalized PA 6 nanofibrous samples, 4 mL of concentrated HNO_3 and 1 mL of concentrated H_2SO_4 was added, followed by an acid digestion in a Milestone MLS-1200 microwave oven. After digestion, 100 µL of the internal standard (IS) was added to 500 µL of the obtained solution, and further diluted to a volume of 10 mL with Milli-Q water. To ± 20 mg of TiO_2 functionalized silica nanofibers 2 mL of concentrated HNO_3 and 1 mL of concentrated HF was added. This was followed by an acid digestion in closed Savillex beakers (24 hours at 90°C). Next, the samples were evaporated and again dissolved in 2 mL of 10% HNO_3, followed by an appropriate dilution for each sample (Silica 0.2 wt%: 1 mL of sample + 100 µL IS – dilution to 10 mL with 1% HNO_3, silica 2 wt% and silica DC 0.12M: 500 µL of sample + 100 µL IS – dilution to 10 mL with 1% HNO_3). Analysis of all samples was carried out with an ICP-OES (Spectra Arcos).

Previous to the X-Ray Diffraction (XRD) analysis, the samples were heated to 1000°C for 4 hours. The samples were milled and side-loaded into the sample holder. The XRD data were collected on a Thermo Scientific ARL X'tra Diffractometer equipped with a Peltier cooled detector. Samples were measured in θ-2θ geometry over an angular range of 5-70 °2θ (CuKα radiation) using a 0.02 °2θ step size and 1 s/step counting time. The Rietveld method for whole-powder pattern fitting was used to investigate the ratios of the crystalline phases (SiO_2 vs $TiSiO_4$). Topas Academic V4.1 software was used for Rietveld refinement [Coelho, A.A., Topas Academic version 4.1. 2007.]. The refined parameters were the measurement specific or sample displacement error, a cosine Chebyshev function of 12 polynomial terms for background correction, phase specific scale factors, unit cell parameters and Lorentzian peak shape broadening parameters.

5.2.5 Photocatalytic activity test

The photocatalytic activity of the membranes was evaluated by photodegradation of aqueous solutions of both Methylene Blue (4.2 mg L^{-1}) and isoproturon (5 and 10 mg L^{-1}) under UV irradiation. Methylene Blue

(MB) was simply dissolved in deionized water, isoproturon was first dissolved in aceton at a mass concentration of 1000 mg L^{-1}. This solution was then diluted with deionized water to a mass concentration of 5 or 10 mg L^{-1}. A schematic diagram of the used set-up is given in Figure 5.2. For each type of membrane, three samples were tested simultaneously. The samples were fixed in a sample holder and immersed in a tempering beaker (15°C) containing the MB or isoproturon solution. The samples were illuminated from a distance of 13 cm by a 300 W Osram Ultra-Vitalux lamp, emitting radiation (mainly UV-A, similar to sunlight) with an intensity of about 5 mW/cm^2. The light emission profile of the Osram Ultra-Vitalux lamp is shown in Figure 5.3. To stabilize the power of its emission spectrum the lamp was switched on 1 h before starting the photocatalytic test. To ensure the attainment of the ad/absorption equilibrium the samples were immersed in the solutions 24 h prior to the photocatalytic test. The Methylene Blue decoloring and isoproturon degradation were followed by measuring the transmission spectra of the solutions after 0 h, 1 h, 2 h, 4 h, 6 h using a Perkin-Elmer Lambda 900 UV-Vis spectrophotometer (Figure 5.4) or via Liquid Chromatography – Mass Spectrometry (LC-MS). The photocatalytic degradation rate of various organic compounds over TiO_2 usually follows pseudo first-order reaction kinetics, which is described by equation (1) [33,34,37,38]. C is the concentration of MB or isoproturon after a specific UV irradiation time t, C_0 is the initial concentration and k is the rate coefficient of the reaction.

$$\ln\left(\frac{C}{C_0}\right) = -kt \quad (1)$$

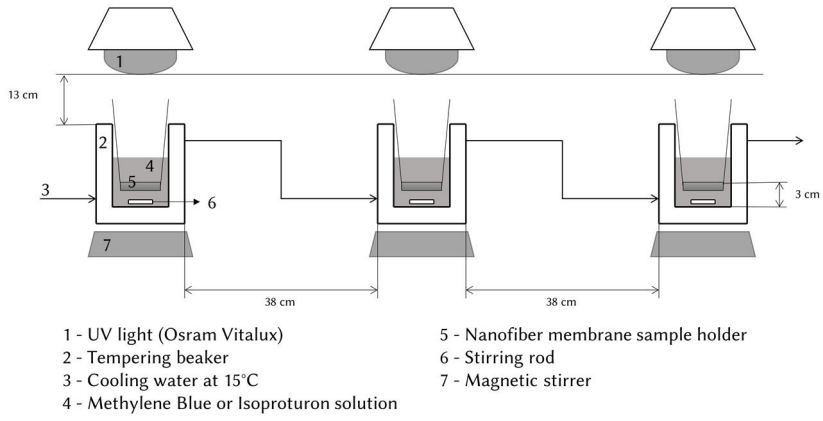

Figure 5.2 Schematic drawing of photocatalytic set-up

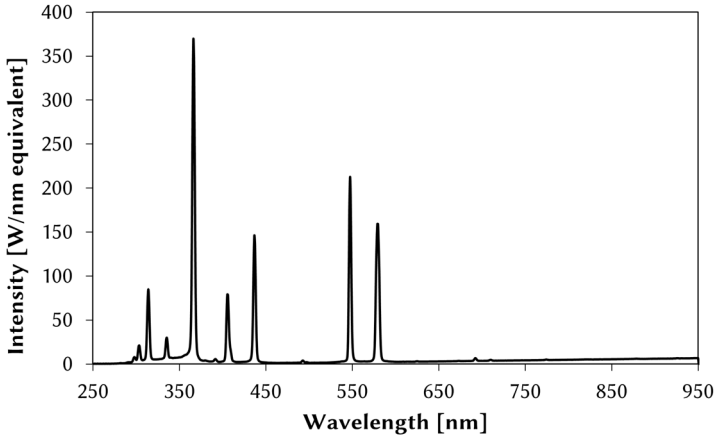

Figure 5.3 Light emission spectrum of Osram Ultra-Vitalux lamp

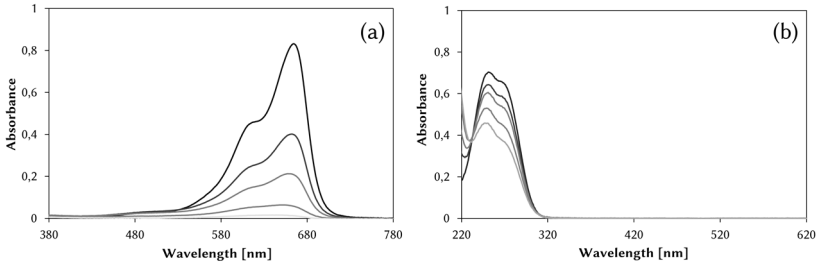

Figure 5.4 UV-Vis spectra demonstrating decoloring of Methylene Blue by PA 6 DC 0.12 M sample (a) and degradation of isoproturon by PA 6 IL 35 wt% sample (b) (IL: inline, DC: dip-coating)

The LC-MS system consisted of a Surveyor HPLC coupled to a Quantum Discovery mass spectrometer (both from Thermo-Scientific, San Jose, CA, USA) equipped with an electrospray-source (ESI), operated in full scan positive ionization mode. Prior to analysis, samples were diluted twice with methanol (MeOH). Subsequently 1 µL was injected. Separation was performed on an Omnispher C18 column 50 x 3 mm (3 µm particle size) protected with a guard column 10 x 2 mm (both from Varian, Sint-Katelijne-Waver, Belgium). The mobile phase consisted of water and MeOH, both containing 0.1% acetic acid and 1mM ammonium acetate. A gradient program was used to elute the isoproturon. After analysis the protonated molecular ion of isoproturon (m/z 207) was extracted from the chromatograms and peak heights were plotted in function of time.

5.3 Characterization of TiO_2 functionalized membranes

An in-depth characterization of the nanofibrous membranes and their TiO_2 loading is indispensable for a correct interpretation of the photocatalytic behavior of the produced membranes. The influence of the TiO_2 addition on the resulting nanofiber morphology was evaluated via SEM, Figure 5.5. Uniform membranes were obtained (Figure 5.5 a,b) and fiber diameters of 220 ± 50 nm were measured for inline (IL) functionalized 2.5 wt% TiO_2 PA 6 membrane, being in line with PA 6 nanofibers without TiO_2 loading, 200 ± 45 nm, and previous research [17],[24]. Smaller diameters, 100 ± 15 nm, were measured for the 35 wt% PA6 sample, since a lower concentration of polymer was present in the solution [25],[26]. The presence of TiO_2 is not visible for the low amounts (Figure 5.5 a), opposed to the 35 wt% PA 6 sample for which the TiO_2 particles are clearly visible, with the formation of clusters or beads (Figure 5.5 b).

Inline functionalization of the silicon oxide sols was possible up to 2 wt% only. SEM images are shown of 0.2 wt% and 2 wt% TiO_2 loaded silica nanofibers. These samples have diameters of 345 ± 45 nm and 320 ± 165 nm, which are again largely unaltered compared to non-functionalized silica nanofibers (300 ± 85 nm) prepared in this work and in previous chapters. At a TiO_2 loading of 2 wt% beads started to become present in the resulting nanofibers. It was not possible to further increase the TiO_2 loading of these membranes by inline functionalization when the same sol preparation procedure was used.

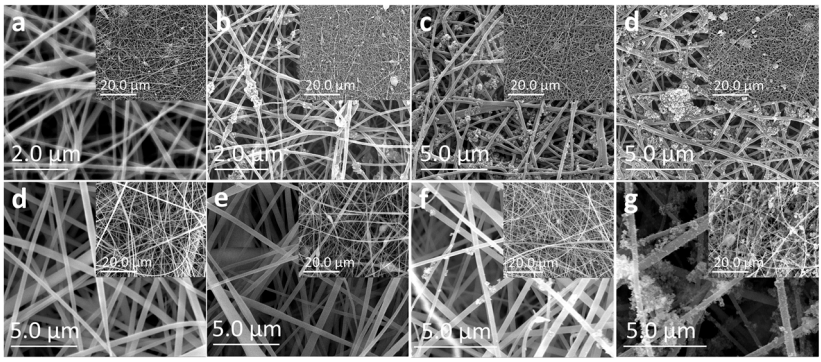

Figure 5.5 SEM images of polyamide 6 inline functionalized with (a) 2.5 wt% and (b) 35 wt%, post-functionalized polyamide 6 membranes with (c) 0.12 M and (d) 0.5 M TiO_2 solution, silica inline functionalized with (d) 0.2 wt% and (e) 2 wt%, and silica post-functionalized with 0.34 M TiO_2 solution as (f) hydrophobic membrane and (g) hydrophilic membrane.

Post-functionalization via dip-coating (DC) was examined since it allows deposition of TiO_2 nanoparticles only at the surface of the nanofibers. This makes the TiO_2 nanoparticles more accessible to the pollutants in the water. However, blocking of the pores of the membranes may be a drawback together with the easier wash-out of TiO_2. Again the membranes were screened using SEM and the comparison was made between PA 6 and silica nanofibrous membranes. For the PA 6 membranes an increased loading is seen with increasing concentration of the solution used for dip-coating (Figure 5.5 c,d), which was also confirmed with TGA (Table 5.1). Moreover, the pores of the PA 6 membranes seem to become blocked upon functionalization with a 0.5 M TiO_2 solution. Due to their low affinity for polyamide the TiO_2 nanoparticles tend to form clusters and upon increasing concentration these clusters block the pores of the membranes.

Dip-coating of the silica nanofibers also resulted in an increased loading with an increasing concentration of the dip-coating solution. The silica nanofibers can change their hydrophilicity in time (as discussed in Chapter 3). Therefore, both hydrophobic and hydrophilic samples were dip-coated, which resulted in a significant difference in TiO_2 loading (Figure 5.5 f,g and Table 5.1). Due to their high affinity for silica, the TiO_2 nanoparticles are much better distributed along the nanofibers compared to PA 6, resulting in only a minimal pore blocking of these silica membranes. This is an important advantage if membrane separation

reactors are aimed for as pore blocking is too be minimized for an optimal reactor performance.

Quantification of the amounts of Ti/TiO_2 present in or on the nanofibers was carried out using multiple techniques. TGA was used for PA 6 membranes (Figure 5.6) , XRD was used for silica membranes and ICP-OES was used for both. An overview of the results obtained via ICP-OES and TGA are shown in Table 5.1. The amounts of TiO_2 present in the inline functionalized membranes was, as expected, in line with the calculated amounts. With increasing concentration of TiO_2 in the dip-coating solutions, an increase in TiO_2 loading on the membranes was measured, which was also confirmed via SEM (Figure 5.5 c,d). Via XRD an amount of 2.19 wt% $TiSiO_4$ was determined for the 2 wt% inline functionalized silica membrane, although crystallinity was not fully developed the result showed to be in line with the calculated amounts and ICP-OES results. A substantial higher TiO_2 loading through dip-coating was noted for the hydrophilic silica samples over the hydrophobic samples.

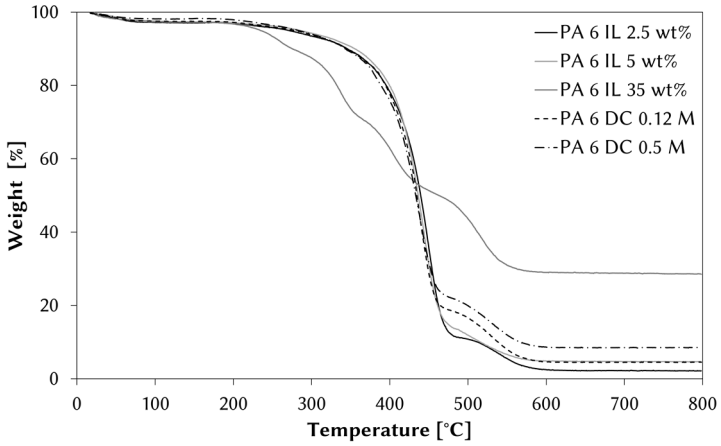

Figure 5.6 TGA thermograms of PA 6 nanofibrous samples functionalized with TiO_2 nanoparticles (IL: inline, DC: dip-coating).

In summary, successful functionalization of both PA 6 and silica nanofibrous membranes was carried out using both inline functionalization and dip-coating and their TiO_2 load was quantified. The photocatalytic behavior of these membranes is evaluated next to identify the most promising membranes for isoproturon degradation.

Table 5.1 Quantification of TiO_2 loading for PA 6 and silica nanofibrous membranes functionalized inline or via dip-coating via ICP-OES and TGA (TiO_2 quantification is not possible via calculation for dip-coated membranes, TGA is not a valid tool for TiO_2 quantification of silica membranes) (IL: inline, DC: dip-coating and H: hydrophilic)

		Calculated amount (mg Ti g^{-1} sample)	ICP-OES (mg Ti g^{-1} sample)	TGA (mg Ti g^{-1} sample)
PA 6	IL 0.5 wt%	3	3.72	-
	IL 2.5 wt%	15	-	31.2
	IL 5 wt%	29	41.2	45
	IL 35 wt%	200	-	187
	DC 0.12 M	-	39.1	42
	DC 0.5 M	-	-	61.7
Silica	IL 0.2 wt%	1.12	0.843	-
	IL 2 wt%	11	8.81	-
	DC 0.12 M	-	8.89	-
	DC 0.34 M	-	23.5	-
	H DC 0.34 M	-	143.1	-

5.4 Photocatalytic behavior of TiO_2 functionalized membranes

The photocatalytic behavior of the TiO_2 functionalized nanofibrous membranes was evaluated subsequently via Tauc plots and the decoloring of Methylene Blue. The properties of the TiO_2 semi-conductor present in the samples was verified by plotting their Tauc plot (Figure 5.7), following the method reported by López *et al* [27]. The estimated band gap energies (E_g) were all in the range 3.18 - 3.30 eV, which is close to the value of 3.2 eV being extensively reported for the commercial P25 TiO_2 nanoparticles [27]. UV-A light, emitted by the chosen Osram Ultra-Vitalux lamp, is thus sufficient to overcome this band gap energy. It can be concluded that the properties of the semi-conductor do not change by incorporation in both the PA 6 and silica nanofibrous membranes.

The photocatalytic activity of the functionalized PA 6 and silica nanofibrous membranes was further characterized by their decoloring of a Methylene Blue (MB) solution. The decoloring of MB is typically used as a probe to demonstrate the activity of a photocatalyst. Since it is generally

accepted that the decoloring of MB follows a pseudo first-order kinetic mechanism [37,38], the photocatalytic activity of the samples was calculated from the logarithmic plots of the pseudo first-order degradation rate of the MB solutions in contact with the functionalized membranes (Figure 5.8). The photolysis of MB under UV light without sample present and the decoloring of the MB solution by non-functionalized samples is also plotted, to demonstrate clearly the influence of the added TiO_2 nanoparticles. The rate coefficient and t_{90} values given in Table 5.2 indicate the differences in photocatalytic activity of all samples.

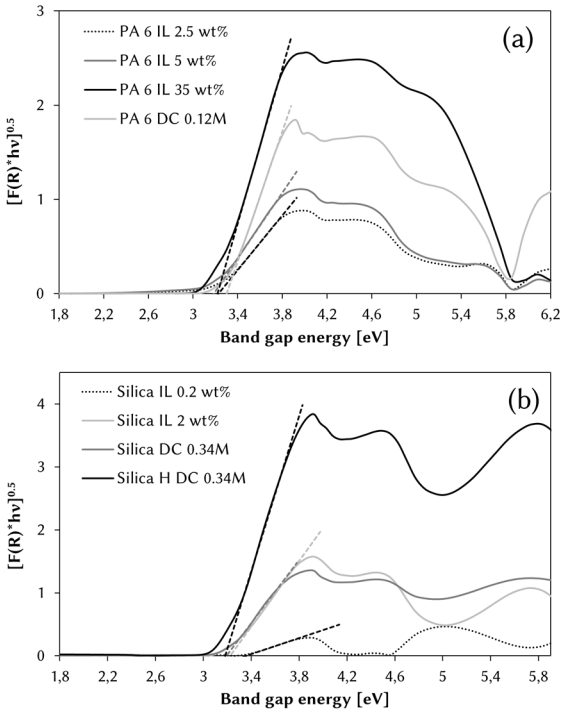

Figure 5.7 Tauc plot illustrating the band gap of the TiO_2 semiconductor present in the different samples: PA 6 membranes (a) and silica membranes (b) being close to 3.2 eV.

Use of non-functionalized membranes resulted in a low removal of MB attributable to a combined effect of MB photolysis and MB ab-/adsorption. The inline addition of TiO_2 to the PA 6 samples resulted in a significant increased removal due to degradation by the photocatalyst. Yet, the inline addition of TiO_2 to the silica membranes did not significantly change the removal rate compared to non-functionalized samples. This can be

explained by the shielding of TiO_2 by the silica [28]–[30]. However, very interesting, the rate coefficients of dip-coated samples are significantly higher than those of inline functionalized samples for both PA 6 and silica. Via TGA and ICP-OES it was quantified that the 0.12 M DC samples had the same TiO_2 loading as the inline functionalized samples with 5 wt% (for PA 6) and 2 wt% (for silica) (Table 5.1). The presence of TiO_2 only at the surface of the nanofibers resulted thus, as expected, in a higher degradation rate. Comparing the MB decoloring results to literature, although not always straightforward due to various testing conditions used, it can be stated that both inline and post-functionalized PA 6 membranes are in line with the results of Daels *et al* [16] and even better than results obtained by Pant *et al* [31] and Kasanen *et al* [32].

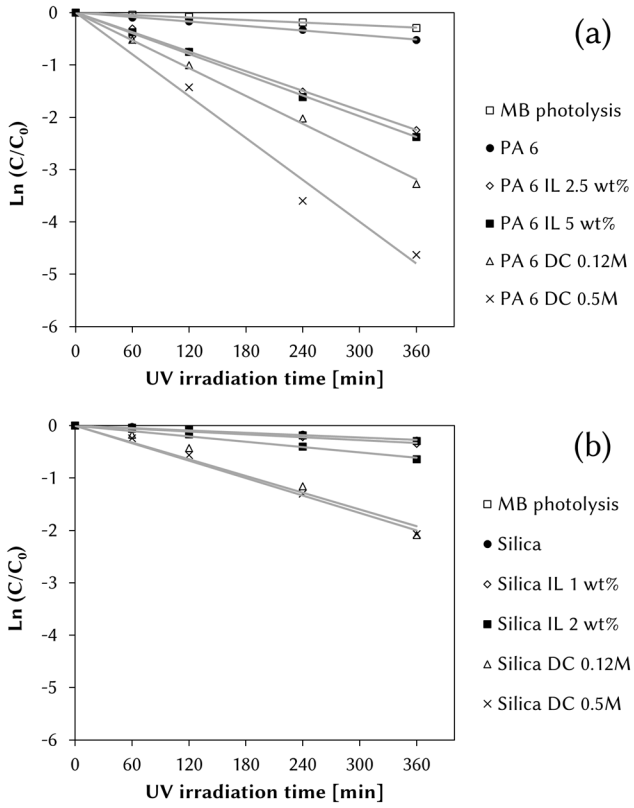

Figure 5.8 Photolysis of Methylene Blue solution under UV and removal of aqueous Methylene Blue solution as a function of time by non-functionalized and TiO_2 functionalized (IL: inline, DC: dip-coating) PA 6 (a) and silica (b) nanofibrous membranes.

Table 5.2 Degradation rate coefficients (k) of aqueous MB solutions in contact with TiO_2 functionalized PA 6 and silica nanofibrous membranes determined via UV-Vis spectroscopy (IL: inline, DC: dip-coating, R^2: coefficient of determination, t_{90}: time necessary for 90% removal).

PA 6	k [min^{-1}]	R^2	t_{90} [h]	Silica	k [min^{-1}]	R^2	t_{90} [h]
MB photolysis	0.0008	0.99	48.2	**MB photolysis**	0.0008	0.99	48.2
PA 6	0.0014	0.99	38.4	**Silica**	0.0008	0.99	48.2
IL 2.5 wt%	0.0062	0.99	6.5	**IL 1 wt%**	0.0009	0.99	38.9
IL 5 wt%	0.0068	0.99	5.5	**IL 2 wt%**	0.0017	0.99	19.5
DC 0.12M	0.0089	0.99	4.3	**DC 0.12M**	0.0053	0.96	6.8
DC 0.5M	0.0133	0.98	2.9	**DC 0.5M**	0.0056	0.99	6.6

When evaluating both the photocatalytic results and the morphology/pore blocking of the membranes after functionalization it can be stated that inline functionalization is preferred for PA 6, since pore blocking is a major concern for PA 6 dip-coated membranes. Moreover, inline functionalization results in sufficiently high removal rates. In contrast to PA 6, dip-coating of the silica samples resulted in membranes where no pore blocking was noticed and high removal rates are seen, making post-functionalization thus preferred for silica nanofibrous membranes. Inline functionalization of silica is no valuable option for the decoloring of MB, due to the shielding effect of the silica. This knowledge now allows to test the potential of the best membranes for their removal of the contaminant isoproturon which is a current challenge during water treatment.

5.5 Degradation of isoproturon

Isoproturon degradation by both PA 6 and silica nanofibrous samples, functionalized with TiO_2 nanoparticles, was followed via both UV-Vis spectroscopy and LC-MS. Sharma *et al* found that the degradation of isoproturon also followed pseudo first-order kinetics [33],[34]. Therefore, the photocatalytic activity was again calculated from the logarithmic plots of the pseudo first-order degradation rate of the isoproturon solutions in contact with the functionalized membranes. The logarithmic plots based on both UV-Vis spectroscopy (Figure 5.9) and LC-MS (Figure 5.10) are given and compared.

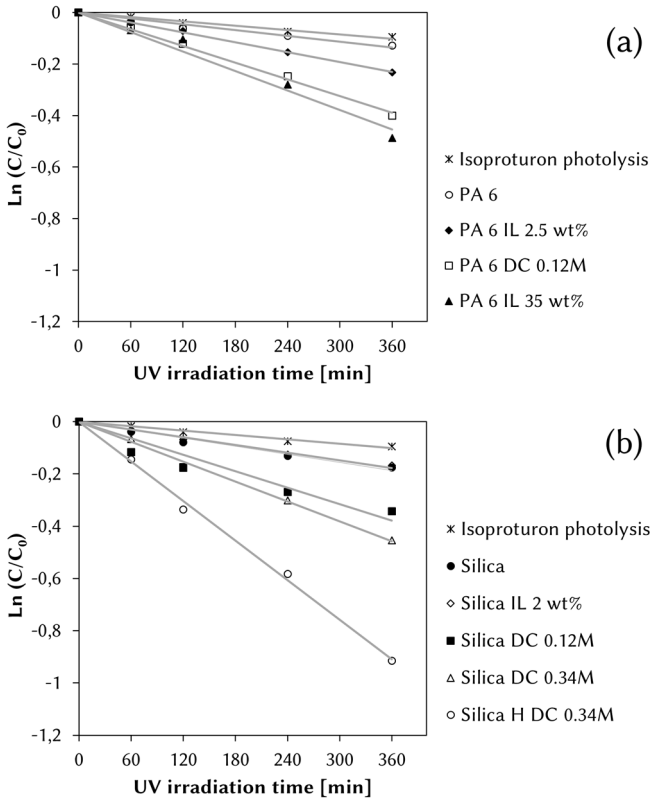

Figure 5.9 Photolysis of isoproturon solution under UV and removal of aqueous isoproturon solution as a function of time by non-functionalized and TiO_2 functionalized (IL: inline, DC: dip-coating and H: hydrophilic) PA 6 (a) and silica (b) nanofibrous membranes based on UV-Vis spectroscopy.

A clear increase in isoproturon removal was seen upon functionalization with TiO_2 for both PA 6 and silica nanofibrous membranes (Table 5.3). The same trends were seen as for the MB decoloring. The functionalization of both PA 6 and silica samples with a substantial increased TiO_2 loading was further optimized using inline functionalization for PA 6 (inline 35 wt%) and via dip-coating for silica nanofibrous membranes (hydrophilic silica, 0.34 M TiO_2, 10 min immersion time) to obtain even better degradation rates. Comparing the different PA 6 samples it is seen that inline functionalization with 2.5 wt% resulted in an increased removal compared to non-functionalized samples, furthermore dip-coating with 0.12 M solution even further increased the removal. The highest removal rate was obtained using the 35 wt% inline functionalized PA 6 samples,

being the PA 6 sample with the highest TiO_2 load. Silica samples inline functionalized with TiO_2 did not result in a higher removal rate compared to non-functionalized samples, similar to MB decoloring. Again confirming that inline functionalization of silica nanofibrous membranes with TiO_2 is not the preferred method for organic components removal. Functionalization of these silica membranes using dip-coating resulted in much higher degradation rates, resulting in the fastest removal of isoproturon for the hydrophilic dip-coated sample, which is the sample with the highest TiO_2 load. This sample gave the best overall rate coefficient of all tested samples and therefore it was studied more in-depth using LC-MS (Figure 5.10 a). Complete removal of isoproturon is seen after 24 hours using a straightforward test set-up. Moreover, to the best of our knowledge this is the first study reporting on TiO_2 functionalized nanofibrous membranes for isoproturon removal.

Comparing the rate coefficients obtained via UV-Vis spectroscopy and LC-MS similar results are obtained, with LC-MS resulting in an even slightly higher degradation rate. Indeed a small underestimation of the degradation rate using UV-Vis spectroscopy can be explained by the presence of degradation products absorbing in the same UV region of the electromagnetic spectrum as isoproturon. However, UV-Vis spectroscopy can clearly be a viable fast, easy accessible method to demonstrate the removal of isoproturon in time.

Table 5.3 Degradation rate coefficients (k) of aqueous isoproturon solutions in contact with TiO_2 functionalized PA6 and silica nanofibrous membranes determined via UV-Vis spectroscopy and LC-MS. (IL: inline, DC: dip-coated and H: hydrophilic, R^2: coefficient of determination, t_{90}: time necessary for 90% removal); the amount of TiO_2 added is expressed as wt% for IL samples, for the DC samples the concentration of TiO_2 in the coating solution is denoted in M (mol L^{-1}).

PA 6	k [min^{-1}]	R^2	t_{90} [h]	Silica	k [min^{-1}]	R^2	t_{90} [h]
UV-Vis							
Isoproturon photolysis	0.0003	0.98	127.8	**Isoproturon photolysis**	0.0003	0.98	127.7
PA 6	0.0004	0.94	127.8	**Silica**	0.0005	0.97	76.4
IL 2.5 wt%	0.0006	0.99	64	**IL 2 wt%**	0.0005	0.98	76.5
DC 0.12M	0.0011	0.99	38.5	**DC 0.12M**	0.0011	0.91	41.9
IL 35 wt%	0.0013	0.97	38.4	**DC 0.34M**	0.0013	0.99	38.3
				H DC 0.34M	0.0025	0.99	12.8
LC-MS							
DC 0.12M	0.0015	0.97	19.5	**DC 0.12M**	0.0012	0.97	37.8
IL 35 wt%	0.0016	0.99	19.2	**H DC 0.34M**	0.0028	0.99	13.1

Thus, optimization of inline functionalized PA 6 samples and dip-coated silica samples results in a significant and even complete removal of isoproturon in time. In this research, a basic set-up was used to characterize the isoproturon degradation, to demonstrate the large potential of these Degussa P25 TiO_2 functionalized nanofibrous membranes for advanced water treatment. These membranes might be used for various organic (micro)pollutants and they are applicable in both membrane separation reactors and contact reactors. PA 6 is the most economical option in non-harsh conditions. However, a slightly slower removal of isoproturon was noted for PA 6 nanofibrous membranes functionalized with TiO_2 (inline 35 wt%) compared to silica (hydrophilic, DC 0.34 M). The best removal rates were obtained with hydrophilic silica nanofibrous membranes functionalized via dipcoating. In addition to the high potential for the degradation of micro pollutants, the ceramic silica nanofibrous membranes offer a high chemical and thermal resistance

making them also promising materials for other effluent treatments such as highly acidic effluents.

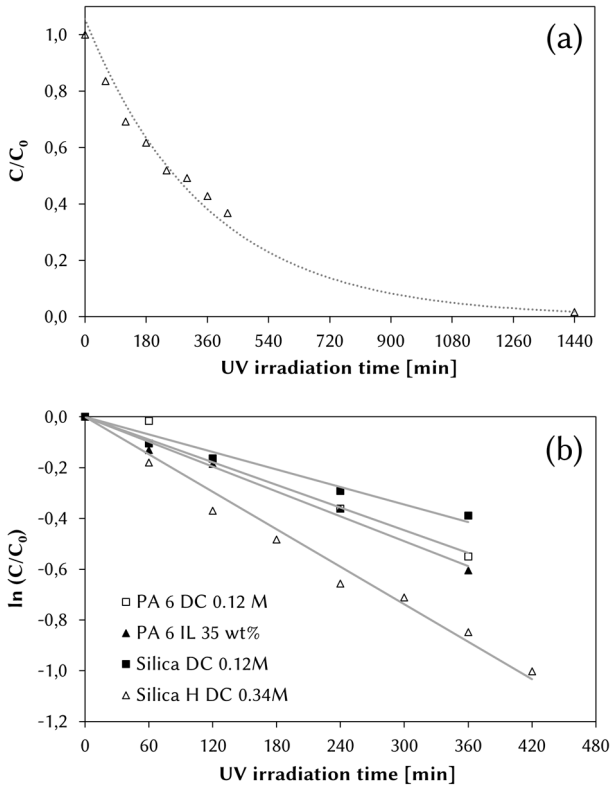

Figure 5.10 Removal of aqueous isoproturon solution as a function of time by hydrophilic silica nanofibrous membrane dip-coated with 0.34 M TiO2 solution (a), removal of aqueous isoproturon solution as a function of time by non-functionalized and TiO2 functionalized PA 6 and silica nanofibrous membranes based on LC-MS measurements (b).

No other reports on nanofibrous supports for isoproturon removal were found, nevertheless limited research has been carried out on immobilized titanium dioxide on inert non-porous substrates. Verma *et al* immobilized Degussa P25 nanoparticles on an inert glass sheet support, resulting in only 70% removal of isoproturon after 420 hours of exposure to sunlight [35]. The best result on a non-porous support was reported by Losito *et al* [36]. Titanium dioxide-poly(vinylidenefluoride) (TiO_2-PVDF) was deposited on glass substrates by casting or spin-coating, giving 70% up to 90% removal in 5 hours, being in the same order as the 60% removal in 6

hours of our best sample. Our results thus confirm the potential of TiO_2 to remove micro pollutants such as isoproturon. Moreover, a correct immobilization on a nanofibrous matrix results in a functionalized highly porous material, ideal for future reactor set-up design.

5.6 Conclusion

Functionalization of polyamide 6 and silica nanofibrous membranes with TiO_2 nanoparticles was optimized via both inline functionalization and dip-coating. Inline functionalization with increased amounts of TiO_2 showed to be the best functionalization method for PA 6, since dip-coating results in pore blocking. For silica, on the contrary, dip-coating was the preferred functionalization method, avoiding shielding of the TiO_2 by the silica shell. Immobilization of these nanoparticles on these porous supports resulted in highly photocatalytically active membranes, which was verified via their Tauc plots and demonstrated via Methylene Blue decoloring. Finally, complete removal of isoproturon, a real concern in current water treatment progresses, was established using a basic set-up. By functionalizing a highly porous and flexible support with commercial available TiO_2 nanoparticles, advanced materials were produced showing a high potential to be used for removal of organic (micro)pollutants. Moreover, these membranes can be applied in both membrane separation reactors as contact reactors. PA 6 is assumed to be the most economical and efficient option for non-harsh environments. Silica nanofibrous membranes, on the other hand, can be highly valuable for removal of organic species in industrial, highly acidic effluents.

References

[1] X. Chen and S. S. Mao, "Titanium dioxide nanomaterials: Synthesis, properties, modifications and applications," *Chem. Rev.*, vol. 107, no. 7, pp. 2891–2959, 2007.

[2] K. Hashimoto, H. Irie, and A. Fujishima, "TiO2 Photocatalyis: A Historical Overview and Future Prospects," *Jpn. J. Appl. Phys.*, vol. 44, no. 12, pp. 8269–8285, 2005.

[3] A. Fujishima, T. N. Rao, and D. a. Tryk, "Titanium dioxide photocatalysis," *J. Photochem. Photobiol. C Photochem. Rev.*, vol. 1, no. 1, pp. 1–21, 2000.

[4] R. Loos, G. Locoro, S. Comero, S. Contini, D. Schwesig, F. Werres, P. Balsaa, O. Gans, S. Weiss, L. Blaha, M. Bolchi, and B. M. Gawlik, "Pan-European survey on the occurrence of selected polar organic persistent pollutants in ground water," *Water Res.*, vol. 44, no. 14, pp. 4115–4126, 2010.

[5] L. Nitschke and W. Schüssler, "Surface water pollution by herbicides from effluents of waste water treatment plants.," *Chemosphere*, vol. 36, no. 1, pp. 35–41, 1998.

[6] A. R. Ribeiro, O. C. Nunes, M. F. R. Pereira, and A. M. T. Silva, "An overview on the advanced oxidation processes applied for the treatment of water pollutants defined in the recently launched Directive 2013/39/EU," *Environ. Int.*, vol. 75, pp. 33–51, 2015.

[7] S. Parra, S. Malato, and C. Pulgarin, "New integrated photocatalytic-biological flow system using supported TiO2 and fixed bacteria for the mineralization of isoproturon," *Appl. Catal. B Environ.*, vol. 36, no. 2, pp. 131–144, 2002.

[8] M. N. Chong, B. Jin, C. W. K. Chow, and C. Saint, "Recent developments in photocatalytic water treatment technology: A review," *Water Res.*, vol. 44, no. 10, pp. 2997–3027, 2010.

[9] M. N. Chong, V. Vimonses, S. Lei, B. Jin, C. Chow, and C. Saint, "Synthesis and characterisation of novel titania impregnated kaolinite nano-photocatalyst," *Microporous Mesoporous Mater.*, vol. 117, no. 1–2, pp. 233–242, 2009.

[10] Z. Sun, Y. Chen, Q. Ke, Y. Yang, and J. Yuan, "Photocatalytic degradation of cationic azo dye by TiO2/bentonite nanocomposite," *J. Photochem. Photobiol. A Chem.*, vol. 149, no. 1–3, pp. 169–174, 2002.

[11] Z. M. Huang, Y. Z. Zhang, M. Kotaki, and S. Ramakrishna, "A review on polymer nanofibers by electrospinning and their applications in nanocomposites," *Compos. Sci. Technol.*, vol. 63, no. 15, pp. 2223–2253, 2003.

[12] R. S. Barhate, C. K. Loong, and S. Ramakrishna, "Preparation and characterization of nanofibrous filtering media," *J. Memb. Sci.*, vol. 283, no. 1–2, pp. 209–218, 2006.

[13] R. Gopal, S. Kaur, Z. Ma, C. Chan, S. Ramakrishna, and T. Matsuura, "Electrospun nanofibrous filtration membrane," *J. Memb. Sci.*, vol. 281, no. 1–2, pp. 581–586, 2006.

[14] R. S. Barhate and S. Ramakrishna, "Nanofibrous filtering media: Filtration problems and solutions from tiny materials," *J. Memb. Sci.*, vol. 296, no. 1–2, pp. 1–8, 2007.

[15] N. Daels, S. De Vrieze, I. Sampers, B. Decostere, P. Westbroek, a. Dumoulin, P. Dejans, K. De Clerck, and S. W. H. Van Hulle, "Potential of a functionalised nanofibre microfiltration membrane as an antibacterial water filter," *Desalination*, vol. 275, no. 1–3, pp. 285–290, 2011.

[16] N. Daels, M. Radoicic, M. Radetic, S. W. H. Van Hulle, and K. De Clerck, "Functionalisation of electrospun polymer nanofibre membranes with TiO2 nanoparticles in view of dissolved organic matter photodegradation," *Sep. Purif. Technol.*, vol. 133, pp. 282–290, 2014.

[17] N. Daels, M. Radoicic, M. Radetic, K. De Clerck, and S. W. H. Van Hulle, "Electrospun nanofibre membranes functionalised with TiO2 nanoparticles: Evaluation of humic acid and bacterial removal from polluted water," *Sep. Purif. Technol.*, vol. 149, pp. 488–494, 2015.

[18] J. Kim and B. Van Der Bruggen, "The use of nanoparticles in polymeric and ceramic membrane structures: Review of manufacturing procedures and performance improvement for water treatment," *Environ. Pollut.*, vol. 158, no. 7, pp. 2335–2349, 2010.

[19] Z. Ma, H. Ji, Y. Teng, G. Dong, J. Zhou, D. Tan, and J. Qiu, "Engineering and optimization of nano- and mesoporous silica fibers using sol-gel and electrospinning techniques for sorption of heavy metal ions," *Journal of Colloid and Interface Science*, vol. 358, no. 2. pp. 547–553, 2011.

[20] S. Wu, F. Li, Y. Wu, R. Xu, and G. Li, "Preparation of novel poly(vinyl alcohol)/SiO(2) composite nanofiber membranes with mesostructure and their application for removal of Cu(2+) from waste water.," *Chem. Commun. (Camb).*, vol. 46, no. 10, pp. 1694–1696, 2010.

[21] R. Xu, M. Jia, Y. Zhang, and F. Li, "Sorption of malachite green on vinyl-modified mesoporous poly(acrylic acid)/SiO2 composite nanofiber membranes," *Microporous Mesoporous Mater.*, vol. 149, no. 1, pp. 111–118, 2012.

[22] S. Ramakrishna, R. Jose, P. S. Archana, A. S. Nair, R. Balamurugan, J. Venugopal, and W. E. Teo, "Science and engineering of electrospun nanofibers for advances in clean energy, water filtration, and regenerative medicine," *J. Mater. Sci.*, vol. 45, no. 23, pp. 6283–6312, 2010.

[23] S. De Vrieze, T. Van Camp, A. Nelvig, B. Hagström, P. Westbroek, and K. De Clerck, "The effect of temperature and humidity on electrospinning," *J. Mater. Sci.*, vol. 44, no. 5, pp. 1357–1362, 2009.

[24] S. de Vrieze, B. De Schoenmaker, and K. De Clerck, "Morphologic study of steady state electrospun polyamide 6 nanofibres," *J. Appl. Polym. Sci.*, vol. 119, no. 7, pp. 2984–2990, 2011.

[25] C. Mit-uppatham, M. Nithitanakul, and P. Supaphol, "Ultrafine electrospun polyamide-6 fibers: Effect of solution conditions on morphology and average fiber diameter," *Macromol. Chem. Phys.*, vol. 205, no. 17, pp. 2327–2338, 2004.

[26] J. Zeng, H. Haoqing, A. Schaper, J. H. Wendorff, and A. Greiner, "Poly-L-lactide nanofibers by electrospinning – Influence of solution viscosity and electrical conductivity on fiber diameter and fiber morphology," *e-Polymers*, vol. 3, no. 9, pp. 1–9, 2003.

[27] R. López and R. Gómez, "Band-gap energy estimation from diffuse reflectance measurements on sol-gel and commercial TiO2: A comparative study," *J. Sol-Gel Sci. Technol.*, vol. 61, no. 1, pp. 1–7, 2012.

[28] A. M. El-Toni, S. Yin, and T. Sato, "Control of silica shell thickness and microporosity of titania-silica core-shell type nanoparticles to depress the photocatalytic activity of titania," *J. Colloid Interface Sci.*, vol. 300, no. 1, pp. 123–130, 2006.

[29] I. A. Siddiquey, T. Furusawa, M. Sato, K. Honda, and N. Suzuki, "Control of the photocatalytic activity of TiO2 nanoparticles by silica coating with polydiethoxysiloxane," *Dye. Pigment.*, vol. 76, no. 3, pp. 754–759, 2008.

[30] A. M. El-Toni, S. Yin, T. Sato, T. Ghannam, M. Al-Hoshan, and M. Al-Salhi, "Investigation of photocatalytic activity and UV-shielding properties for silica coated titania nanoparticles by solvothermal coating," *J. Alloys Compd.*, vol. 508, no. 1, pp. L1–L4, 2010.

[31] H. R. Pant, B. Pant, P. Pokharel, H. J. Kim, L. D. Tijing, C. H. Park, D. S. Lee, H. Y. Kim, and C. S. Kim, "Photocatalytic TiO2-RGO/nylon-6 spider-wave-like nano-nets via electrospinning and hydrothermal treatment," *J. Memb. Sci.*, vol. 429, pp. 225–234, 2013.

[32] J. Kasanen, J. Salstela, M. Suvanto, and T. T. Pakkanen, "Photocatalytic degradation of Methylene Blue in water solution by multilayer TiO2 coating on HDPE," *Appl. Surf. Sci.*, vol. 258, no. 5, pp. 1738–1743, 2011.

[33] M. V. P. Sharma, V. Durgakumari, and M. Subrahmanyam, "Solar photocatalytic degradation of isoproturon over TiO2/H-MOR composite systems," *J. Hazard. Mater.*, vol. 160, no. 2–3, pp. 568–575, 2008.

[34] M. V. Phanikrishna Sharma, V. Durga Kumari, and M. Subrahmanyam, "Photocatalytic degradation of isoproturon herbicide over TiO2/Al-MCM-

41 composite systems using solar light," *Chemosphere*, vol. 72, no. 4, pp. 644–651, 2008.

[35] A. Verma, N. T. Prakash, and A. P. Toor, "Photocatalytic degradation of herbicide isoproturon in TiO2 aqueous suspensions: study of reaction intermediates and degradation pathways," *Environ. Prog. Sustain. Energy*, vol. 33, no. 2, pp. 402–409, 2014.

[36] I. Losito, A. Amorisco, F. Palmisano, and P. G. Zambonin, "X-ray photoelectron spectroscopy characterization of composite TiO 2-poly(vinylidenefluoride) films synthesised for applications in pesticide photocatalytic degradation," *Appl. Surf. Sci.*, vol. 240, no. 1–4, pp. 180–188, 2005.

[37] T. Zhang, T. Oyama, A. Aoshima, H. Hidaka, J. Zhao, and N. Serpone, "Photooxidative N-demethylation of methylene blue in aqueous TiO2 dispersions under UV irradiation," *J. Photochem. Photobiol. A,* vol.140, pp. 163-172, 2001.

[38] G.A. Epling, and C. Lin, "Photoassisted bleaching of dyes utilizing TiO2 and visible light," *Chemosphere,* vol. 46, pp. 561-570, 2002

6

Sensitive membranes: Dye-functionalized silicon oxide nanofibers for HCl and NH_3 sensing

Colorimetric sensors for monitoring and visual reporting of acidic environments both in water and air are highly valuable in various fields, such as safety, defense and technical textiles. Until now sol-gel based colorimetric sensors are usually non-flexible bulk glass or thin film sensors. Large area, flexible sensors usable in strong acidic environments are not available today. In this chapter, two pH-indicator dyes are immobilized in the silica nanofibers resulting in flexible sensor materials with a high sensitivity and fast response time for pH-changes in water, HCl and NH_3 vapors, and biogenic amines.

Parts of this chapter are published in:

J. Geltmeyer, G. Vancoillie, I. Steyaert; B. Breyne, G. Cousins, K. Lava, R. Hoogenboom, K. De Buysser, and K. De Clerck, "Dye Modification of Nanofibrous Silicon Oxide Membranes for Colorimetric HCl and NH_3 sensing," *Adv. Funct. Mater.*, vol. 26, pp. 5987-5996, 2016.

6.1 Introduction

As discussed in Chapter 1, ceramic sol-gel based sensors are highly valuable due to their high chemical and temperature resistance. The majority of the studied sol-gel sensors are sensors for pH-measurements [1]–[5]. These pH-sensors are usually optical bulk glass or thin films [4],[6]–[9]. pH-sensors are not only developed to detect acidity changes in aqueous solutions, also the detection of HCl and NH_3 gas has recently attracted significant attention [10]–[13]. The detection of these gases via optical sensors in industrial processes are of great interest, due to their simplicity and sensitivity.

Halochromic nanofibrous polymer sensors have been successfully developed [14]–[17]. However, as mentioned in Chapter 1, one of the challenges in the development of these sensors remains dye immobilization. Extended research on immobilization of pH-indicator dyes has shown that a covalent linkage between dye and matrix is the most efficient manner to inhibit dye migration [2],[18]–[22]. In addition to the superior chemical resistance, the sol-gel process offers through the availability of various sol-gel precursors the ease of functionalization. The functionalization of an appropriate sol-gel precursor with a selected halochromic dye allows for covalent functionalization of the dye in the sol-gel network. In this chapter, incorporation of the pH-indicators in the sol-gel matrix is carried out via both doping and covalent bonding to the selected precursor.

The aim of this chapter is to develop colorimetric nanofibrous sensors that can be used for both pH-sensing in aqueous solution as well as hydrogen chloride and ammonia vapor sensing. This shows potentials for multiple applications such as environmental control, industrial plants, protective clothing and equipment. APTES is selected as the additional precursor for functionalization. Thus, the electrospinning of tetraethylorthosilicate-(3-aminopropyl)triethoxysilane (TEOS-APTES) sols needs to be tackled. The pH-indicator dyes Methyl Yellow (MY) and Methyl Red (MR) are added to these sols via dye doping. The carboxylic acid group of Methyl Red offers the possibility for covalent linking to the APTES precursor and thus covalent immobilization in the silicon oxide nanofibers. These different types of nanofibrous membranes will be evaluated both for pH-sensing in water and for sensing of hydrogen chloride and ammonia vapors. Their sensitivity to biogenic amines was screened to evaluate the versatility of

the membranes. Colorimetric sensors with a clear color change in response to changing acidity or alkalinity of water or air are aimed for. Flexible, large scale, reusable sensors which can be highly valuable for personal protective equipment are envisioned.

6.2 Materials and Methods

6.2.1 Materials

Dichloromethane (DCM, ≥ 99.8%), n-hexane (n-hex, 95%) and ethyl acetate (≥ 99.7%) were supplied by Sigma-Aldrich and used as received. Magnesium sulfate (dried) was supplied by Fisher Chemical. N,N'-dicyclohexylcarbodiimide (DCC) was obtained from Sigma-Aldrich. DCC was purified by dissolving in DCM and drying using $MgSO_4$, yielding a pure wax solid after evaporation of the solvent.

Biogenic amines: dimethylamine (DMA), trimethylamine (TMA) and histamine were obtained from Fluka. Putrescine and Cadaverine were obtained from Acros Organics and Tyramine was obtained from Sigma Aldrich. DMA and TMA were both solutions of 40 wt% in H_2O. Their chemical structures are given in Table 6.1.

6.2.2 Functionalization of APTES with Methyl Red

Methyl red (MR, 0.510 g, 1.89 mmol, 1 eq) and DCC (0.494 g, 2.39 mmol, 1.26 eq) were dissolved in DCM (10 mL, anhydrous). This mixture was cooled to 0 °C after which APTES (0.44 mL, 1.88 mmol, 0.99 eq) was added dropwise. The temperature was allowed to heat up to room temperature while stirring. The reaction was followed using TLC (Silica, EtOAc/n-Hex 1/1, $R_{f,MR}$ = 0.2, $R_{f,MR\text{-}APTES}$ = 0.4) and appeared to be finished after 36 h after which the solvent was evaporated and the residual red sticky viscous solid was further purified using column chromatography yielding the product as a dark red solid. Yield: 0.321 g (36%), MS(ESI): m/z = 473.20 ($[M+H]^+$).

^{1}H NMR spectroscopy (300 MHz, DMSO-6d; Bruker Avance 300 MHz spectrometer): δ(ppm) 8.55 (t, J = 5.6 Hz, 1H, -C=O-*NH*-CH_2-), 7.85 – 7.39 (m, 6H, Ar H), 6.93 – 6.76 (m, 2H, Ar H), 3.82 – 3.62 (m, 6H, -O-*CH_2*-CH_3), 3.28 (t, overlaps H_2O, -NH-*CH_2*-CH_2-), 3.08 (s, 6H, -N-*$(CH_3)_2$*), 1.61 (dt, J = 12.6, 8.0 Hz, 2H, -CH_2-*CH_2*-CH_2-), 1.24 – 1.05 (m, 9H, -O-CH_2-*CH_3*), 0.71 – 0.50 (m, 2H, -CH_2-*CH_2*-Si-). (Figure 6.1)

Table 6.1 Chemical structures of biogenic amines

Biogenic amine	Chemical structure
Dimethylamine (DMA)	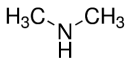
Trimethylamine (TMA)	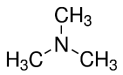
Histamine	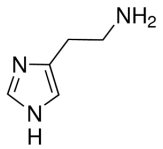
Putrescine	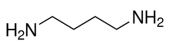
Cadaverine	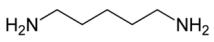
Tyramine	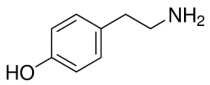

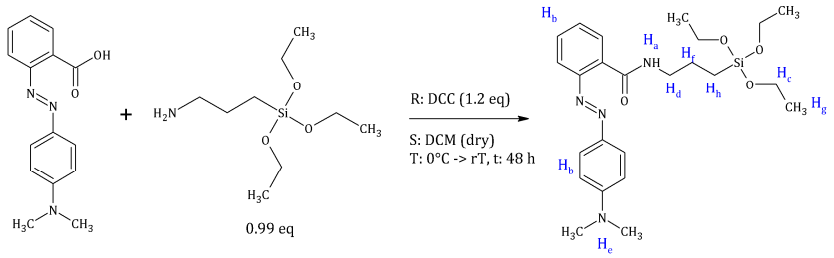

Figure 6.1 Synthesis of Methyl Red – (3-aminopropyl)triethoxysilane with proton annotations for ^{1}H NMR spectroscopy.

6.2.3 Sol preparation and electrospinning

The dye doped sols were prepared in an open set-up from a TEOS:APTES:MR(or MY):ethanol:water:HCl mixture with a molar ratio of respectively 1:0.0024:0.0024:2.2:2:0.01. Firstly, TEOS was mixed with APTES, ethanol and Methyl Red or Methyl Yellow in a beaker. Secondly, aqueous HCl was added dropwise to the mixture under vigorous stirring. After completion of the hydrolysis reaction, the sols were heated at 80 °C until the desired viscosity was reached. Finally, the sol was cooled down to room temperature. The same method was used for the sols for which MR was covalently bond to APTES. The molar ratio of TEOS:MR-APTES was again 1:0.0024. Also dye doped sols without APTES were prepared with a similar TEOS:MR:ethanol:water:HCl molar ratio of 1:0.0024:2.2:2:0.01 respectively. Again the same preparation method was used.

The electrospinning experiments were executed on a mononozzle set-up with a rotating drum collector, resulting in samples with an average size of 30 x 20 cm. The tip-to-collector distance was fixed at 15 cm, the flow rate at 1 mL h^{-1} and the voltage was adjusted in between 20 and 24 kV to obtain a stable electrospinning process. All the experiments were executed at a relative humidity of 34% RH ± 10% of and a room temperature of 22°C ± 2°C. Nanofibrous membranes with a density of ± 13 g/m^2 were obtained.

6.3 Functionalization of APTES with Methyl Red

The first goal was to modify the silica-precursor APTES with a suitable, pH-responsive dye to enable covalent immobilization of the chosen dye into the fabricated, silica-based halochromic material. APTES was chosen as its amino group can easily be modified through carbodiimide-assisted amide coupling with the carboxylic acid group present in MR. [23] Similar MR was selected as dye because of the straightforward modification of its carboxylic acid group as well as its interesting pH-responsive color change for sensing of strong acid vapors. Dye modification was performed by the Supramolecular Chemistry group of prof. dr. Richard Hoogenboom at the department of Organic and Macromolecular Chemistry.

Various methods for the amide formation were investigated involving different coupling reagents including 1-ethyl-3-(3-dimethylaminopropyl) carbodiimide (EDC), *N*,*N*′-dicyclohexylcarbodiimide (DCC) and *N*,*N*′-diisopropylcarbodiimide (DIC) or a preceding activation step of MR as activated ester with *N*-hydroxysuccinimide (NHS) or pentafluorophenol (PFP) in an attempt to simplify the purification. Eventually, the modification was optimized to a simple one-step DCC-assisted coupling at room temperature and purification using a short silica column (eluent: EtOAc/n-Hexane 1/1). By adding APTES in excess, the MR-APTES could easily be isolated after complete consumption of MR since the residual APTES and formed dicyclohexylurea are completely retained on the column. After evaporation of the solvent, a dark red solid was obtained. The disadvantage of using a silica-based column for the purification of a silica precursor was the significant immobilization of MR-APTES on the column material, reducing the yield to 36%. The simple DCC-assisted coupling and the straightforward purification, however, does allow for the synthesis of large batches (> 1 g MR-APTES).

6.4 Halochromic behavior of MY, MR and MR-APTES aqueous solutions

The functionalization of APTES with MR may have an influence on the color and color transitions of the dye, as the free carboxylic acid group is modified into an amide moiety. Therefore, it is essential to study and compare the behavior of the dyes MY, MR and MR-APTES in solution. MR and MY have been profoundly studied in literature [24]–[26]. An overview of the changes in the molecular and electronic structure, responsible for the color changes on protonation are visualized in Figure 6.2.

When APTES is coupled to MR, a covalent amide bond is formed between the carboxylic acid group of MR and the amine group of APTES removing the acidic proton of MR. As a consequence, the carboxylic acid group of the dye is no longer available to take part in the structural changes for the color transitions and it may be anticipated that the halochromic behavior of MR-APTES will be similar to that of MY (Figure 6.2 b,c).

Visible spectra of the three solutions (380 nm – 780 nm) were recorded at pH values from pH 1 to pH 12. The normalized absorbance spectra at

pH 2 and pH 12 are shown in Figure 6.3 a. The alkaline form of the dyes MR, MR-APTES and MY with λ_{max} of 432 nm, 451 nm and 446 nm, respectively, is responsible for the yellow color. Upon acidification all solutions change color from yellow over orange to red. MR has two red forms, one form associated with the monoprotonated form and the second with the diprotonated form, at pH 2 the λ_{max} of 519 nm can be attributed to the diprotonated form. [25] For MY and MR-APTES, on the contrary, the red color can be attributed to the monoprotonated form of the dye, having a λ_{max} of respectively 514 nm and 517 nm. A shift in pK_a is seen from 4.9 ± 0.2 for the MR solution to 3.1 ± 0.1 for the MR-APTES solution (Figure 6.3 b), being similar to the pK_a of MY in solution 3.3 ± 0.01 (Figure 6.3 c).

In conclusion, the blocking of the acidic proton of MR as a result of APTES functionalization, results in a shift of the pK_a making the halochromic behavior of MR-APTES similar to MY. All three dyes showed a clear color shift in response to pH-changes, making them suitable for preparation of colorimetric sensors. The absence of the carboxylic acid group on the dye MY, however, makes it not suitable for covalent immobilization onto the silicon oxide nanofibers.

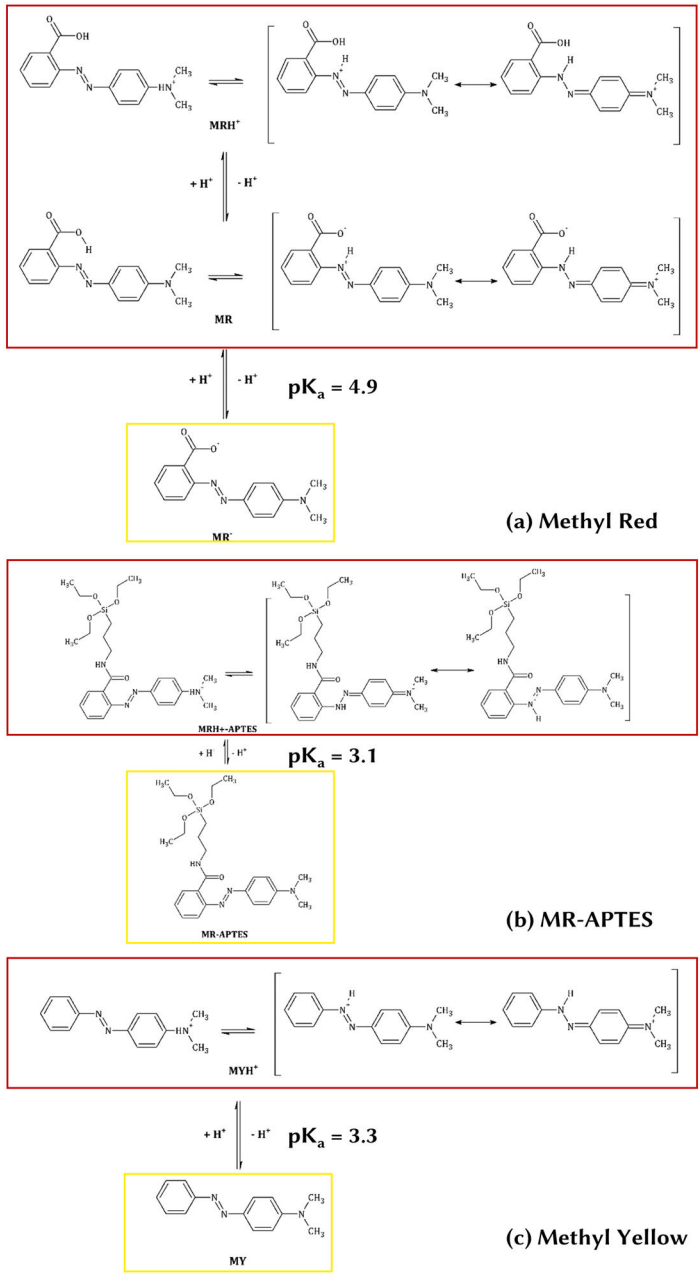

Figure 6.2 The acid-base equilibria of the dyes Methyl Red (a), MR-APTES (b) and Methyl Yellow (c). The color of the frames visualizes the color of the dyes in their alkaline and protonated forms.

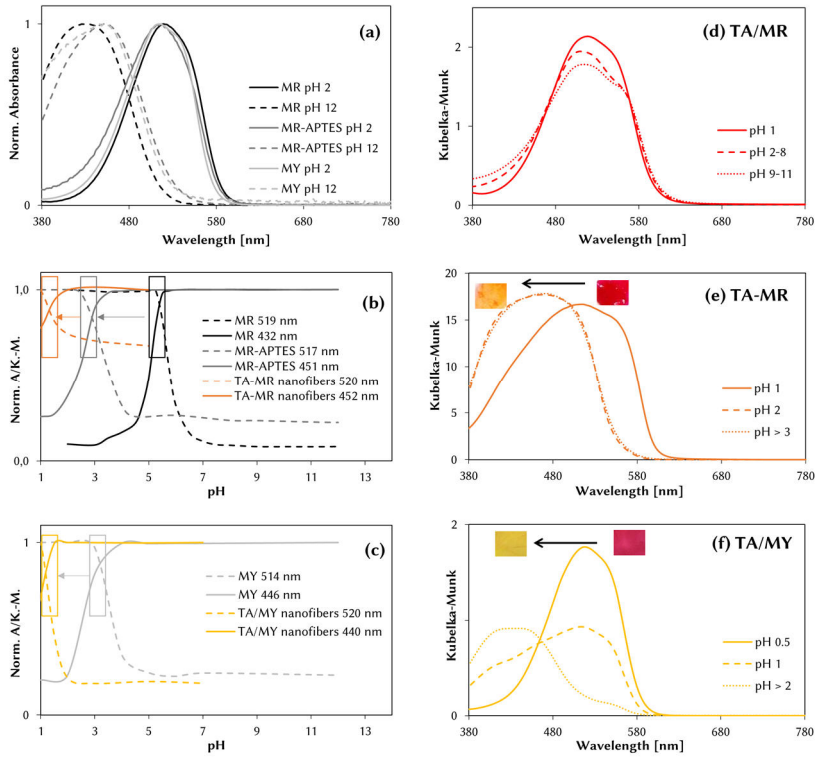

Figure 6.3 Normalized visible spectra of aqueous solutions of MR, MR-APTES and MY illustrating their halochromic behavior (a). Visible reflection spectra of the nanofibrous structures illustrating the halochromic behavior of covalently coupled TA-MR nanofibers (e), dye doped TA/MY nanofibers (f) and illustrating the absence of halochromic behavior of dye doped TA/MR nanofibers (d). An overview of the pH-sensitivity window of the MR, MR-APTES aqueous solutions and TA/MR nanofibers (b) and MY aqueous solution and TA/MY nanofibers (c) is given, showing the clear shift in pK_a upon covalent linking of MR to APTES and the shift in pH-sensing range by incorporation into nanofibers.

6.5 Electrospinning of dye-functionalized nanofibers

To produce colorimetric nanofibrous membranes, Methyl Yellow (MY), Methyl Red (MR) and MR-APTES were added to the sols prior to electrospinning. To electrospin TEOS-APTES sols with the aim for functionalized nanofibers, a sufficient amount of APTES needs to be selected that however still allows for a stable electrospinning process. Too

high amounts of APTES, molar ratios of TEOS:APTES > 1:0.005, resulted in sols for which the viscosity increased too fast and gelation occurred too quick. A molar ratio of TEOS:APTES 1:0.0024 was found to correspond to a sufficient color depth of the final nanofibrous membranes as well as a good electrospinnability.

MY was added to TEOS/APTES sols, MR was added to both TEOS/APTES sols and pure TEOS sols. In summary, four types of sols were electrospun, namely dye doped sols further referred to as T/MR (TEOS/MR) sols, TA/MR (TEOS/APTES/MR) sols and TA/MY (TEOS/APTES/MY) sols; and covalently bonded sols, further referred to as TA-MR (TEOS/MR-APTES) sols. T/MR membranes were produced according to the conditions in Chapter 3 and Chapter 4 (open system), no influence of dye addition on electrospinning and the fiber properties was seen. This is in line with dye doping of polymer nanofibers where no influence of doping on the electrospinning process is seen [16],[17],[27],[28].

The optimum viscosity range for electrospinning of TA/MR, TA-MR and TA/MY sols was in between 500 and 800 mPa s. In this viscosity range a stable electrospinning process was obtained and uniform, beadless nanofibrous membranes were produced. SEM images of the membranes are shown in Figure 6.4. The reproducibility of these nanofibrous TA/MR, TA-MR and TA/MY membranes was confirmed, with a similar average fiber diameter of 570 ± 140 nm, 585 ± 130 nm and 675 ± 190 nm respectively. Electrospinning of these sols was done for 2 hours resulting in uniform, flexible, large (20 x 30 cm) nanofibrous membranes with a clear color.

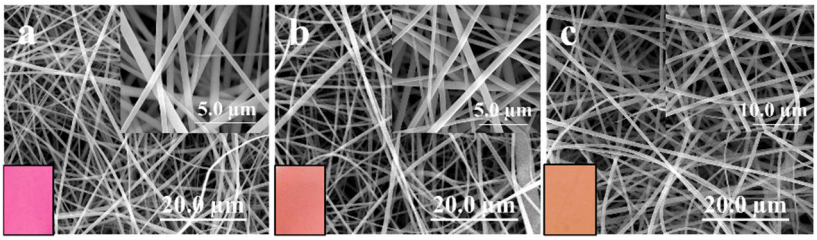

Figure 6.4 SEM images of TA/MR nanofibrous membrane (a), SEM images of TA-MR nanofibrous membrane (b) and SEM images of TA/MY nanofibrous membrane (c) (color of the respective membranes is illustrated by pictures as inset).

The color of the TA/MR, TA-MR and TA/MY samples was clearly different as shown in the inset of Figure 6.4. T/MR and TA/MR sols resulted in pink nanofibrous membranes while TA-MR and TA/MY sols resulted in orange nanofibrous membranes. This color difference can be attributed to the difference in pK_a of MR, MR-APTES and MY, respectively 4.9 ± 0.2, 3.1 ± 0.1 and 3.3 ± 0.01. A pH of 3.6, 4.0 and 3.7 was measured for TA/MR, TA-MR and TA/MY membranes, respectively, by first wetting with a drop of water followed by measuring the pH with a flat contact electrode. As a consequence, the MR in the TA/MR nanofibers is trapped in in its protonated forms (pH TA/MR membrane < pKa MR). This results in the pink color of the membrane. MY and MR-APTES in the TA/MY and TA-MR nanofibrous membranes are trapped almost fully in their alkaline form (pH TA-MR and TA/MY membranes > pKa MR-APTES and MY, respectively), which gives an orange color to the membrane.

6.6 Halochromic behavior of dye-functionalized nanofibrous membranes

The hydrophilic properties of the non-functionalized silica nanofibrous samples change in time, as discussed in Chapter 3. The halochromic behavior of the nanofibrous membranes was tested both immediately after electrospinning and after storing for 21 days at high humidity (90%RH). During storing at high humidity, the samples became hydrophilic. This was again confirmed via contact angle measurements on the TA/MR and TA-MR nanofibrous membranes. An average value of 136° ± 2° was found when a water droplet was placed onto the membranes before storing at high humidity. Afterwards, a contact angle was no longer measurable (or thus 0°) and immediate wetting of the samples was seen. Based on the ATR-FTIR spectra (Figure 6.5) the same conclusion could be made as for the pure silica nanofibers, described in section 3.5. It was confirmed that once the membranes become hydrophilic their properties are stable in time. The samples evaluated after storing at high humidity showed the same halochromic behavior as the samples before, but with a much faster response time. It is known that the wettability of the nanofibrous samples is a determining factor in the sensor response time [16]. This wettability is directly linked to the poor hydrophilicity of the as-spun nanofibers. Since the halochromic behavior is the same before and

after storing, only the hydrophilic samples will be discussed in detail in the following.

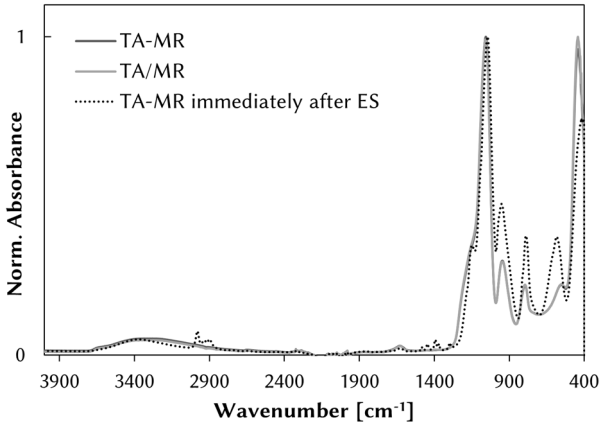

Figure 6.5 ATR-FTIR spectra of TA-MR and TA/MR nanofibers 2 months after electrospinning and TA-MR nanofibers measured immediately after electrospinning showing a broadening of the OH peak (3300 cm^{-1}) in time and the disappearance of residual solvent and alkyl groups.

The halochromic behavior of all samples is evaluated by immersing the samples in pH-baths from pH 1 till pH 12 (with a step of 1 pH-unit). The T/MR and TA/MR nanofibrous membranes did not show a color change, Figure 6.3 d. This is attributed to the leaching of the dye from the silica matrix (Figure 6.6), which was expected since no chemical bond is formed between the dye and the silicon oxide network. Although the fabric did not change color as only the dye is retained that is not exposed to the aqueous environment, the leached dye did change color in the aqueous solution with the same halochromic behavior as the pure MR in aqueous solution.

The TA-MR nanofibrous membranes showed a more interesting halochromic behavior. A clear color change was seen from pink to orange, Figure 6.3 e. After immersion of the TA-MR samples for 24 hours almost no dye leaching (less than 2%) was seen and the samples remained deeply colored (Figure 6.6). Due to the hydrophilic behavior and the highly porous nature of the material, these nanofibrous sensors revealed a response time within less than a second. The samples, which were orange at the start, changed to pink at pH 1. Increasing the pH above 2 resulted in the original orange color, with the color change being reversible. The acidic peak maximum and the alkaline peak maximum are found at 520

nm and 452 nm, respectively. Compared to MR-APTES in aqueous environment no peak shift was seen. However, a shift in pH-transition region to lower pH-values was noted compared to MR-APTES, for which a pKa of 3.1 ± 0.1 was found (Figure 6.3 b). A second shift of the pH-range is thus seen compared to MR-APTES in solution and pure MR in solution, Figure 6.3 b. The change in transition pH can be attributed to the covalent bond formation of the MR-APTES with the silicon oxide matrix and the interaction of MR with the surrounding silicon matrix. This is in line with results on polymeric matrices where a shift in pK_a is seen when pH-indicator dyes are incorporated due to the dye-matrix interactions [16],[29]. These TA-MR nanofibrous membranes can thus be used as acid sensor in aqueous environment.

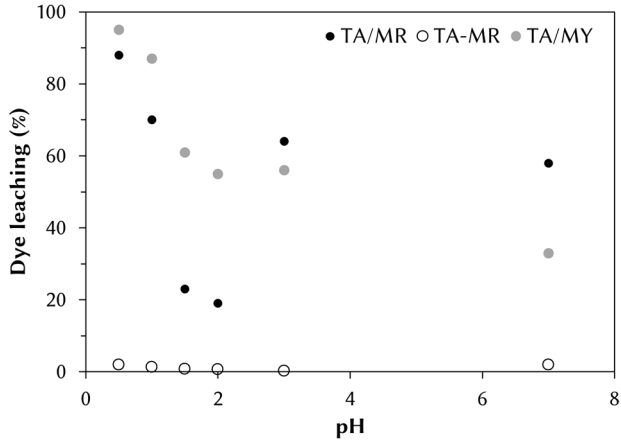

Figure 6.6 Dye leaching (%) of dye dunctionalized nanofibrous membranes as a function of pH

The TA/MY nanofibrous membranes show a highly similar halochromic behavior as the TA-MR membranes (Figure 6.3 f), however, dye leaching showed to be a major issue (Figure 6.6). The samples went from pink at pH 0.5 and pH 1 to yellow at pH 2 and higher. The acidic peak maximum at 520 nm shifts to the alkaline peak maximum at 440 nm, thus almost no difference in peak shift is noted compared to MY in solution. Nonetheless, a shift was seen in the pH-transition region to lower pH-values compared to MY in solution, for which a pKa of 3.3 ± 0.01 was found (Figure 6.3 c). This can again be attributed to the interaction of the dye with the surrounding silicon matrix. Due to the high dye leaching, 95% after 24h

immersion at pH 0.5, the TA/MY samples are not reusable as pH-sensor in aqueous environment.

In summary, the TA-MR membranes are highly suitable as pH-sensor in strong acidic environment, where polymers are no longer usable. Moreover, a covalent bond between matrix and dye showed to be essential to obtain a fast, reversible and reusable pH-sensor that can operate in aqueous environment.

6.7 HCl and NH_3 gas sensing

Sensing acid or alkaline atmospheres in an easy manner with a fast visual signal is highly valuable in industrial processes or in personal protective equipment and clothes. The color change of the TA/MR, TA-MR and TA/MY nanofibers are evaluated and compared when they are exposed to HCl vapors and NH_3 vapors. T/MR nanofibers show a similar behavior as TA/MR and are not discussed in further detail.

The samples were placed in a closed cuvette and the partial pressure of the tested gas was increased gradually. The TA/MR nanofibers, which were pink from the start, showed no color shift when exposed to HCl vapors (Figure 6.7 a). However, a reduction of the peak width is measured with increasing partial pressure of HCl, which will lead to a brighter color. A difference in ΔE around 3 was measured, thus not clearly visual for the naked eye. The acidic peak maximum is slightly shifted from 504 nm to 508 nm upon exposure to HCl. As stated above, the TA/MR nanofibers have a pink color from the start and the MR is already trapped inside the nanofibers in its mono- and diprotonated forms. This is again confirmed with the HCl sensing by the absence of a color change. On the other hand, exposing the TA/MR nanofibers to NH_3 vapors resulted in an immediate visual color change of the fibers. They gradually change color from pink to yellow when the partial pressure of ammonia is gradually increased (Figure 6.7 d). This is explained by the gradual deprotonation of the dye to the alkaline form, corresponding with a yellow color. The peak maximum shifts from 504 nm for the original sample to 456 nm when the sample is exposed to an excess of NH_3.

The fast response time of seconds can be attributed to the typical characteristics of nanofibrous membranes: their high specific surface area

and high porosity. When the samples are taken out of the cuvettes, they go back to their original color in around 20 minutes. This lag time provides a memory function that allows visual read-out up to 20 minutes after the exposure to NH_3 vapor, which is strongly desirable, for example, for personal protective equipment. These TA/MR membranes are thus ideal for sensing of NH_3 vapors.

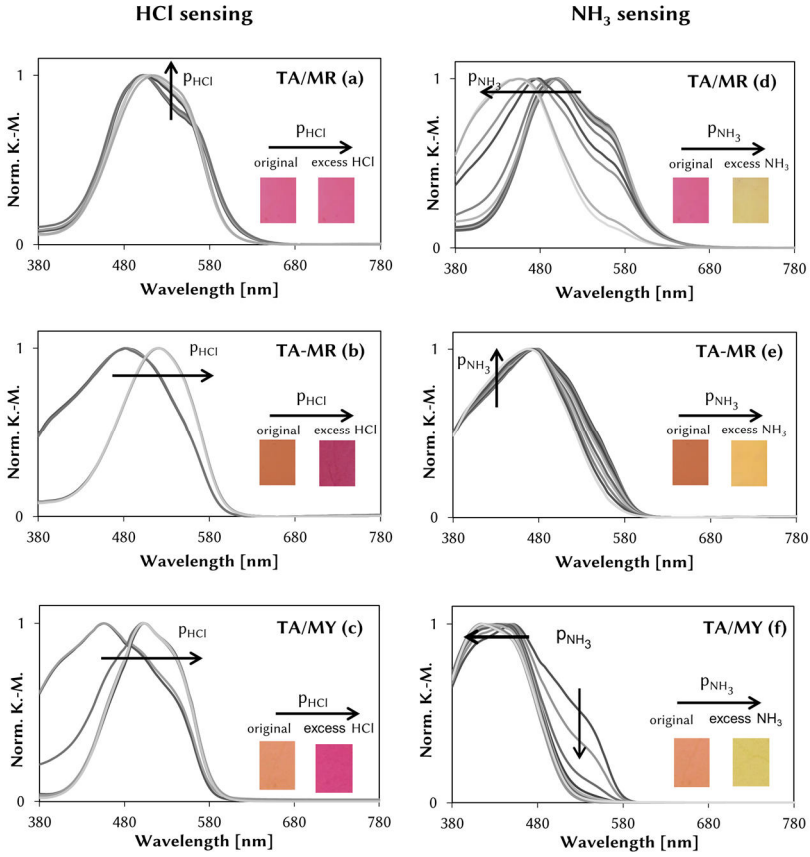

Figure 6.7 Normalised visible Kubelka-Munk spectra of TA/MR with increasing partial pressure of HCl (a) and NH3 (d), Normalised visible Kubelka-Munk spectra of TA-MR with increasing partial pressure of HCl (b) and NH3 (e), and normalised visible Kubelka-Munk spectra of TA/MY with increasing partial pressure of HCl (c) and NH3 (d) (insets: pictures of sample showing the corresponding color transitions after exposure to vapors)

HCl and NH_3 vapor sensing using the orange TA-MR and TA/MY nanofibrous membranes gives complementary results. These nanofibers

give a clear and immediate color change from orange to pink when exposed to HCl vapors (Figure 6.7 b,c). The dye shifts from the alkaline to the protonated form. The peak maximum shows a bathochromic shift from 484 nm tot 524 nm for TA-MR and from 456 nm to 504 nm for TA/MY upon exposure to HCl. The response to NH_3 vapors for these membranes is less clear. The color changes from orange to yellow (Figure 6.7 e,f). This less pronounced color shift, results from a peak narrowing for TA-MR and a peak shift from 452 nm to 416 nm for TA/MY. Again, the color change was immediate upon exposure to the vapors. A small amount of the dye seems to be present in the protonated form, shifting to the alkaline form upon exposure to NH_3, resulting in a color change from orange to yellow. A similar time period, around 20 min, was noted for the samples to go back to their original color after exposure to the vapors, again providing a valuable memory function. Complementary to the TA/MR nanofibrous, these TA-MR and TA/MY membranes are thus ideal for sensing of HCl vapors. In addition, they can be used for NH_3 sensing as well, although with a less clear visual response.

The sensitivity of the nanofibrous membranes was evaluated by gradually increasing the amount of HCl or NH_3 vapors to the closed cuvettes. Figure 6.8 visualizes the color change ΔE as a function of partial pressure. HCl sensing was possible for TA-MR and TA/MY nanofibrous membranes with a visual color shift from orange to pink in between 160 ppm - 300 ppm, and 100 – 300 ppm respectively (partial pressure of 1×10^{-4} bar/5×10^{-5} bar - 2×10^{-4} bar, ΔE of 21 and 27 respectively), Figure 6.8 a. These ppm values correspond to the AEGL-2[2] level of 100 ppm for HCl vapors. For TA/MR there was no visual color shift with increasing partial pressure of HCl. NH_3 sensing was possible starting from 220 ppm or $2{,}85 \times 10^{-4}$ bar (ΔE of 14) when using the TA/MR membranes, Figure 6.8 b. This sensing value of 220 ppm corresponds to the AEGL-2 level of NH_3. For these membranes the color shifted gradually, going from pink over orange to yellow. The excess amount of NH_3 resulted in a color difference ΔE of 40. A certain color can thus be linked with a certain partial pressure of NH_3 vapors. For the TA-MR and TA/MY nanofibrous membranes, a gradual shift from orange to yellow with gradual increasing partial pressure of NH_3 is seen. Although visually less clear to distinct, a yellow color started to appear at 220 ppm ($2{,}85 \times 10^{-4}$ bar). The color difference between the

[2] AEGL-2 is the airborne concentration (ppm) above which the general population would experience irreversible or other serious, long-lasting adverse health effects.

original sample and an excess of NH_3 is clearly visible (ΔE of 22 and 25, respectively), Figure 6.8 b.

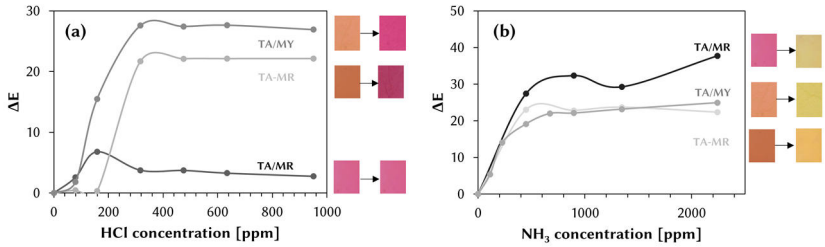

Figure 6.8 Color difference ΔE between original sample and sample exposed to HCl vapors as a function of HCl vapor concentration (a), color difference ΔE between original sample and sample exposed to NH_3 vapors as a function of NH_3 vapor concentration (b) (insets: pictures of sample showing the corresponding color transitions after exposure to vapors)

Finally, the reversibility, reusability and reproducibility is visualized in Figure 6.9. The TA/MR, TA-MR and TA/MY samples were exposed to 10 cycles of HCl vapors alternated with NH_3 vapors. Each time an immediate color change was seen from pink to yellow or reversed. Thus confirming the reusability and stability of the colorimetric sensors.

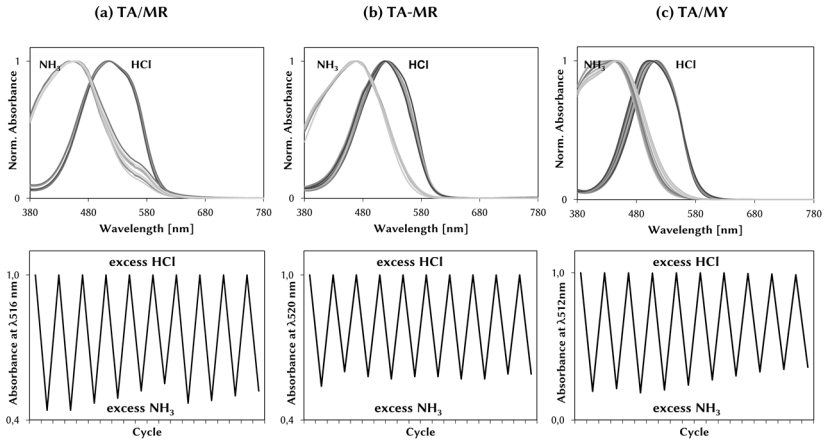

Figure 6.9 Reproducibility and reversibilty of HCl and NH3 sensing with TA/MR, TA-MR and TA/MY nanofibrous membranes: (top) normalised absorbance spectra of 10 cycles of excesses of HCl and NH_3; (bottom) absorbance at acidic peak maximum as a function of the cycle HCl or NH_3 of TA/MR (a), TA-MR (b), and TA/MY (c).

6.8 Biogenic amines sensing

In addition to the sensing of ammonia and especially to demonstrate the versatility of the samples, the sensitivity of the samples for various biogenic amines that are released during decomposition of meat and fish was screened. The visual color change of TA/MR and TA-MR membranes were evaluated upon immersion in aqueous solutions of various biogenic amines with concentrations in the order of the limits that are allowed in food (Table 6.2) [30],[31]. The TA/MR nanofibrous samples showed a clear color change within less than a minute from pink to orange or yellow (Figure 6.10), whereas the TA-MR gave a less visual but still noticeable color change from orange to yellow (Figure 6.11). The results demonstrate that all tested amines except for tyramine resulted in clear visual color changes up to concentrations of 100 ppm and even 20 ppm for putrescine. In addition, TA/MR samples change color from pink to orange within 10 minutes above a 500 ppm TMA and DMA solution. Direct contact with the solution is thus not necessary, which offers the potential to use these membranes for food spoilage detection by incorporation in food packaging. These samples might thus, in addition to protective equipment, also be highly valuable for control and monitoring of food quality. Future work can focus on reduced dye leaching and covalent bonding of amine sensitive dyes on more compatible matrices for food applications.

Table 6.2 Color change of TA/MR and TA-MR membranes after immersion in biogenic amines solutions with various concentrations.

	TA/MR				**TA-MR**	
	5000 ppm	500 ppm	100 ppm	20 ppm	500 ppm	100 ppm
Histamine	+	+	+	-	+	+
Tyramine	-	-	-	-	-	-
Putrescine	+	+	+	+	+	+
Cadaverine	+	+	+	-	+	+
TMA	+	+	+	-	+	-
DMA	+	+	+	-	+	-

+: visual color change - : no visual color change

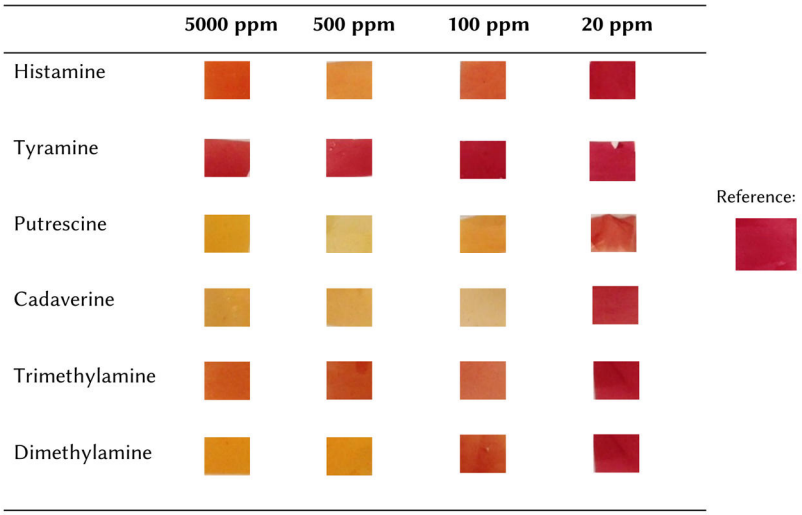

Figure 6.10 Color change of TA/MR nanofibrous membranes after immersion in biogenic amine solutions (Histamine, Tyramine, Putrescine, Cadaverine, dimethylamine and trimethylamine) with concentrations of 5000 ppm, 500 ppm, 100 ppm and 20 ppm.

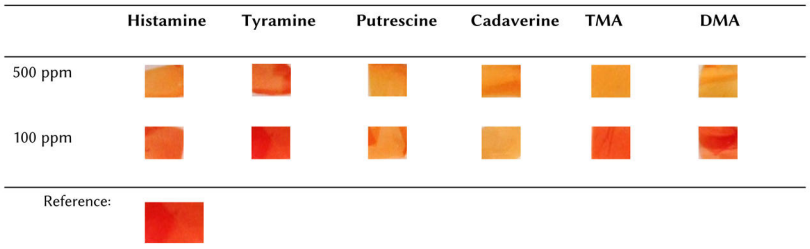

Figure 6.11 Color change of TA-MR nanofibrous membranes after immersion in biogenic amine solutions with concentrations of 500 ppm and 100 ppm.

6.9 Conclusion

In summary, large area, flexible, reusable colorimetric nanofibrous silicon oxide sensors were developed for the detection of pH-changes in water, HCl and NH_3 vapors, and biogenic amines. The importance of a covalent link for the use of these membranes in water is proven, and thus only the covalently coupled MR membranes were suitable to be used as pH-sensor in aqueous acidic environments. Colorimetric sensors were developed

that allow fast and accurate detection of local signals without the need of additional electronic devices. These nanofibrous membranes thus show to be ideal to be used as a visual warning patch in personal protective clothes or equipment since an immediate and clear color change is obtained upon exposure to hydrogen chloride or ammonia vapors. The more economical dye doped membranes can thus be used for solid state gas sensing applications where dye leaching is no issue, covalently functionalized membranes are however indispensable for applications where the sensors are exposed to liquids, e.g. rain. Finally, the sensitivity of these membranes to biogenic amines showed their high versatility for multiple applications such as control of food quality.

The use of these colorimetric nanofibrous sensors can be broadened to the sensing of other analytes. Optical sensors that enable the continuous monitoring of several solvents are highly relevant for applications in chemical and food industries, as well as in environmental control and personal protective clothing and equipment [32]. Chapter 7 involves the study of these colorimetric sensors for the detection of solvents.

References

[1] O. Belhadj Miled, D. Grosso, C. Sanchez, and J. Livage, "An optical fibre pH sensor based on dye doped mesostructured silica," *J. Phys. Chem. Solids*, vol. 65, no. 10, pp. 1751–1755, 2004.

[2] C. Rottman, A. Turniansky, and D. Avnir, "Sol-gel physical and covalent entrapment of three methyl red indicators: a comparative study," *J. Sol-Gel Sci. Technol.*, vol. 13, pp. 17–25, 1998.

[3] C. J. Brinker and G. W. Scherer, *Sol-Gel Science: The Physics and Chemistry of Sol-Gel Processing*. 1990.

[4] I. M. El-Nahhal, J. Livage, S. M. Zourab, F. S. Kodeh, and A. Al swearky, "Entrapment of phenol red (PR) pH indicator into sol–gel matrix in presence of some surfactants," *J. Sol-Gel Sci. Technol.*, vol. 75, no. 2, pp. 313–322, 2015.

[5] E. Wang, K.-F. Chow, V. Kwan, T. Chin, C. Wong, and A. Bocarsly, "Fast and long term optical sensors for pH based on sol-gels," *Anal. Chim. Acta*, vol. 495, pp. 45–50, 2003.

[6] B. Gu, M. Yin, a P. Zhang, J. Qian, and S. He, "Biocompatible fiber-optic pH sensor based on optical fiber modal interferometer self-assembled with sodium alginate/polyethylenimine coating," *IEEE Sens. J.*, vol. 12, no. 5, pp. 1477–1482, 2012.

[7] F. R. Zaggout, "Entrapment of phenol red pH indicator into a sol–gel matrix," *Mater. Lett.*, vol. 60, no. 8, pp. 1026–1030, 2006.

[8] F. R. Zaggout, N. M. El-Ashgar, S. M. Zourab, I. M. El-Nahhal, and H. Motaweh, "Encapsulation of methyl orange pH-indicator into a sol-gel matrix," *Mater. Lett.*, vol. 59, no. 23, pp. 2928–2931, 2005.

[9] S. Dong, M. Luo, G. Peng, and W. Cheng, "Broad range pH sensor based on sol–gel entrapped indicators on fibre optic," *Sensors Actuators B Chem.*, vol. 129, no. 1, pp. 94–98, 2008.

[10] E. Wang, K.-F. Chow, W. Wang, C. Wong, C. Yee, A. Persad, J. Mann, and A. Bocarsly, "Optical sensing of HCl with phenol red doped sol-gels," *Anal. Chim. Acta*, vol. 534, pp. 301–306, 2005.

[11] A. Persad, K.-F. Chow, W. Wang, E. Wang, A. Okafor, N. Jespersen, J. Mann, and A. Bocarsly, "Investigation of dye-doped sol-gels for ammonia gas sensing," *Sensors Actuators B Chem.*, vol. 129, pp. 359–363, 2008.

[12] Y.-Y. Lv, J. Wu, and Z.-K. Xu, "Colorimetric and fluorescent sensor constructing from the nanofibrous membrane of porphyrinated polyimide for the detection of hydrogen chloride gas," *Sensors Actuators B Chem.*, vol. 148, pp. 233–239, 2010.

[13] B. Ding, M. Wang, J. Yu, and G. Sun, "Gas Sensors Based on Electrospun Nanofibers," *Sensors*, vol. 9, pp. 1609–1624, 2009.

[14] L. Van Der Schueren, T. Mollet, Ö. Ceylan, and K. De Clerck, "The development of polyamide 6.6 nanofibres with a pH-sensitive function by electrospinning," *Eur. Polym. J.*, vol. 46, no. 12, pp. 2229–2239, 2010.

[15] L. Van Der Schueren, K. Hemelsoet, V. Van Speybroeck, and K. De Clerck, "The influence of a polyamide matrix on the halochromic behaviour of the pH-sensitive azo dye Nitrazine Yellow," *Dye. Pigment.*, vol. 94, no. 3, pp. 443–451, 2012.

[16] L. Van der Schueren, T. De Meyer, I. Steyaert, Ö. Ceylan, and K. Hemelsoet, "Polycaprolactone and polycaprolactone/chitosan nanofibres functionalised with the pH-sensitive dye Nitrazine Yellow," *Carbohydr. Polym.*, vol. 91, pp. 284–293, 2013.

[17] I. Steyaert, G. Vancoillie, R. Hoogenboom, and K. De Clerck, "Dye immobilization in halochromic nanofibers through blend electrospinning of a dye-containing copolymer and polyamide-6," *Polym. Chem.*, 2015.

[18] S. Trupp, M. Alberti, T. Carofiglio, E. Lubian, H. Lehmann, R. Heuermann, E. Yacoub-George, K. Bock, and G. J. Mohr, "Development of pH-sensitive indicator dyes for the preparation of micro-patterned optical sensor layers," *Sensors Actuators, B Chem.*, vol. 150, no. 1, pp. 206–210, 2010.

[19] G. J. Mohr, H. Müller, B. Bussemer, A. Stark, T. Carofiglio, S. Trupp, R. Heuermann, T. Henkel, D. Escudero, and L. González, "Design of acidochromic dyes for facile preparation of pH sensor layers," *Anal. Bioanal. Chem.*, vol. 392, no. 7–8, pp. 1411–1418, 2008.

[20] A. Lobnik, I. Oehme, I. Murkovic, and O. S. Wolfbeis, "pH optical sensors based on sol-gels: Chemical doping versus covalent immobilization," *Anal. Chim. Acta*, vol. 367, no. 1–3, pp. 159–165, 1998.

[21] L. Van Der Schueren, K. De Clerck, G. Brancatelli, G. Rosace, E. Van Damme, and W. De Vos, "Novel cellulose and polyamide halochromic textile sensors based on the encapsulation of Methyl Red into a sol-gel matrix," *Sensors Actuators, B Chem.*, vol. 162, no. 1, pp. 27–34, 2012.

[22] S. Tao, G. Li, and J. Yin, "Fluorescent nanofibrous membranes for trace detection of TNT vapor," *J. Mater. Chem.*, vol. 17, no. 26, p. 2730, 2007.

[23] Y. Yi, M. J. Farrow, E. Korblova, D. M. Walba, and T. E. Furtak, "High-sensitivity aminoazobenzene chemisorbed monolayers for photoalignment of liquid crystals," *Langmuir*, vol. 25, no. 2, pp. 997–1003, 2009.

[24] K. M. Tawarah and H. M. Abushamleh, "a Spectrophotometric Study of the Tautomeric and Acid-Base Equilibria of Methyl-Orange and Methyl Yellow in Aqueous Acidic Solutions," *Dye. Pigment.*, vol. 16, no. 3, pp. 241–251,

1991.

[25] K. M. Tawarah and H. M. Abushamleh, "A spectrophotmetric study of the acid-base equilibria of o-methyl red in aqueous solutions," *Dye. Pigment.*, vol. 17, pp. 203–215, 1991.

[26] S. Bell, A. Bisset, and T. J. Dines, "Ab initio and density functional study of the resonance Raman spectra of Methyl Red, Ethyl Red and their protonated derivatives," *J. Raman Spectrosc.*, vol. 29, no. 6, pp. 447–462, 1998.

[27] A. Camposeo, F. Di Benedetto, R. Stabile, R. Cingolani, and D. Pisignano, "Electrospun dye-doped polymer nanofibers emitting in the near infrared," *Appl. Phys. Lett.*, vol. 90, no. 14, p. 143115, Apr. 2007.

[28] A. Agarwal, A. Raheja, T. S. Natarajan, and T. S. Chandra, "Development of universal pH sensing electrospun nanofibers," *Sensors Actuators, B Chem.*, vol. 161, pp. 1097–1101, 2012.

[29] T. De Meyer, I. Steyaert, K. Hemelsoet, R. Hoogenboom, V. Van Speybroeck, and K. De Clerck, "Halochromic properties of sulfonphthaleine dyes in a textile environment: The influence of substituents," *Dye. Pigment.*, vol. 124, pp. 249–257, 2016.

[30] FAO/WHO [Food and Agriculture Organization of the United Nations/World Health Organization], "Public Health Risks of Histamine and other Biogenic Amines from Fish and Fishery Products," 2013.

[31] A. Naila, S. Flint, G. Fletcher, P. Bremer, and G. Meerdink, "Control of Biogenic Amines in Food-Existing and Emerging Approaches," *J. Food Sci.*, vol. 75, no. 7, pp. R139–R150, 2010.

[32] P. C. a Jerónimo, A. N. Araújo, and M. Conceição B S M Montenegro, "Optical sensors and biosensors based on sol-gel films.," *Talanta*, vol. 72, no. 1, pp. 13–27, 2007.

7

Sensitive membranes: solvatochromic silicon oxide nanofibrous membranes

Further enhancement in the versatility of the colorimetric sensors as reported in Chapter 6 is carried out by developing solvatochromic sensor materials. Silicon oxide nanofibrous membranes are functionalized with the dye C.I. Disperse Red 1 via three functionalization techniques, namely dye doping, inline covalent immobilization and covalent immobilization by post-functionalization via coating. Although further research is needed to design true solvatochromic materials, the post-functionalization via coating was the best route to reduce the dye leaching and to improve the sensor properties.

7.1 Introduction

Chapter 6 demonstrated the versatility of Methyl Red and Methyl Yellow functionalized silicon oxide nanofibers by colorimetric sensing of pH-changes in water, HCl and NH_3 vapors and biogenic amines. In sensor technology, developments continuously aim at an improved sensitivity, simplicity, response time, reproducibility and selectivity [1],[2]. Similar to pH-sensitive colorimetric sol–gel sensor materials, solvatochromic dyes have been immobilized in sol-gel based porous films to obtain solvatochromic sensors [3],[4]. Simon *et al* [3] immobilized solvatochromic dyes on porous glass films. High dye leaching was noticed reducing the applicability in time. Covalent coupling of the dye resulted in decreased leaching but no proof of solvatochromic sensitivity was seen.

Limited research has been carried out on the development of solvatochromic fibrous membranes via electrospinning [5]. Davis *et al* [6] and Yoon *et al* [7] both produced polydiacetylene (PDA) embedded micro/nanofibers via electrospinning. Polydiacetylene is a conjugated polymer changing color from blue to red upon response to heat, mechanical stress and organic solvents; which is broadly explored as colorimetric sensing material. Both authors used TEOS to enforce the nanofibrous mats and to enhance their chemical resistance. However, a major limitation of the applicability of these sensor mats is that the solvatochromic changes were found to be irreversible.

In this chapter, focus is given to the dye C.I. Disperse Red 1 (DR1) to obtain solvatochromic sensors. It is known from Chapter 6 that a covalent linkage between dye and matrix is essential to prevent dye leaching. DR1 is selected for its primary alcohol present which is excellent for functionalization. Chlorotriethoxysilane (CTES) is selected as sol-gel precursor for covalent coupling to DR1. A first step is thus the functionalization of the dye DR1 with CTES, resulting in the modified dye DR1-CTES. Next, the modified dye DR1-CTES is used to functionalize the nanofibrous membranes. Similar to Chapter 6, DR1-CTES is added inline (prior to electrospinning) resulting in covalent immobilization of the dye in the sol-gel network of the nanofibers. Additionally, DR1-CTES is also applied on pure hydrophilic silica nanofibers by post-functionalization via coating. To fully understand the importance of the covalent linkage, the comparison is made with DR1 doped nanofibrous membranes. The solvatochromic behavior of all membranes is evaluated via a detailed

study of dye leaching, materials stability and sensor performance in various solvents. The coating technique explored in this chapter broadens the applicability of the solvatochromic sensor layer from silica nanofibrous membranes to other substrates. This is highly relevant when various end-applications are envisioned.

7.2 Materials and Methods

7.2.1 Materials

The solvent tetrahydrofuran (THF) and catalyst pyridine were both supplied by Sigma-Aldrich. THF was dried using flasks whereas pyridine was sourced in small quantities in its dry form and used as such. Dry DCM used for coating of the nanofibrous membranes was obtained from Sigma-Aldrich.

The solvatochromic behavior was evaluated for eight different solvents: dimethylsulfoxide (DMSO), ethanol, methanol, acetone, dimethylformamide (DMF), dichloromethane (DCM), diethylether and cyclohexanone. All of the solvents, except ethanol, were supplied by Sigma-Aldrich and used as received. Ethanol absolute was obtained from Fiers.

7.2.2 Functionalization of CTES with DR1

The functionalization was based on the modification of C.I. Disperse Red 19 with alkoxysilane groups according to Paoprasert *et al* [8]. C.I. Disperse Red 1 (DR1, 1g, 3.18 mmol) and pyridine (0.39g, 4.77 mmol) were dissolved in dry tetrahydrofuran (THF, 100 mL). The system was kept under an inert argon atmosphere. Next, the sol-gel precursor chlorotriethoxysilane (CTES) was added dropwise to the mixture. The temperature was kept at 50 °C and the mixture was continuously stirred. After completion of the reaction the unwanted pyridinium salt was eliminated by filtration and the solvent evaporated using a rotary evaporator. Thin-layer chromatography (TLC) was used to check the purity of the product. The red sticky viscous solid was then further purified via column chromatography for the removal of all unreacted DR1.

A reaction time of 3 days was used for the production of DR1-CTES. The reaction scheme of DR1-CTES is given in Figure 7.1. DR1-CTES was used for the production of inline functionalized nanofibrous membranes (TC-DR) and for coating of pure hydrophilic silica nanofibrous membranes. MS(ESI): m/z = 478.20 ($[M+H]^+$), m/z = 824.20 (Crosslinked product, Figure 7.2). ^{1}H NMR spectroscopy (300 MHz, $CDCl_3$; Bruker Avance 300 MHz spectrometer): δ(ppm) 8.2 (2H, Hg), 7.8 (4H, Hf and He), 6.7 (2H, Hd), 3.9 and 3.5 (6H, Hc), 3.8 (6H, Hb), 1.2 (12H, Ha). (Figure 7.2)

The integration of the peaks in the ^{1}H NMR spectrum does not fully correspond to pure DR1-CTES (Figure 7.2), indicating that already some internal crosslinking may be initiated as a result of the followed synthesis conditions. This was also supported by the MS data.

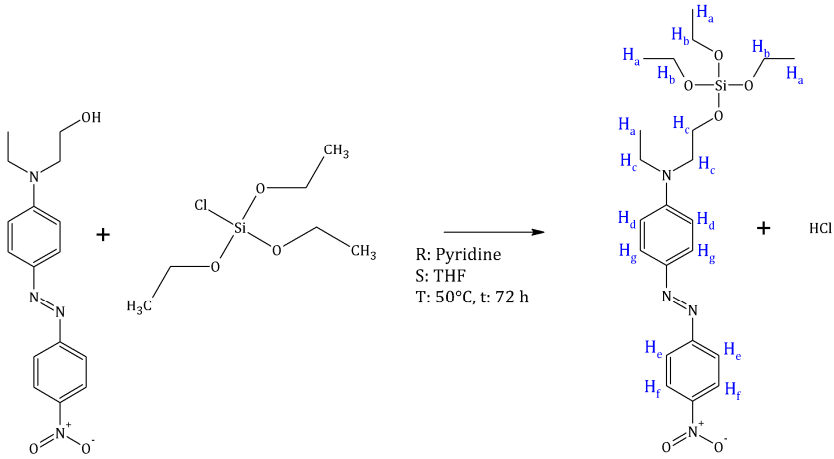

Figure 7.1 Synthesis of C.I. Disperse Red 1- chlorotriethoxysilane with proton annotations for ^{1}H NMR spectroscopy.

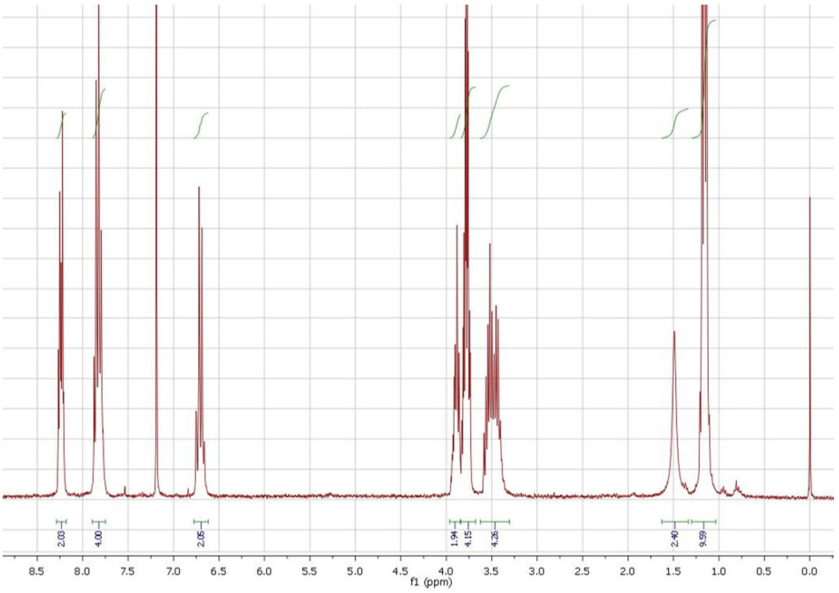

Figure 7.2 ^{1}H-NMR spectrum of DR1-CTES.

7.2.3 Sol preparation and electrospinning

All sols were prepared using an open set-up. A mixture of TEOS:CTES:DR1:ethanol:H_2O:HCl was used for the dye doped TEOS/CTES sol with a molar ratio of 1:0.0025:0.0025:2.2:2:0.01 respectively. First, TEOS and CTES were mixed in a beaker together with DR1 and ethanol. Next, aqueous HCl is added dropwise under vigorous stirring. After completion of the hydrolysis reactions, the sol is heated to 80°C and this is maintained until the desired viscosity is reached. Finally, the sol is cooled down to room temperature. The dye doped TEOS/CTES sols will be denoted as TC/DR sols. The same method was used for the sol for which DR1 was covalently coupled to CTES. The molar ratio of TEOS:DR1-CTES was 1:0.0025, similar to the ratio of the dye doped sols. These covalently immobilized sols will be denoted as TC-DR sols. DR1 doped TEOS sols are also prepared using a similar method, a molar ratio of TEOS:DR1:ethanol:H_2O:HCl 1:0.0025:2:2:0.01 was used. These dye doped TEOS sols will be denoted as T/DR sols. Pure silica nanofibers used for coating were also prepared using sols with a molar ratio of

TEOS:ethanol:H_2O:HCl 1:2:2:0.01 and a similar preparation procedure (open set-up, Chapter 2).

The electrospinning of all sols was carried out using a mononozzle set-up with a rotating drum collector. The tip-to-collector distance was fixed at 15 cm, the flow rate at 1 mL h^{-1} and the voltage was adjusted in between 20 and 24 kV to obtain a stable electrospinning process. All experiments were executed at a relative humidity of 33% RH ± 10% of and a room temperature of 22°C ± 2°C. Nanofibrous membranes with a density of ± 13 g/m^2 were obtained.

7.2.4 Coating of silica nanofibers with DR1-CTES

Hydrophilic silica nanofibers (aged for 1 year) were coated with DR1-CTES by immersing a nanofibrous sample in 135 mL of dry DCM with 1 g of the functionalized dye. An inert atmosphere was maintained using nitrogen gas. The nanofibrous membrane was left in the bath for 24 hours at 50°C. The uncoupled DR1-CTES was removed from the nanofibrous membrane via soxhlet extraction with ethanol for 6 hours. The samples were dried overnight in an oven at 50 °C. Silica nanofibrous membranes coated with the dye DR1-CTES will be denoted as C-DR coated TEOS.

7.3 Functionalization of CTES with DR1

The sol-gel precursor CTES was modified with the solvatochromic dye C.I. Disperse Red 1 (DR1) to enable covalent immobilization of the dye in and onto the resulting nanofibers. The procedure followed was based on a recipe found in literature by Paoprasert *et al* [8]. The terminal nucleophilic hydroxyl group of DR1, separated from the chromophore, reacts easily with the chlorine group of CTES, forming the functionalized DR1-CTES product and hydrochloric acid (Figure 7.1). MS and ^{1}H NMR analysis revealed the presence of some crosslinked CTES, initiated by the applied reaction conditions (Figure 7.2). Dye modification was performed by the Supramolecular Chemistry group of prof. dr. Richard Hoogenboom at the department of Organic and Macromolecular Chemistry.

7.4 Solvatochromic behavior of the dyes DR1 and DR1-CTES

It is known that the optical properties of indicator dyes may be very sensitive to immobilization reactions and/or the environment [9]–[11], which is also demonstrated in Chapter 6. Both the dyes DR1 and DR1-CTES were dissolved in eight solvents with varying polarity, and visual spectra (380 nm – 780 nm) were recorded (Figure 7.4). The wavelength at maximum absorption (λ_{max}) and the visual color of the solutions are given in Table 7.1.

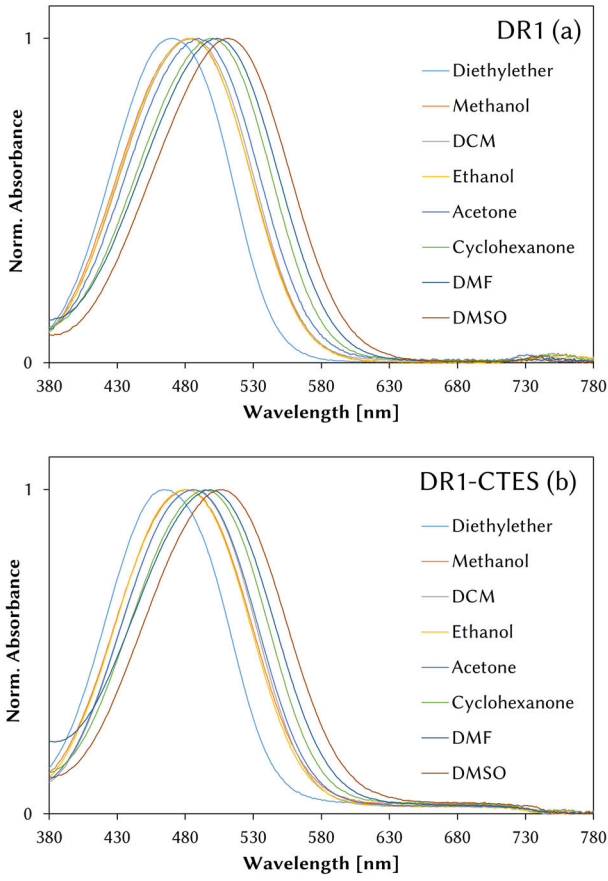

Figure 7.3 Normalized absorbance spectra of the dyes DR1 and DR1-CTES_1 in various solvents

Upon modification of DR1 to DR1-CTES a hypsochromic shift is seen of λ_{max} for all solvents, except for DCM were no shift was noted. This shift can be attributed to two effects. The removal of the hydroxyl group and the replacement by a (O-Si) group changes the electron releasing properties [12]. In addition, the disappearance of the hydroxyl group makes hydrogen bonding no longer possible there. The hypsochromic shift, however, did not significantly influence the visual color of the solutions. In conclusion, both dyes DR1 and DR1-CTES show a clear solvatochromic behavior in solution and thus both are further studied to modify the nanofibrous membranes.

Table 7.1 Wavelength at maximum absorption (λ_{max}) of the dyes DR1 and DR1-CTES in various solvents and the respective visual color of the solutions

Solvent	DR 1 λ_{max} [nm]	DR1-CTES λ_{max} [nm]	Visual color
Diethylether	471	464	Yellow
Methanol	482	480	Orange
DCM	485	485	Orange
Ethanol	486	479	Orange
Acetone	490	486	Orange
Cyclohexanone	500	494	Peach
DMF	503	498	Pink
DMSO	512	505	Pink

7.5 Functionalization of nanofibers with DR1 and DR1-CTES

Colored nanofibrous membranes were produced using three functionalization techniques, namely via dye doping with DR1, via inline covalent coupling using the modified dye DR1-CTES and by post-functionalization via coating with the modified dye DR1-CTES. Doped samples were produced by addition of the dye DR 1, to both pure TEOS and TEOS/CTES sols. Covalent immobilization inside the nanofibers was achieved by addition of DR1-CTES to TEOS sols prior to electrospinning. These samples will be denoted with T/DR, TC/DR and TC-DR, respectively, and will be referred to as inline functionalized samples. A fourth sample type was made by coating of pure hydrophilic silica nanofibers with the modified dye DR1-CTES, denoted as C-DR coated TEOS.

To electrospin TEOS-CTES sols as to generate functionalized fibers a proper amount of CTES had to be selected. A molar ratio of TEOS:CTES 1:0.0025 showed to allow for sols with rheological properties permitting electrospinning and yet resulting in a sufficient color depth of the intended colored membranes. It was thus selected for further study. The electrospinning of TEOS/CTES sols without added dye was tackled first to enable stable electrospinning. TEOS/CTES sols with varying viscosities were electrospun and a viscosity range of 100 – 250 mPa·s was found as optimum for electrospinning.

The dye DR1 was added to both pure TEOS sols and TEOS/CTES sols. The modified dye DR1-CTES was added to TEOS sols aiming for covalent immobilization in the sol-gel network. All sols were prepared via the open set-up. Addition of the dyes to pure TEOS and TEOS/CTES sols did not significantly influence the electrospinning process, similar to both the results in Chapter 6 and dye doping of various polymer nanofibers [13]–[15]. The T/DR, TC/DR and TC-DR nanofibrous membranes had an average nanofiber diameter of 330 ± 90 nm, 395 ± 80 nm and 350 ± 75 nm, respectively (Figure 7.4 a,b,c). The color of the membranes is visualized in the inset of Figure 7.4 and is for all samples similar, being pink. Electrospinning was carried out for 2 hours, resulting in sufficiently uniform, flexible, large and deeply colored nanofibrous membranes.

No influence on the nanofiber morphology such as pore blocking is seen after application of the dye DR1-CTES via coating (Figure 7.4 d). However some broken fibers were noticed in the C-DR coated TEOS sample which might be induced by the stirring of the membrane for 24 hours during the coating process. An average fiber diameter of 305 ± 90 nm was measured, similar to pure silica nanofibers. The color shown in the inset of Figure 7.4 d for the C-DR coated TEOS is the color obtained after soxhlet extraction of the uncoupled dye DR1-CTES, being paler pink compared to the T/DR, TC/DR and TC-DR nanofibrous samples. In summary, via all techniques uniform, flexible and sufficiently colored nanofibrous membranes were obtained.

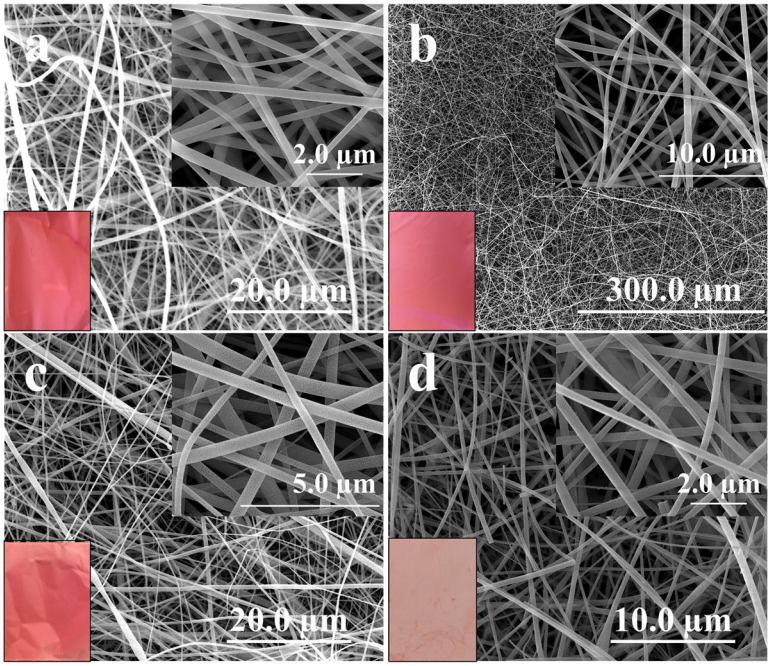

Figure 7.4 SEM images of T/DR (a), TC/DR (b), TC-DR (c) and C-DR coated TEOS (d) nanofibrous membranes, the color of the respective membranes is visualized by the inset in the images.

7.6 Solvatochromic behavior of DR1 functionalized nanofibers

The solvatochromic properties of the membranes were evaluated by immersing them in eight different solvents, namely diethylether, methanol, dichloromethane (DCM), ethanol, acetone, cyclohexanone, dimethylformamide (DMF) and dimethylsulfoxide (DMSO). For both the DR1 and DR1-CTES dyes in solution a clear color shift was seen with a maximal shift in λ_{max} of 41 nm when changing the solvent from diethylether to DMSO or inverse.

For all inline functionalized nanofibrous membranes (T/DR, TC/DR and TC-DR) high dye leaching was noticed (Figure 7.5 a). Covalent linkage of the dye within the sol-gel matrix did thus not seem to inhibit dye migration. The resistance of the samples to the solvents was evaluated

subsequently by immersing the samples for 24 hours in the different solvents (Figure 7.5 b). In contrast to pure TEOS as well as TEOS-APTES nanofibers, the TEOS-CTES samples showed a non-negligible degradation in most of the selected solvents as can be observed via monitoring their weight loss. This was true for both the TC/DR and the TC-DR nanofibrous membranes. High dye leaching was thus not only induced by the absence of the covalent linkage but also by dissolution of the nanofibrous membranes. Additionally, the presence of internally crosslinked DR1-CTES is suggested as an additional cause for the chemical instability. Thus, all inline functionalized nanofibrous membranes (T/DR, TC/DR and TC-DR) cannot be used as a solvatochromic sensor.

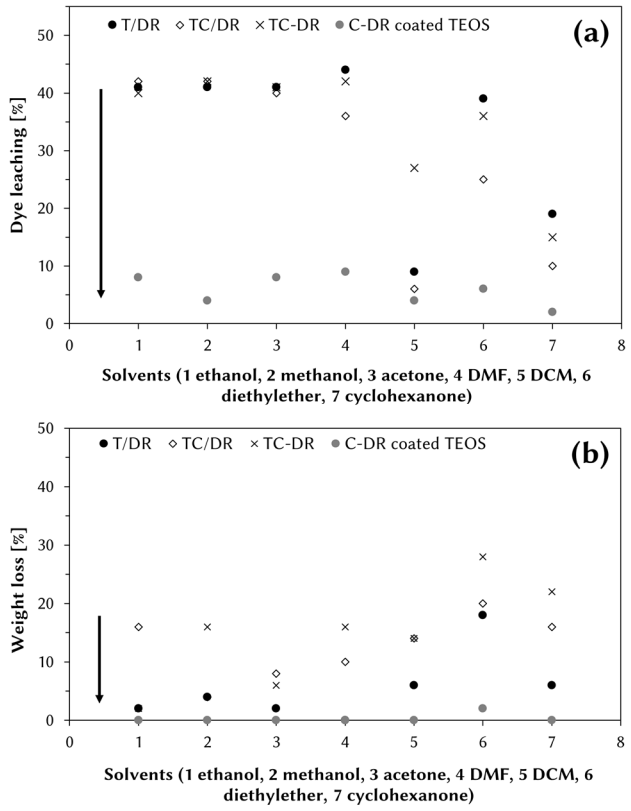

Figure 7.5 Dye leaching (a) and weight loss (b) of T/DR, TC/DR, TC-DR and C-DR coated TEOS nanofibrous membranes.

Immersion of C-DR coated TEOS in all solvents resulted in significantly lower dye leaching (Figure 7.5 a). Moreover, the samples showed to be resistant to the solvents in time as well (Figure 7.5 b), making these membranes better suited as solvatochromic sensor. The solvatochromic behavior was evaluated by immersing the C-DR coated TEOS samples in all eight different solvents (Figure 7.6 a). Only a small shift in λ_{max} of 8 nm was noticed upon immersion in DMF (Table 7.2). This resulted in a weak, yet visible color shift for the naked eye ($\Delta E = 7.6$) , visualized in the insets in Figure 7.6 a. Additionally, by immersing the same sample in different solvents, the reversibility was noted. Nevertheless, the polarity of the local silica environment seems to dominate the color of the solvatochromic dye, resulting in only a very minor color change, no longer visible to the naked eye, upon immersion in the other listed solvents.

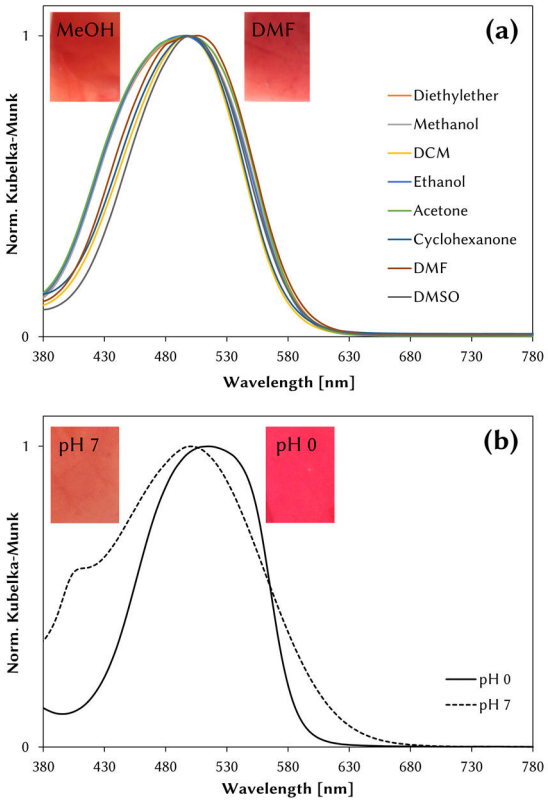

Figure 7.6 Solvatochromic (a) and halochromic (b) behaviour of C-DR coated TEOS nanofibrous membranes demonstrated with their normalized visible Kubelka-Munk spectra.

Table 7.2 Wavelength at maximum absorption (λ_{max}) of the dyes DR1 and DR1-CTES, and the C-DR coated TEOS nanofibrous membrane in various solvents.

Solvent	DR 1 λ_{max} [nm]	DR1-CTES λ_{max} [nm]	C-DR coated T λ_{max} [nm]
No solvent	-	-	496
Diethylether	471	464	496
Methanol	482	480	496
DCM	485	485	496
Ethanol	486	479	496
Acetone	490	486	496
Cyclohexanone	500	494	496
DMF	503	498	504
DMSO	512	505	500

In addition, the halochromic properties of the C-DR coated TEOS samples were evaluated as well (Figure 7.6 b). A much clearer color change (ΔE = 25) is seen going from pink at pH 0 to orange at pH 7 upon immersion in pH-baths. The reversibility was again confirmed. As expected, protonation and deprotonation of the dye is still possible, since coupling of DR1 to CTES is established via the hydroxyl group being isolated from the conjugated system. This thus seems to confirm the dominancy of the polarity of the silica surface resulting in a less pronounced solvatochromic behavior. Skrdla *et al* [4] noted as well that not all indicator dyes resulted in a significant difference in spectroscopic properties when doped in a sol-gel thin film. Future work should focus on proper dye and sol-gel precursor selection resulting in a more profound color shift upon exposure to various solvents. It can however be emphasized that coating of the functionalized dye significantly reduced dye leaching. Moreover, these samples were highly resistant to all solvents.

7.7 Conclusion

In summary, proper dye immobilization remains to be an essential prerequisite to obtain colorimetric sensor materials. Dye doped and inline covalently coupled samples showed to be unusable as solvatochromic sensor materials due to the absence of the covalent linkage and/or their non-resistance to the solvents. Covalent functionalization of pure TEOS nanofibers via coating showed to be ideal to tackle both problems. However, only a minor solvatochromic color change was noted for these samples. It is believed that by adjustment of the dye and sol-gel precursor a higher sensitivity might be obtained. Moreover, functionalization via coating is not only relevant for functionalization of nanofibrous membranes but is widely applicable for other materials as well. Therefore, it is assumed that these results can be highly valuable for future optimization of solvatochromic sensor materials applicable in various applications such as process control in food industry or chemical industry; or protective clothing and equipment, but further studies are still needed.

References

[1] B. Ding, M. Wang, X. Wang, J. Yu, and G. Sun, "Electrospun nanomaterials for ultrasensitive sensors," *Mater. Today*, vol. 13, no. 11, pp. 16–27, 2010.

[2] I. Steyaert, H. Rahier, and K. D. E. Clerck, "Nanofibre-based sensors for visual and optical monitoring," in *Electrospinning for High Performance Sensors*, A. Macagnano, E. Zampetti, and E. Kny, Eds. 2015, pp. 157–177.

[3] D. N. Simon, R. Czolk, and H. J. Ache, "Doped sol-gel films for the development of optochemical ethanol sensors," *Thin Solid Films*, vol. 260, no. 1, pp. 107–110, 1995.

[4] P. J. Skrdla, S. B. Mendes, N. R. Armstrong, and S. S. Saavedra, "Planar integrated optical waveguide sensor for isopropyl alcohol in aqueous media," *J. Sol-Gel Sci. Technol.*, vol. 24, no. 2, pp. 167–173, 2002.

[5] S. Chigome and N. Torto, "A review of opportunities for electrospun nanofibers in analytical chemistry," *Anal. Chim. Acta*, vol. 706, no. 1, pp. 25–36, 2011.

[6] B. W. Davis, A. J. Burris, N. Niamnont, C. D. Hare, C.-Y. Chen, M. Sukwattanasinitt, and Q. Cheng, "Dual-mode optical sensing of organic vapors and proteins with polydiacetylene (PDA)-embedded electrospun nanofibers.," *Langmuir*, vol. 30, no. 31, pp. 9616–22, 2014.

[7] J. Yoon, S. K. Chae, and J. M. Kim, "Colorimetric sensors for volatile organic compounds (VOCs) based on conjugated polymer-embedded electrospun fibers," *J. Am. Chem. Soc.*, vol. 129, no. 11, pp. 3038–3039, 2007.

[8] P. Paoprasert, B. Park, H. Kim, P. Colavita, R. J. Homers, P. G. Evans, and P. Gopalan, "Dipolar chromophore functional layers in organic field effect transistors," *Adv. Mater.*, vol. 20, no. 21, pp. 4180–4184, 2008.

[9] I. Steyaert, G. Vancoillie, R. Hoogenboom, and K. De Clerck, "Dye immobilization in halochromic nanofibers through blend electrospinning of a dye-containing copolymer and polyamide-6," *Polym. Chem.*, 2015.

[10] G. J. Mohr, H. Müller, B. Bussemer, A. Stark, T. Carofiglio, S. Trupp, R. Heuermann, T. Henkel, D. Escudero, and L. González, "Design of acidochromic dyes for facile preparation of pH sensor layers," *Anal. Bioanal. Chem.*, vol. 392, no. 7–8, pp. 1411–1418, 2008.

[11] B. Ding, M. Wang, J. Yu, and G. Sun, "Gas Sensors Based on Electrospun Nanofibers," *Sensors*, vol. 9, pp. 1609–1624, 2009.

[12] Y. Cui, M. Wang, L. Chen, and G. Qian, "Synthesis and spectroscopic characterization of an alkoxysilane dye containing C. I. Disperse Red 1," *Dye. Pigment.*, vol. 62, no. 1, pp. 43–47, 2004.

[13] L. Van der Schueren, T. De Meyer, I. Steyaert, Ö. Ceylan, and K. Hemelsoet, "Polycaprolactone and polycaprolactone/chitosan nanofibres functionalised with the pH-sensitive dye Nitrazine Yellow," *Carbohydr. Polym.*, vol. 91, pp. 284–293, 2013.

[14] I. Steyaert, M. P. Delplancke, G. Van Assche, H. Rahier, and K. De Clerck, "Fast-scanning calorimetry of electrospun polyamide nanofibres: Melting behaviour and crystal structure," *Polym. (United Kingdom)*, vol. 54, no. 25, pp. 6809–6817, 2013.

[15] L. Van Der Schueren, K. Hemelsoet, V. Van Speybroeck, and K. De Clerck, "The influence of a polyamide matrix on the halochromic behaviour of the pH-sensitive azo dye Nitrazine Yellow," *Dye. Pigment.*, vol. 94, no. 3, pp. 443–451, 2012.

8

Concluding remarks and outlook

This chapter summarizes the main conclusions of this PhD work and highlights some future perspectives.

Electrospinning of silica nanofibers without organic polymer addition is regarded as a highly promising methodology for the production of thermal and chemical resistant nanofibrous materials applicable in various advanced applications. The combination of sol-gel technology and the electrospinning process allows for the production of ceramic nanofibrous membranes. By proper control of the sols rheology, addition of an organic polymer can be skipped in the nanofibers preparation procedure. This broadens their applicability since an additional heat treatment, typically used to remove the organic polymer, can be avoided if not necessary. Moreover, it allows for functionalization of these nanofibrous membranes with various components that would otherwise not withstand the heat treatment.

Thus far, however, the electrospinning of these pure sol-gel precursors is not well understood nor studied in detail. Moreover, the full potential of these silica nanofibrous membranes for multiple applications such as water treatment and colorimetric sensors has not yet been uncovered. Analysis of the parameters influencing electrospinning of pure sols and subsequent investigation of the obtained nanofibers and their possibility for functionalization with different compounds, are thus necessary. Therefore, this PhD work explored the potential of electrospinning of pure sols without organic polymer and their functionalization with titanium dioxide nanoparticles and color changing dyes envisioning water treatment and sensor applications, respectively. To do so, tetraethyl orthosilicate (TEOS) was selected as sol-gel precursor for these silica nanofibers, since TEOS is the most commonly used and most thoroughly studied sol-gel precursor.

The significant influence of the viscosity on the electrospinning process was demonstrated. A clear viscosity region was found for which electrospinning was most stable. Lower viscosities resulted in beads, higher viscosities resulted in blocking of the needle during electrospinning. The resistance of these nanofibers towards a heat treatment at 1000°C was confirmed. Moreover, interesting changes in hydrophilic properties upon aging and after heat treatment were seen.

To gain a more in-depth knowledge on the parameters influencing the electrospinning process, three preparation set-ups were compared and the sols were characterized via various techniques. All parameters, including colloidal particle sizes, solvent concentration, degree of

crosslinking and viscosity showed to have a major influence on the electrospinning process and they all showed to be related. Proper control of these parameters is thus essential in the electrospinning of silica nanofibers. As a consequence, upscaling was possible resulting in the production of larger, flexible silica nanofibrous membranes usable to be examined for different end-applications.

The unique properties of nanofibrous membranes makes them ideal for a wide range of filtration applications. Moreover, they show to be an excellent porous support for the immobilization of TiO_2 nanoparticles. These TiO_2 nanoparticles are capable of oxidizing many organic (micro)pollutants. In this PhD the comparison was made between polyamide 6 and silica nanofibrous membranes as a porous support for water treatment applications. Two techniques for immobilization were explored, namely inline functionalization and dip-coating. It was shown that for polyamide 6 inline functionalization was the best method, since dip-coating results in pore blocking. Silica nanofibers on the contrary are preferably functionalized via dip-coating, avoiding shielding of the TiO_2 by the silica shell. A basic set-up was used to evaluate the high photocatalytic activity of the membranes. Decoloring of the dye Methylene Blue was easily established. Moreover, complete removal of the micro pollutant isoproturon, a herbicide, was achieved. Functionalization of a highly porous and flexible nanofibrous support with TiO_2 nanoparticles allows for the production of advanced materials, applicable in different water treatment set-ups. Polyamide 6 is believed to be the most economical option in non-harsh environments. The chemical and temperature resistance of silica nanofibers makes them a promising material for other effluent treatments including highly acidic effluents.

The use of nanofibers significantly improves the sensitivity and the response time of colorimetric sensors. In this PhD work, nanofibrous membranes were developed changing color under influence of pH changes, HCl and NH_3 vapors, biogenic amines and solvents. As a first step to enable covalent immobilization in or on the nanofibrous membrane, the color-changing dye was attached to a sol-gel precursor. Two strategies for immobilization were explored, inline addition of the dye-modified sol-gel precursor and coating with the dye-modified sol-gel precursor.

Aiming for color changing dye-modified silicon oxide nanofibers, focus was first given to sensor materials changing color under influence of pH

changes in water, HCl/NH_3 vapors and biogenic amines. To do so the comparison was made between dye doping and inline covalent functionalization. The importance of the covalent linkage was proven, as only the membranes with a covalently link between dye and sol-gel matrix were suitable to be used as pH-sensor in aqueous acidic environments. Nevertheless, all nanofibrous membranes showed an immediate and clear color change upon exposure to hydrogen chloride and ammonia vapors. For solid state gas sensing nanofibrous membranes can thus be applied without covalent linkage since dye leaching is not always an issue. When these sensors are however exposed to liquids a covalent linkage is indispensable. Also the sensitivity to biogenic amines was demonstrated, showing the high versatility of these membranes for various applications including control of food quality. Color changing large area, flexible, reusable sensors were thus developed that are highly valuable for advanced applications including personal clothing and equipment.

Further enhancements in the versatility of these colorimetric sensor materials were enabled by developing solvatochromic sensors. In addition to inline covalent functionalization, also coating with the dye-modified precursor was investigated as a new technique. A limiting factor in the production of these membranes was the dissolution of the membranes, to which the additional (dye-functionalized) CTES precursor was added, in the solvents. High dye leaching of the inline functionalized membranes was thus a major problem as well. These membranes were not applicable as solvatochromic sensor. To overcome this problem the coating technique was applied. Dye leaching and dissolution in the solvents was proven to be significantly reduced. However, only a minor color change was noted upon immersion of these coated membranes in the solvents and further studies are thus necessary.

In conclusion, the development of silica nanofibers without addition of an organic polymer in the preparation procedure showed to be realistic. Moreover, two possible end-applications have been explored and both showed to be highly promising. Even though this PhD presents a major step forward, certain aspects still remain to be researched.

First, within this PhD some first steps towards the influence of a heat treatment on the silica nanofibers have been explored. This resulted in highly interesting results on changing hydrophilic properties of the membranes. However, more detailed studies focusing on this heat

treatment and the influence on the nanofibrous membranes are advised. An in-depth study on the influence of this heat treatment on the mechanical properties and hydrophilic properties of these membranes will demonstrate their broad potential for the intended end-applications. When relating these properties to water treatment and sensor applications and going even further to product design also handling, storage, lifetime become important factors and should be included in future studies.

Secondly, the sol-gel process is known to be an ideal technique for functionalization due to the availability of various sol-gel precursors and by their applicability via multiple techniques including coating. When aiming at solvatochromic sensors in this PhD, the introduction of a sol-gel precursor different than TEOS resulted in a decreased chemical resistance of the membranes. Further studies on proper sol-gel precursor selection should thus be carried out. In addition, the application of dye modified precursors via coating may be a promising alternative. Moreover, these coatings can be applied on other substrates such as films and glass, significantly broadening the applicability of this technique.

Thirdly, dye selection remains an essential prerequisite when aiming at colorimetric sensors. In order to better understand the influence of a nanofibrous matrix on the color-changing properties, future studies in molecular modeling can supplement experimental results and allow for a better informed dye selection.

In conclusion, the work presented in this PhD illustrates the major potential of novel silica nanofibers and their applicability for advanced applications including water treatment and colorimetric sensors. This research can lead to various follow-up investigations towards the same or different end-applications. Therefore, I truly believe that my research and findings will help to pave the way towards advanced nanofibrous products.